THE $FE^{3+/2+}$ REDOX COUPLE IN LIQUID AND SOLID SOLVENTS

Lynn Christie

A Thesis Submitted for the Degree of PhD
at the
University of St Andrews

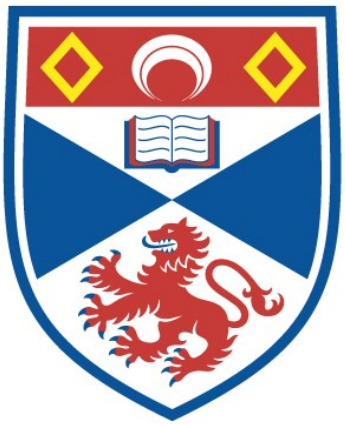

1996

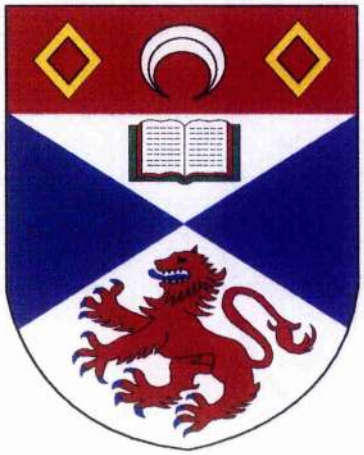

THE $FE^{3+/2+}$ REDOX COUPLE

IN LIQUID AND SOLID SOLVENTS

A thesis presented for the degree of

Doctor of Philosophy

in the Faculty of Science of the University of St. Andrews

by Lynn Christie, *B.Sc.*

Centre for Electrochemical

and Material Sciences

School of Chemistry

St. Andrews

September, 1995

DECLARATION

I, Lynn Christie, certify that this thesis has been composed by myself, that it is a record of my own work, and has not been submitted in any previous application for a higher degree.

Signed: Date:

I was admitted to the Faculty of Science in the University of St. Andrews under Ordinance General No. 12 on 1 October, 1991 and as a candidate for the degree of Doctor of Philosophy on 1 October, 1992.

Signed: Date: 28/9/95

CERTIFICATION

I hereby certify that Lynn Christie, B.Sc. has spent twelve terms of research work under my supervision, and that she has fulfilled the conditions of the Resolution and Regulations appropriate to the degree of Doctor of Philosophy.

Signed: Date: 27/9/95

P.G. Bruce

Director of Research

LIBRARY DECLARATION

In submitting this thesis to the University of St. Andrews, I understand that I am giving permission for it to be made available for use in accordance with regulations of the University Library for the time being in force, subject to any copyright vested in the work not being affected thereby. I also understand that the title and abstract will be published, and that a copy of the work may be made and supplied to any bona fide library or research worker.

Signed: Date: 28/9/95

Dedicated to the ones I love

Acknowledgements

Thanks must be given to my supervisor, Professor Peter Bruce, for his guidance and constructive comments throughout my Ph.D years, and for giving encouragement to work with my own ideas. I would like to express my appreciation to Professor Colin Vincent and all the members of *C.E.M.S.*, past and present, for their general good humour and stimulating discussions.

My thanks are also due to Dr. Stephen Cambell, Jim Rennie and Bob Cathcart for the design and construction of the solid state polymer cell, and other members of the technical staff at St. Andrews who have helped with many odd requests. Thanks are also due to the EPSRC and Yuasa for CASE funding.

Special thanks must go to my family for their support over my many years of study. Finally, I would like to thank Ali, my husband and colleague, for standing by me through the highs and lows of the last four years, and without whom this thesis would never have been completed.

ABSTRACT

The $Fe^{3+/2+}$ redox couple, in the form of Fe (II) and Fe (III) trifluoromethane sulphonate, has been investigated in several non-aqueous solvents: propylene carbonate (PC), acetonitrile (ACN), tetrahydrofuran (THF), dimethyl sulphoxide (DMSO) and dimethyl formamide (DMF), as well as in tetraethyleneglycol dimethylether, a low molecular weight liquid polyether, and poly(ethylene oxide), a high molecular weight solid polyether. It has been shown that the $Fe^{3+/2+}$ couple exhibits a simple one electron transfer reaction in all cases. The influence of the solvent on the electrode kinetics of the $Fe^{3+/2+}$ redox couple has been investigated with a view to identifying the factors controlling the rate of the simple electron transfer process for this redox couple. The standard apparent rate constant (k_{sh}) in each system was determined via ac impedance spectroscopy. For studies in the solid polyether solvent a new technique has been developed involving ac impedance spectroscopy at an ultramicroelectrode. This new technique proved to be a very powerful tool in the identification of interfacial processes occurring in highly resistive media

Using the Marcus and the Levich, Dogonadze & Kuznetsov theories for activation of electron transfer, kinetic data were interpreted in terms of inner and outer sphere contributions from the solvent. For the liquid solvents a correlation between k_{sh} and the donor number of the solvent was found, indicating inner sphere activation of electron transfer via vibration of the coordinate bond. However, for the solid solvent activation of electron transfer was found to be influenced by outer sphere solvent dynamics as solvent reorganisation in the polymer is slower than in the liquid solvents.

TABLE OF CONTENTS

CHAPTER 3

CHAPTER 4

CHAPTER 5

CHAPTER 8

List of commonly used symbols

A	Area of electrode
C	Capacitance
C_{dl}	Double layer capacitance
C_e	Electrode capacitance
C_b	Bulk capacitance
c_i	Concentration of species i
c_O^σ, c_R^σ	Surface concentrations of O and R
c_O^∞, c_R^∞	Bulk concentrations of O and R
C_r	Concentration of reduced species
C_o	Concentration of oxidised species
D_0	Diffusion coefficient
D_i	Diffusion coefficient of species I
D_{op}, D_s	Square of refractive index and static dielectric constant respectively
E	Applied potential
E_e	Equilibrium potential
E_e^θ	Standard equilibrium potential
E_p	Peak potential
E_{max}	Potential amplitude
e	elementary charge
$E_{1/2}$	Half-wave potential
E_a	Activation energy

E_f	Fermi energy
E	Energy
ε_s	Static permittivity
ε_{op}	Optical permittivity
ε	Permittivity
ε_0	Permittivity of free space
F	Faraday Constant
G	Free energy
G^*	Free energy of activation
I	Current density
I_0	Exchange current density
I_p	Peak current density
i	Current
k_0	Rate constant at 0V vs. the reference electrode
k_s	Standard rate constant for a redox couple
k_{sh}	Standard apparent rate constant for a redox couple
k	Boltzmann constant
K_p	Equilibrium constant
k_j	Force constant of jth vibrational level
κ	Electronic transmission coefficient
λ	Reorganisational energy
l	Length between electrodes
n	Number of electrons
O	Oxidised species

q	Charge
q_j	Bond length
R	Reduced species
R	Resistance
R	Gas constant
R_s	Solution/electrolyte resistance
R_m	Electrode resistance
R_b	Bulk resistance
R_u	Uncompemsated solution resistance
R_e	Electrode resistance
R_{ct}	Charge transfer resistance
T	Temperature
t	Time
τ_l	Longitudinal relaxation time
U	Potential energy
v	Sweep rate
ν_n	Nuclear frequency factor
V	Voltage
ω	Angular frequency
Y	Admittance
Z	Impedance
Z'	Real impedance
Z''	Imaginary impedance
Z_w	Warburg impedance

z	Charge valency
η	Overpotential

Constants

Elementary charge	e	=	1.602177×10^{-19}C
Faraday constant	F	=	96485 C mol^{-1}
Boltzmann constant	k	=	1.38066×10^{-23} mol^{-1}
Avagadro constant	N	=	6.02214×10^{23} mol^{-1}
Gas constant	R	=	8.31451 JK^{-1} mol^{-1}
Vacuum permittivity	ε_0	=	8.85419×10^{-12} $J^{-1} C^2 m^{-1}$

CHAPTER 1

INTRODUCTION

1.1 The Importance of Electrochemistry

Electrochemistry involves chemical phenomena that are associated with charge separation which often leads to charge transfer. Charge transfer can occur homogeneously in solution, or heterogeneously at electrode surfaces. Electrochemistry is not only a subject within physical chemistry but is one which spans science from biology to chemistry to physics and materials science as the world is full of interfaces, the majority of which are charged. The goal of physics is understanding how these charges move and by putting them together into cells brings in the materials science of electrodes and the organic and inorganic chemistry of the species inside the cell.

Electrochemistry involves the study of interfaces and the passage of charge across these junctions. From this viewpoint it is possible to derive a relationship between electrochemistry and other interdisciplinary fields involved in the study of charge transfer at interfaces (figure 1.1). The following examples give a small insight into the importance of electrochemistry in other fields. The list is very limited as a full discussion of this would itself be a thesis but it is hoped that the brief discussion will give an insight into the importance of electrochemistry.

Thermodynamics of this situation at equilibrium

Metallurgy of defects on metal surface

Quantum mechanics of transfer of electrons through barrier at interface

Fick's second law **diffusion theory** of time dependence of concentration

Crystallography of surface

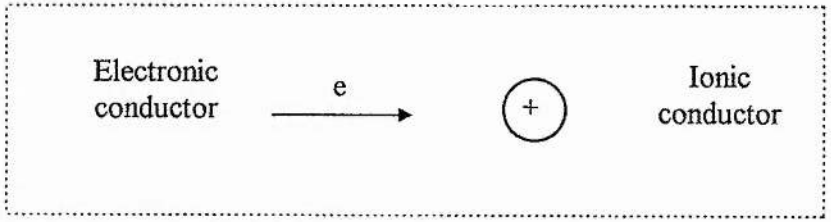

Electronics of circuitry to control potential across interfaces

Physical chemistry of solutions

Statistical mechanics of particle distribution near interface in field

Physics of energy levels in metals and semiconductors

Surface chemistry of intermediate radicals on surface; and adsorption

Spectroscopy of acceptor particles, gives energy levels for electrons

Hydrodynamics of flow of solution, transports ions to surface

Surface physics of electron overlap potential very near surface of metal

Physical chemistry of surface reactions

Metallurgy, e.g. sputtered film formation on surface

Optics of examination of surfaces

Figure 1.1 Relationship between electrochemistry and other interdisciplinary fields.

In *metallurgy* the stability and properties of the materials, the extraction of metals from ores dissolved in molten salts, and the separation of metals from mixtures in solution all have electrochemical aspects associated with them. Soil movements in *geology* have an electrochemical base: movement of the soil depends on interactions of the double layers between colloidal particles which in turn depends on the concentration of ions which affect the field across the double layer and cause the colloidal structures upon which the soil's consistency depends to repel each other and remain stable. The use of electrochemistry in *industry* is widespread. Examples of such uses include electrolysis and electrosynthesis, electrodeposition and metal finishing [1-3] and water and effluent treatment. Other examples include the production of batteries and fuel cells [4,5] which are electrochemical power sources. In *biology* food is converted to mechanical work by biochemical mechanisms involving electrochemical reactions. Transmission of nerve impulses, the stability of blood and macromolecules involved in biological processes all depend on electrochemistry via electrochemical charge transport and double layer interactions. Also important is the application of electrochemical methods in biology i.e. *bioelectrochemistry* and the development of *bioelectroanalysis* [6-10] which has in turn led to biosensors [9,11].

As well as electrochemistry being important in other sciences many basic principles of chemistry have their origins in electrochemistry. For example the third law of thermodynamics was born from observations of temperature variations in heat content and free energy changes in cell reactions. Other examples include pH and dissociation constant concepts which were studied as a part of the electrochemistry of solutions,

and also Brϕnsted – Bjerrum theory and ionic reaction kinetics which are expressed in terms of Debye-Huckel theory.

The subject of electrochemistry may be divided into two sub topics: ionics and electrodics. Ionics is concerned with the behaviour of ions in solution, whilst Electrodics is concerned with the theory of charged interfaces and the conditions governing the transfer of charge across them.

1.2 Ionics

1.2.1 Electrolyte Solutions

In electrochemistry the structure of both phases on either side of the interface need to be well understood. The structure of the electrode, whether it be a metal, semiconductor etc., is mainly the domain of solid state physics. On the other hand ionics, the study of bulk electrolyte phenomena is the domain of chemistry, and electrochemists in particular. The majority of the work of ionics was completed from about 1920 to 1950 and concentrated on, for example, activity coefficients of dilute aqueous solutions, electrical conductivity in molten salts or electrostatic effects on the dissociation constants of acids and bases in aqueous solutions.

Electrolytes can be divided into different classes, these are aqueous solutions, non-aqueous solutions, molten salts, solid ceramic electrolytes and solid polymer electrolytes. The electrochemistry of aqueous solutions has been studied exhaustively

since the last century. However, the relative reactivity of water puts limitations on the potentials which can be used when looking at redox species and their electrochemical behaviour, especially if the oxidation and reduction potentials fall outside the stability window of water which is less than 2.1V. As an example of the limitations of water consider the development of high voltage (>3V) batteries: in modern lithium battery research a completely water - free environment is required as any water present will react with the lithium [12,13] or carbon electrodes which are located at ≈ -3V vs. H^+/H_2 couple, outside the stability range of water. For these reasons other solvents have been used in most recent electrochemical studies. These solvents tend to be aprotic e.g. DMSO, DMS, PC, THF, ACN, or lower dielectric solvents, e.g. benzene [14] and liquid polymers [13] e.g. tetraethyleneglycol dimethyl ether (tetramer). These solvents allow a much greater range of investigations to be carried out electrochemically and they have extended greatly the scope of electrochemistry. These solvents also allow the studies of compounds that have not been possible before due to the reactive nature of the compound with water or because the compound is only soluble in organic solvents. (e.g. the plating and stripping of lithium and sodium). Technological advances have necessitated the most recent advance in the production of new electrolytes: smaller and more environmentally safe power resources are required that can produce the same amount of energy as conventional ones. As the geometry and size of some of these power sources must be small and very flexible (for example batteries for heart pacemakers) and not in the least bit corrosive or poisonous liquid solvents are not desirable. To this effect solid polymer electrolytes, that can be bent and shaped to any geometry, have been developed.

1.2.1.1 Solid Polymer Electrolytes

Polymer electrolytes are ionically conducting phases formed by the dissolution of salts into suitable coordinating polymers, for example poly(ethylene oxide) (PEO) [15]. There are three important criteria governing the suitability of the polymer to act as a host:

(i) the polymer molecules must have polar groups or donor atoms capable of forming coordinate bonds with the cation,

(ii) the distance between coordinate groups must be such as to maximise the polymer-cation interaction,

(iii) the polymer must be capable of adopting low energy conformations to allow multiple inter- and intra- molecular coordinations.

To form a good polymer electrolyte there must be a compromise between strong cation-polymer interaction to compensate for the loss of salt lattice energy and the cation-polymer bond lability to facilitate ion transport. The dissolution of salts in the polymer host is governed by the hard and soft acid base theory (HSAB theory). PEO can be regarded as a hard base and it most likely to form stable complexes with hard acids. An example of such a system is a lithium salt complex of poly(ethylene oxide) [16]. In the PEO complexes it is the ether oxygens which coordinate the cations. Polymer electrolytes can be thought of as solid solvent systems, allowing the investigations of solvent effects on electrochemical phenomena to be taken to the final stage of study in the solid state.

As polymer electrolytes are solid solvent systems, the motion of ions through the polymer complex is different to that in liquid solvent systems. All ionic motion is frozen below the glass transition temperature (T_g) of the system. Above T_g ionic motion occurs and there are three main theoretical models for motion in polymer electrolytes: the Free Volume Theory of Cohen and Turnbull [17], the Configurational Entropy Model of Adam, Gibbs and DiMarzio [18,19] and the Dynamic Bond Percolation Theory of Ratner, Nitzan and Druger [20,21].

Free Volume Theory: Cohen and Turnbull [17]. Cohen and Turnbull proposed that molecular transport occurred as a result of movement of molecules into voids greater than a certain critical size formed by the redistribution of the free volume of the system. They suggested that diffusive motion would occur if another molecule jumped into the hole vacated by the first before it could return. They defined the free volume of the molecule to be equal to the volume of the molecule in its cage less that occupied by the molecule itself. For the diffusion of each molecule to be non-zero, the volume of the void had to be greater than a critical value v*. A molecule can only jump into a void if the motion of the short polymer chain fragments provides an empty hole adjacent to the molecule that is going to jump. Hence, the segmental motion of the polymer chains governs the diffusion of ions or molecules through the polymer matrix.

Configurational Entropy Theory: Adam, Gibb and DiMarzio [18,19]. This theory proposed that the total configurational entropy of a system was a linear function of the fraction of bonds flexed out of their low energy orientations. The flexing of these

bonds, i.e. the motion of the polymer chain segments again governs the motion of ions: the polymer chain sections have to attain a certain configuration or array providing a site adjacent to the ion into which the ion can move.

Although the free volume or configurational entropy approaches describe adequately many of the transport properties in polymer electrolytes, they are not based on a microscopic treatment and therefore, local mechanistic information is lost. Motions of ions in polymer electrolytes is strongly dependent on segmental motion of the polymer host. Ratner, Nitzan and Druger [20,21] proposed a microscopic model to describe the transport mechanisms in polymer electrolytes: the *Dynamic Bond Percolation (DBP) Theory.* In this model cation motion and anion motion are considered to be fundamentally different. Cation motion can be described as being the making and breaking of coordinate bonds with motion between coordinating sites: the whole segment of polymer coordinating the cation moves before passing on the ion. Anion motion is regarded as a hopping between an occupied site and a void that is large enough to contain the ion and this only occurs between neighbouring sites. This motion has an associated probability of hopping occurring. Due to polymer motion the configuration of the polymer is continually changing and sites involved in hopping move with respect to each other. Ions can only move to a new coordination site, or hop, if the polymer chains move to a configuration that provides a coordination site or void adjacent to the moving ion.

These three models of ionic motion each provide a mathematical model. All three mathematical models coincide with each other.

Following on from early studies [22] that indicated over a certain temperature range many $\sigma(T)$ curves followed either Arrhenius (eqn. 1) or Vogel-Tamman-Fulcher (VTF) [23] behaviour (eqn. 2), it has subsequently been found that most polymer electrolytes show one of four patterns of behaviour for ionic motion:

Eqn. 1	Eqn. 2
Arrhenius behaviour:	VTF behaviour
$D_0 = A \exp(-E_a / RT)$	$D_0 = C \exp[-B / (T-T_0)]$
A is a constant	C is a weakly temperature dependent constant; ($C \alpha T^{-1/2}$)
E_a is the activation energy for the process	T_0 is a reference temperature
	B is a constant

(i) VTF over observable temperature range

(ii) Arrhenius behaviour for low temperatures and VTF at higher temperatures

(iii) Arrhenius behaviour over whole temperature range falling into two regions : one with a high activation energy at low temperatures and the second with a low activation energy at higher temperatures

(iii) VTF behaviour at low temperatures and Arrhenius at higher temperatures.

As has just been discussed, the process by which net ionic motion takes place in polymer electrolytes is different from that in low molecular weight solvent-based systems, since long range displacement of the solvent is not observed. Ionic transport

occurs via local relaxation processes in the polymer chains which may provide liquid-like degrees of freedom [24]. Intra- and inter- polymer transitions between ion coordinating sites, and segmental motion of the chains are believed to play a major role in the ion conduction mechanism thus bringing cations to the interfacial region. The disadvantage of this type of ionic motion however, means that diffusion of the electroactive species to and from the interfacial region is slow when compared to liquid systems (typically three orders of magnitude slower). As the polymer electrolyte is a solid it has one more disadvantage associated with it, with respect to electrochemical studies: it has a very high bulk resistance. This along with the slower diffusion can be overcome by the appropriate design of electrochemical experiments. This is dealt with later in Chapter 3.

The advantages of polymer electrolytes over classical liquid electrolytes are:

(i) There are not the leakage problems associated with liquid electrolytes,

(ii) The materials are often soft and form good interfacial contact with electrodes. They can often accommodate the volume changes associated with the ion-electrode exchange process,

(iii) The materials can be produced in a variety of geometries including thin films.

However, the full scope of the use of polymer electrolytes has not yet been fully realised [20].

1.2.1.2 Solid Ceramic Electrolytes

Migration of ions does not occur to any appreciable extent in most ionic and covalent solids such as oxides and halides. In contrast, there is a small group of solids called solid electrolytes (also known as superionic conductors and fast ion conductors), that usually have a rigid framework structure, but within which one set of ions forms a mobile sublattice. Solid electrolytes contain tunnels or layers through which their mobile ions may move. In this respect solid electrolytes are intermediate between typical ionic solids, in which none of the ions can move from their lattice sites, and liquid electrolytes, in which all the ions are mobile. There are two main structural requirements for high ionic conductivity in these materials: (i) there must be empty sites available for ions to hop into and (ii) the energy barrier that ions have to overcome in order to hop between sites must be small. Like polymer electrolytes, solid electrolytes have distinct advantages over liquid electrolytes. Research into the applications of these materials, especially in the development of high energy density storage systems, has grown rapidly in recent times [4,5].

1.3 Electrodics

1.3.1 The Electrode/Electrolyte Interface

Electrodics involves the study of electrified interfaces existing between two media. Interfaces occur between two immiscible solutions, two solid materials, and an electrode and an electrolyte, whether the electrolyte is a solid or a liquid. For interfaces between an electrode and an electrolyte the most fundamental process that

occurs is electron transfer and this is at the heart of electrochemistry. Electron transfer occurs via electron tunnelling across the interface either from the electrode into the electrolyte or vice versa.

The electrochemical interface has been the topic of research for many decades, probably starting with Helmholtz in 1879 [25]. The interface in aqueous systems is well documented and relatively well understood. The interface between aprotic liquid solvent systems and electrodes, although less well understood than aqueous systems, is a rapidly moving discipline, but is still in its infancy [26-31].

When studying electrode reactions it is very important to consider the interfacial region as it is in this area where the act of electron transfer occurs, the interfacial area governing the driving force of the reaction and how it takes place. Therefore, a knowledge of the potential distribution and the position of the reactant species with respect to the electrode when electron transfer occurs is important.

In his model Helmholtz [25] considered the ordering of the negative and positive charges in a rigid fashion on both sides of the interface, the interactions of which did not extend any further into the solution, this led to the term 'double layer'. Helmholtz's model (figure 1.2) can be compared to the classical parallel-plate capacitor. The first plate would be on the contact surface of the metal/solution, the second would be formed by ions of opposite charge from the solution rigidly linked to the electrode and would pass through the centres of these ions. The distance of closest approach would therefore be the ionic radius of these ions. This model fails on

two points: firstly it ignores interactions that occur further from the electrode than the first layer of adsorbed species and secondly it does not allow for any electrolyte concentration dependence.

Early in this century (1910-1913) Gouy [32] and Chapman [32] independently developed a model for the double layer in which they considered the influence of electrolyte concentration and applied potential on the double layer capacitance. The double layer was of variable thickness, the ions being free to move, and was called the diffuse double layer (figure 1.3).

In 1924 Stern [33] combined the Helmholtz and the Gouy-Chapman models. The double layer was now considered to be formed of a compact layer of ions next to the electrode followed by a diffuse layer extending into the bulk solution (figure 1.4). If the electrolyte is concentrated then the thickness of the diffuse layer is less important and the potential drop is rapid. The transition between the compact and diffuse layer occurs at the distance x_H. This separation plane is known as the *Outer Helmholtz Plane* (*OHP*).

Although Stern distinguished between ions adsorbed on the electrode surface and those in the diffuse layer, the double layer theory was again modified in 1928 by Grahame [34]. Grahame developed the model to allow for the existence of specific adsorption and thus has three regions (figure 1.5). A specifically adsorbed ion loses its solvation shell and so can approach closer to the electrode surface. It can also have the same charge as the electrode or be of opposite charge. The centre of these ions

defines the *Inner Helmholtz Plane* (*IHP*). The *OHP* passes through the centre of the non-specifically adsorbed solvated ions and the diffuse region is outside the *OHP*, and, as in the Stern model, the potential varies linearly with distance until the *OHP* is reached then exponentially in the diffuse layer.

Although extensively covered, the structure of the double layer is far from being well established and evaluated. The Helmholtz, Gouy-Chapman, Stern and Grahame models are all based on electrostatic considerations. Further 'chemical' models, have been developed that consider the electronic distribution of the atoms inside the electrode. The first of these models to be proposed was done so by Damaskin and Frumkin [35] and the model has been reviewed recently by Trasatti [36] and Parsons [37]. From his model, Frumkin derived a correction that allows for loss of potential across the diffuse double layer. The *Frumkin correction* is required when calculating the true standard rate constant of electrode kinetics.

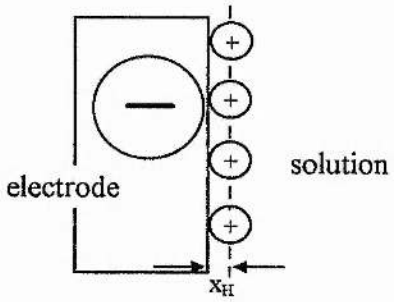

Rigid arrangement of ions

Figure 1.2 Helmholtz's model of the double layer.

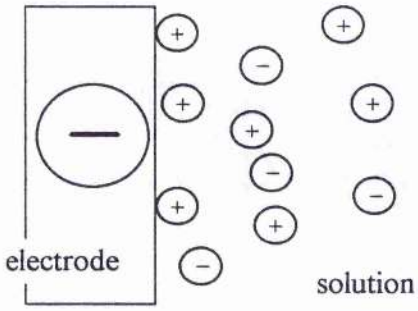

Arrangement of ions in diffuse way

Figure 1.3 The Gouy-Chapman model for the double layer

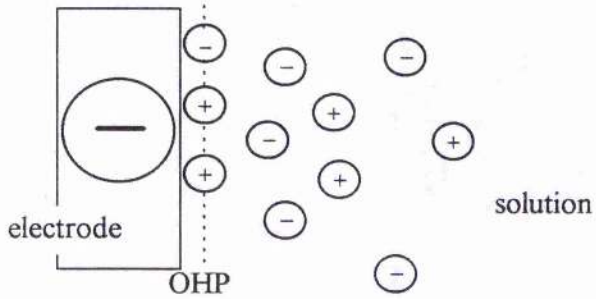

Arrangement of ions in compact and diffuse layer

Figure 1.4 The Stern model for the double layer

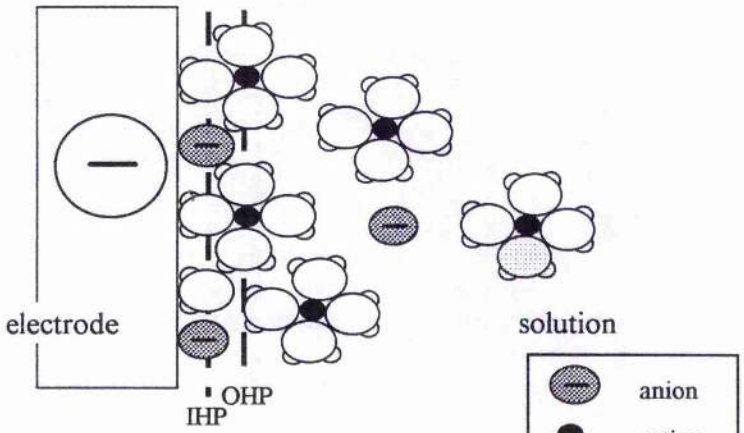

(a) Arrangement of the ions

Figure 1.5 The Grahame model of the double layer

1.3.2 Electron Transfer

Although electron transfer is now known to be the most fundamental process in many reactions, and not only in electrochemistry, it has taken many years for an understanding of this process to be developed. At about the same time that models for the double layer were being postulated chemists were trying to understand the principles governing electrochemical reactions. At the turn of the century electrochemical cells in equilibrium were being treated thermodynamically, i.e. there was no net current passing across the interface in the cell and therefore there was no net cell reaction. The thermodynamic view was that electrochemical energy was lost or gained when an electric charge was taken around a circuit made from the electrochemical cell and its two electrode/solution interfaces. The lost or gained electrochemical energy was thought to be an algebraic sum of the potential differences in the cell multiplied by the charge transferred in the reactions at each interface. This electrochemical energy sum was then equal to the change in free energy occurring in the net chemical reaction taking place in the electrochemical cell. This thermodynamical view was postulated by Nernst in 1891.

Although this view represented a great advance in the history of chemistry it had two major negative consequences on the development of electrochemistry. Firstly, it assumed that electrochemical reactions across the interface were *potential-centric* and not *current-centric*, that is when the current changed it was thought that the corresponding changes in the electric potential was due to some malfunction in the cell. The thought that the net flow of electrons across interfaces occurred only because the potential difference across them was made to differ from the Nernst

equilibrium was suppressed in favour of the thermodynamic approach. For about 50 years on from 1910, electrochemists were in awe of the thermodynamic treatment which regarded potential as the variable dependent on current. They did not try to develop a kinetic treatment for interfacial charge transfer. For example, irreversible electrode reactions were still being treated by approximations based on reversible thermodynamics as late as 1947.

By 1950 electrochemists in America and Europe had begun to think of the immediate cause of current flowing across an interface as being the influence of an external power source which caused a change in the electric potential difference across the double layer from values corresponding to the zero current situation of equilibrium. That is the concept of overpotential (η). Overpotential related current densities to deviations of electric potential from values when the interface was at equilibrium, i.e. η was the current provoking quantity. The thermodynamic view that equilibrium was disturbed *by* the passage of electrons across the interface was finally laid to rest.

This idea of overpotential had been earlier implied by Butler in 1924 and explicitly stated by Volmer and Erdey-Gruz in 1930. However in Russia this idea had been firmly adopted by Frumkin *et. al.* as early as the 1930's and 1940's. Electrochemistry became more structural and kinetic in attitude and electrochemists began to talk in terms of molecular structure at the interface and the effect of the interfacial field on electron transfer. The kinetic interpretation of equilibrium corresponding to electrons crossing the interface at the same rates in both directions became widespread with the publication of the first book in 1961 written by Vetter on electrode kinetics.

However, the electrochemists who developed these ideas were not very discerning about the type of electron transfer; they assumed classical electron emissions where electrons were climbing over barriers to get in and out of electronically conducting phases. In the 1960's electrochemists, considering what types of electron transfer would correspond to the ranges of rates of charge transfer observed at the metal/solution interfaces, found that classical electron emissions did not explain the differences. The theory of classical electron emission was producing rates that were many orders of magnitude smaller than those experimentally observed. Electron transfer was therefore begun to be thought of as being quantum mechanical, where the electron 'tunnelled' through the interface into or out of the electrode. This quantum mechanical approach was in fact first published by Gurney in 1931 [38].

Today the importance of electron transfer and its kinetic treatment is well established and it is possible to measure the rate at which electrons transfer across the interface. Electron transfer rates for several redox couples have been calculated in recent years [39-47]. A basic understanding of the electron transfer process has led to the development of materials such as semiconductors [29-31] which represent one of the largest advances in modern electrochemistry, and the characteristics of semiconductors are of great practical and technological importance [48-50]. This knowledge of electron transfer has also led to a much greater understanding of biological processes [6-10]. It has been suggested that molecular electron transfer is vital in the growth of cancerous cells [51], as well as in the biological regulation of organisms' defence. There are many other processes [52] linked with electrochemical reactions including photosynthesis, nerve excitation, blood coagulation, vision, smell,

thyroid gland function as well as the origin of the biological potential etc. The basic knowledge of the electron transfer process has also led to a greater understanding of the kinetics and mechanisms of biological phenomena such as nerve impulse conduction, muscle contraction, photosynthesis, energy conversion and storage, effects of hormones and drugs, clotting of blood and many others [52].

Although the tunnelling process in electron transfer is quite well understood, the parameters influencing the rates of electron transfer are not so well understood. Many theories have been put forward to try and explain possible influences on electron transfer and although substantial progress has been made, much remains to be done. Investigation into these influences is becoming a vast research field in itself.

An important factor controlling the rate of electron transfer is the nature of the solvent in which the redox couple is dissolved. Attempts to understand the influence of the solvent have been limited by the solvent characteristics, for example high resistance and slow diffusion in a solvent can hamper any electrochemical measurements made in conventional three electrode cells where the working electrode is of normal dimensions. These problems have recently been overcome by probably the greatest advance in electrochemical techniques in recent times: the development of the ultramicroelectrode by Fleischmann *et. al.* [53]. An ultramicroelectrode is an electrode with at least one dimension small enough that its properties are a function of its size and most ultramicroelectrodes have radii in the range 0.5-25μm. There are many different forms of ultramicroelectrode for example disk, hemisphere, band and ring etc. Due to the reduction in size of the electrode ohmic losses that arise from the

resistance of the solvent are much reduced, and mass transport rates to and from the electrode are increased due to non-planar diffusion. This development has allowed investigations in electrochemistry that were previously thought to be impossible.

1.4 Aims of Thesis

Shedding light on the factors influencing electron transfer is a difficult task and the work presented in this thesis tries to achieve this goal. The rates of electron transfer for the $Fe^{3+/2+}$ redox couple in the presence of the trifluoromethane sulphonate (triflate) anion has been studied in the following media: Acetonitrile (ACN), propylene carbonate (PC), tetrahydrofuran (THF), dimethylsulphonate (DMSO) dimethylformamide (DMF), poly(ethylene oxide) (PEO) and tetraethyleneglycol dimethylether (tetramer).

In order to understand how the solvent contributes to electron transfer with such a couple these media differ in their donor number, polarity, permittivity and structure. By studying the effects of concentration and temperature on the standard apparent rate constant (k_{sh}) in each medium, it is hoped that the major parameters influencing electron transfer may be identified. A second but important objective is the development of a better understanding of redox reactions in solid polymer electrolytes. This has necessitated the development of a new technique: ac impedance spectroscopy at an ultramicroelectrode.

REFERENCES

1 A.T. Kuhn (ed.), *Techniques in electrochemistry, corrosion an metal finishing - a handbook,* Wiley, London, 1987

2 C.J. Rands in *Modern bioelectrochemistry* eds. F. Gutmann and H. Keyser, Plenum, New York, 1986.

3 J.P Hoare & M.L. Laboda in *Modern bioelectrochemistry* eds. F. Gutmann and H. Keyser, Plenum, New York, 1986

4 A.F. Sammells, *J. Chem. Ed.*, 60, 320, 1983

5 M. Hayes, *Chem. Brit.*, 22, 1101, 1986

6 S. Srinivasan, Yu.A. Chizmadzehav , J.O'M. Bockris, B.E. Conway & E. Yeager, (eds.), *Comprehensive treatise of electrochemistry,* Plenum, New York, vol. 10, 1985

7 G. Milazzo (ed.), *Topics in bioelectrochemistry and bioenergetics,* Wiley, 1978

8 F. Gutmann & H. Keyser (ed.), *Modern bioelectrochemistry,* Plenum, New York, 1986

9 A.P.F. Turner, I. Karubi & G.S. Wilson (eds.), *Biosensors, fundamentals and applications,* Oxford University Press, 1987

10 G. Milazzo et.al., *Experientia,* 36, 1243, 1980

11 A.E.G. Cass (ed.), *Biosensors: a practical approach,* IRL Press, Oxford, 1990

12 J.P Gabano, ed. *Lithium Batteries,* Academic Press, 1983

13 A.M. Christie, *Thesis for PhD.*, University of St. Andrews, Scotland, 1995

14 E. Long *Thesis for PhD.*, 1993, Liverpool University

15 C.A. Vincent, *Pro. Solid State Chem.*, 17, 145, 1987

16 *Polymer Electrolyte Reviews*, vols 1 & 2 (Edited by C.A. Vincent and J.R MacCallum), Elsevier Applied Science, London and New York 1991

17 M.H. Cohen & D. Turnbull, *J. Chem. Phys.*, 31(5), 1164, 1959

18 J.H. Gibbs & E.A. DiMarzio, *J. Chem. Phys.*, 43(1), 373, 1958

19 G. Adam & J.H. Gibbs, *J. Chem. Phys.*, 43(1), 139, 1965

20 *Polymer Electrolyte Reviews* 1, eds. J.R. MacCallum and C.A. Vincent, Elsevier Applied Science.

21 S.D. Druger, M.A. Ratner & A. Nitzan, *Solid State Ionics*, 9&10, 1115, 1983

22 M.B. Armand, J.M. Chabagno & M.J. Duclot, *Fast Ion Transport in Solids*, Ed. P. Vashista, J. Mundy & G.K. Shenoy, North Holland and New York, 1978

23 G.S. Fulcher, *J. Amer. Chem. Soc.*, 8, 3339, 1925

24 *Solid Polymer Electrolytes*, F.M. Gray, VCH, New York 1991

25 H.L.F. von Helmholtz, *Ann. Physik*, 89, 211, 1853; 7, 337, 1879

26 E.S. Saidi, *Thesis for PhD.*, Heriot-Watt, Scotland, 1993

27 P.G. Bruce, E.S. McGregor & C.A. Vincent, in *Second International Symposium on Polymer Electrolytes* (ed. B. Scrosati) Elsevier, London, pp357, 1990

28 A.F. Silva ed., *Trends in interfacial electrochemistry,* Proceedings of NATO, A51, 1984, Reidel Dordecht, 1985

29 S.R. Morrison, *Electrochemistry at semiconductor and oxidised metal electrodes*, Plenum, New York, 1980

30 K. Uosaki & H. Kita, *Modern aspects of electrochemistry*, Plenum, New York, ed. R.E. White, J.O'M. Bockris & B.E. Conway, 18, 1, 1986

31 A. Hamnett, in *Comprehensive chemical kinetics*, ed. R.G. Compton, Elsevier, Amsterdam, 27, chapt. 2, 1987

32 G. Gouy, *Compt.Rend.*, 149, 654, 1910; D.L. Chapman, *Phil.* Mag., 25, 475, 1913

33 O. Stern, *Z. Elektrochem.*, 30, 508, 1924

34 D.C. Grahame, *Chem. Rev.*, 41, 441, 1947

35 B.B. Damaskin & A.N. Frumkin, *Electrochim. Acta*, 19, 173, 1974

36 S. Trasatti, *Trends in interfacial electrochemistry*, Proceedings of NATO ASI, pp 25-48, 1984

37 R. Parsons, *Chem. Rev.*, 90, 813, 1990

38 Gurney, R.W., *Proc. Roy. Soc.*, London A 134, 137, 1931

39 J.H. Espenson & J.R. Pladziewkz, *J. Phys. Chem.*, 75, 1971

40 W.R. Fawcett & M. Opallo, *J. Electroanal. Chem.*, 331, 815, 1992

41 W.F. Kinard & R.H. Phile, *J. Electroanal. Chem.*, 25, 373, 1970

42 R.W. Murray & C.R. Leidner, *J.A.C.S.*, 106, 1606, 1984

43 R.W. Murray, T.T. Wooster, Longmire & M. Watanabe, *J. Phys. Chem.*, 95, 5315, 1991

44 J.R. Pladziewicz & J.H. Espenson, *J.A.C.S.*, 95, 56, 1973

45 S. Pons, J.W. Pons, J. Daschback & D. Blackwood, *J. Electroanal. Chem.*, 237, 269, 1987

46 I. Ruff, V.J. Fredrich, K. Demeter & K. Csulag, *J. Phys. Chem.*, 75, 1971

47 M.J. Weaver, T.T.T. Li & C.H. Brabaker jr., *J.A.C.S.*, 104, 2381, 1982

48 Yu.V. Pleskov & Yu.Ya. Farevivh, *Semiconductor photoelectrochemistry*, Plenum, New York, 1986

49 S.U.M. Khan & J.O'M. Bockris, *Modern aspects of electrochemistry*, Plenum, New York, ed. R.E. White, J.O'M. Bockris & B.E. Conway, 14, 151, 1982

50 Yu.V. Pleskov, *Solar energy conversion. A photochemical approach*, Springer-Verlag, Berlin, 1990

51 A. Szent-Gyorgyi, *Science*, 161, 988, 1968

52 H. Berg in *Transient techniques in electrochemistry*, (D.D. Macdonald), Plenum Press, New York, 1977

53 M. Fleischmann, S. Pons, D.R. Rolison & P.P, Schmidt eds., *Ultramicroelectrodes*, Datatech Systems, Inc., 1987

CHAPTER 2

EXPERIMENTAL PROCEDURES

2.1 Preparation and Purification of Salts

2.1.1 Lithium trifluoromethane sulphonate

$$Li_2CO_3 + 2CF_3SO_3H \rightarrow 2LiCF_3SO_3 + H_2O + CO_2$$

The appropriate quantity of Li_2CO_3 (Aldrich 99+%) was suspended in 100ml of distilled water. To this was added 10g of neat trifluoromethane sulphonic acid (triflic acid) (Aldrich 99+ %).The solution was stirred for 4 hours until all the carbonate had been digested by the triflic acid. The resulting solution was filtered through a fine sinter and the bulk water removed from the filtrate by rotary evaporation, yielding the hydrated salt. The hydrated salt was heated under vacuum at 150°C for 24 hours to produce the anhydrous salt, which was then directly transferred to an mBraun dry box (argon atmosphere) after slow cooling.

2.1.2 Iron (II) trifluoromethane sulphonate

$$Fe + 2CF_3SO_3H \rightarrow Fe(CF_3SO_3)_2 + H_2\uparrow$$

An aqueous solution of trifluoromethane sulphonic acid (10g of neat acid in 100ml of distilled water) was slowly added to an excess of iron filings. The mixture was stirred

until a pale blue solution was obtained (approximately 6 hours). The resulting solution was then filtered through a fine sinter to remove any insoluble iron oxides or hydroxides that may have formed. The bulk water was removed from the filtrate by rotary evaporation, and an hydrated salt was collected. The hydrated salt was dissolved in dried acetonitrile (see section 2.2.2) and again the bulk solvent was removed from the salt via rotary evaporation. This process was repeated twice to remove water soluble impurities. The resulting salt was dried under vacuum at 80°C for 48 hours to produce the anhydrous salt. The salt was stored in an argon filled dry box after cooling.

2.1.3 Iron (III) trifluoromethane sulphonate

$$Fe(CF_3SO_3)_2 + CF_3SO_3^- + H_2O_2 + 3H^+ \rightarrow Fe(CF_3SO_3)_3 + 2H_2O + H^+$$

Iron (II) triflate (iron II trifluoromethane sulphonate) was produced as in 2.1.2 but in the presence of excess acid. The iron (II) triflate was then oxidised to iron (III) triflate by adding hydrogen peroxide to the acidic solution of the iron (II) salt. The addition of the hydrogen peroxide solution was carried out drop-wise with constant stirring. The acidity of the solution was monitored at all times, as hydrogen peroxide oxidation reactions need to be carried out under acidic conditions to prevent the formation of hydroxides and hydroxide bridged gels. The bulk of the solvent was removed by rotary evaporation and the salt dried at 80°C under vacuum for 48 hours then transferred directly to a dry box.

2.1.4 Lithium perchlorate

Lithium perchlorate ($LiClO_4$, Aldrich 99%+) was dried by heating the salt at 160°C for 48 hours under vacuum. After cooling slowly, the dry sample was transferred to an argon filled glove box for storage.

2.1.5 Lithium hexafluoroarsenate

Lithium hexafluoroarsenate (FMC company, electrochemical grade, 'Lectro Salt' anhydrous) was used as received.

2.1.6 Tetrabutylammonium perchlorate

Tetrabutylammonium perchlorate ($C_{16}H_{36}NClO_4$, Fluka puriss electrochemical grade) was dried for 72 hours under vacuum at 80°C, and after cooling transferred to and stored in a dry box.

2.1.7 Tetraethylammonium tetrafluoroborate

The salt ($(C_2H_5)_4N(BF_4)$, Fluka, puriss > 99%) was dried under vacuum at 80°C for 72 hours, then transferred to dry box after cooling.

2.1.8 Tetraethylammonium hexafluorophosphate

The salt ($(C_2H_5)_4N(PF_6)$, Fluka, purum >98%) was dried for 72 hours under vacuum at 80°C and stored under argon in a dry box after cooling.

2.1.9 Poly(ethylene oxide)

The polymer (Aldrich, $(-CH_2CH_2O-)_n$ ave. molar mass 4 million) was dried under vacuum at 50°C for 48 hours and stored under argon in a dry box after cooling.

2.2 Solvent Purification

2.2.1 Tetraethyleneglycol dimethylether and Propylene carbonate

Tetraethyleneglycol dimethylether [$CH_3(OCH_2CH_2)_4OCH_3$], and propylene carbonate [$C_4H_5O_3$], abbreviated in this thesis to tetramer and PC respectively (both Aldrich, 99%) were purified by vacuum distillation at 10^{-3} mbar using Fischer HMS 500C distillation apparatus with 90 theoretical plates (figure 2.1).

SOLVENT	Bath temp. ^{o}C	Mantle temp. ^{o}C
Tetramer	147	90
Propylene Carbonate	120	57

Table 1 Temperature settings for Fischer HMS 500C when distilling solvents

After refluxing for at least 1 hour, the first 20% cut was collected at a rate of ca. 25cm^3hr^{-1} Only the middle 60% cut was kept for use and transferred to a glove box.

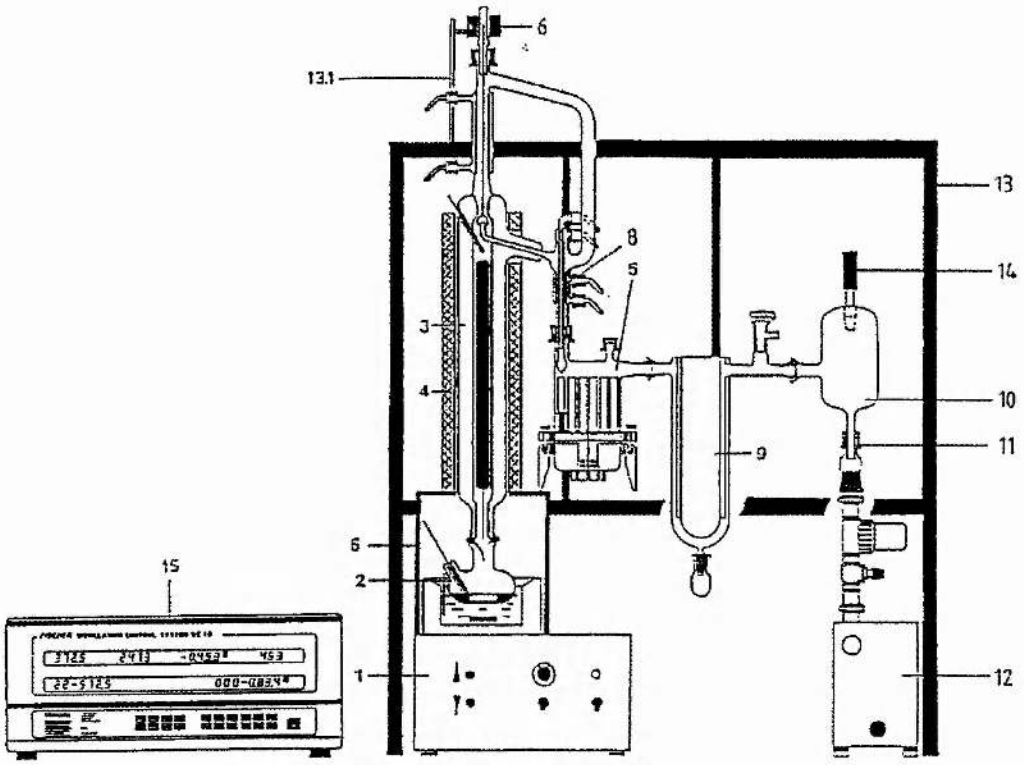

Figure 2.1. General view of the Fischer distillation apparatus HMS 500C.

Legend for Figure 2.1:

1	Oil bath	10	Buffer vessel
2	Distillation flask	11	Vacuum line
3	SPALTROHR™ column	12	Vacuum pump
4	Heating mantle	13	Mounting frame
5	Fraction collector	13.1	Support rod
6	Solenoid coil	14	Vacuum sensor
8	Distillate cooler	15	Distillation control device
9	Cold trap		

The purity of the solvents collected was tested by cyclic voltammetry at an ultramicroelectrode. Previous attempts [1] at purification of PC reported difficulties in removing the commonly found impurity 1,2 propanediol sometimes produced during distillation. 1,2 propanediol is formed by base catalysed ring cleavage and hydrolysis of the cyclic carbonate during distillation. The presence of this impurity, and water results in a cathodic peak at +1.4V vs. Li^+/Li which increases in magnitude with increased concentration of each impurity. Figure 2.2 shows the cyclic voltammograms obtained for PC distilled using the Fischer HMS 500C apparatus with 90 theoretical plates (a), PC distilled using 33 theoretical plates (b) and PC as received (c). The second solvent to be distilled was tetramer the cyclic voltammogram of which is shown in figure 2.3. As can be seen from figures 2.2 and 2.3 the solvents produced in this way are purer than any other previously reported [1]. Neither of these solvents are electrochemically active in the potential range of the investigations carried out in this thesis.

2.2.2 Acetonitrile , Dimethyl sulphoxide and Dimethyl formamide

Small traces of water remaining in the as received solvents, despite being specified as anhydrous, {(CH_3CN, Aldrich, anhydrous, 99+%); ($(CH_3)_2SO$, Aldrich, anhydrous, 99+%); ($HCON(CH_3)_2$, Aldrich, anhydrous, 99+%)} were removed by storing over sieves for 24 hours. The sieves had been dried under vacuum at 350°C for 72 hours before being cooled and transferred to a glove box.

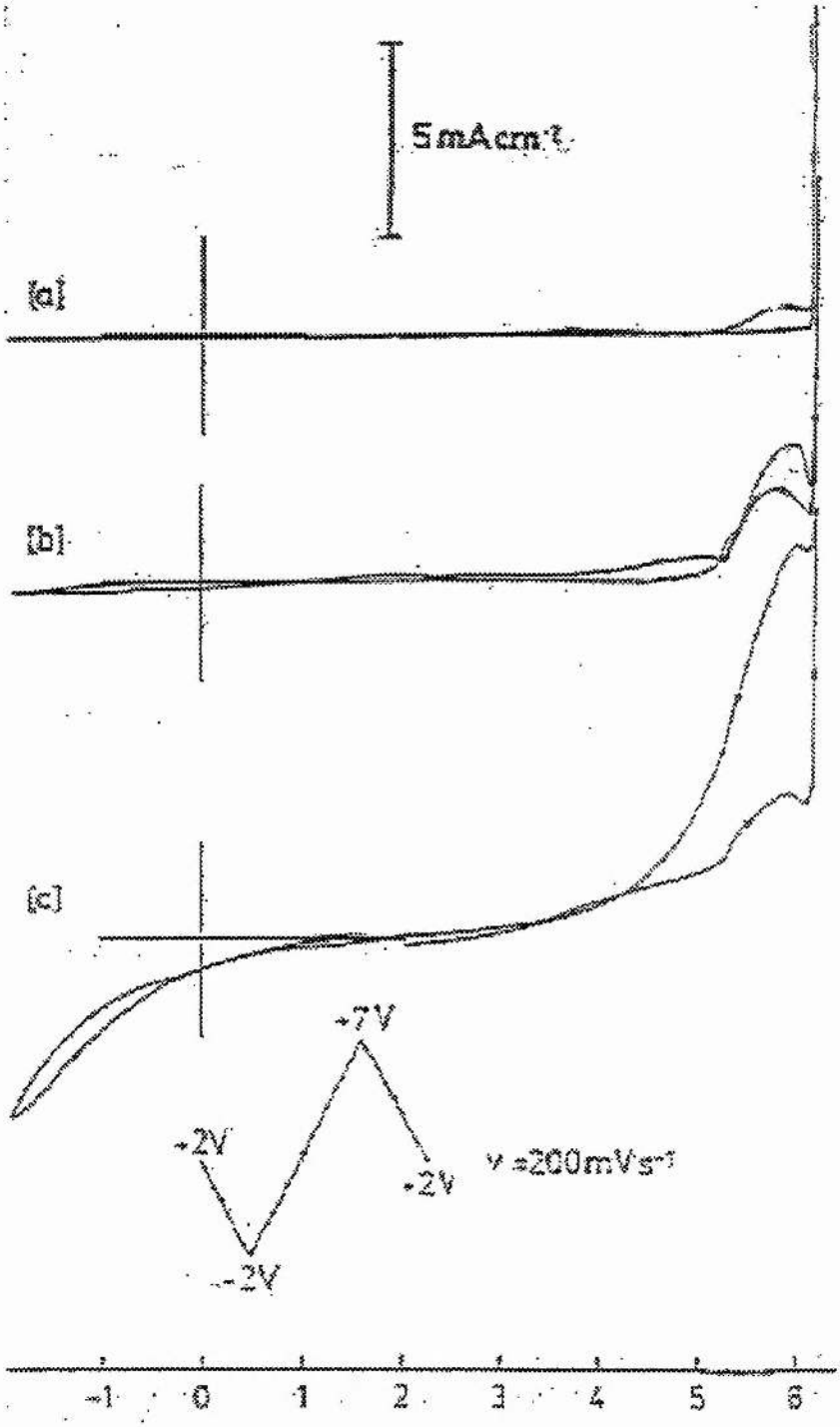

Figure 2.2 Cyclic voltammograms for PC distilled using 90 theoretical plates (a), PC distilled using 33 theoretical plates (b) and PC as received (c).

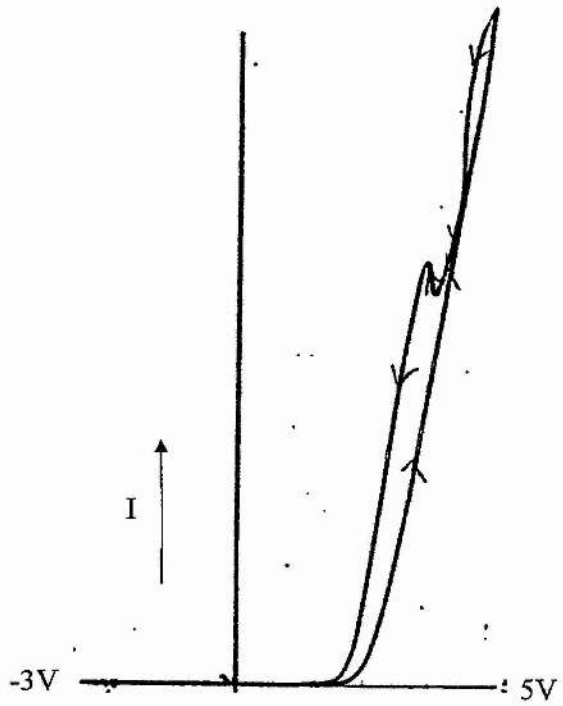

Figure 2.3 Cyclic voltammogram at a 25μm diameter Pt electrode for pure tetramer vs. Li^+/Li

2.2.3 Tetrahydrofuran

Tetrahydrofuran {$(CH_2)_4O$, Aldrich, anhydrous, 99.9%} was refluxed at 65-67°C over fresh lithium under dynamic vacuum. Benzophenone was added as an indicator, changing the colour of the refluxed reaction mixture to a deep blue when the water content was reduced to below 10ppm. The middle 60% cut of the solvent was collected and transferred to a glove box for storage. The storage vessel was blacked out as THF degrades in sunlight.

2.3 Preparation of Polymer Electrolytes

All preparations were carried out in an argon filled dry box.

2.3.1 Cryogrinding [2]

The appropriate dried salt was ground with a pestle and mortar, and a mixture of this and the PEO was transferred to a stainless steel tube containing ball bearings. The tube was sealed using a rubber bung and removed from the dry box. The whole system was then shaken for 20 minutes to half an hour with the tube dipped into a bath of liquid nitrogen. At liquid nitrogen temperatures the polymer becomes brittle and fractures under the action of the ball bearings. In this way an intimate, homogeneous mixture of the salt and polymer was produced. When grinding was complete the system was left to equilibrate to room temperature for 4 hours before being transferred back into the dry box. A variety of compositions of the mixture were produced by altering the proportions of salt and polymer (figure 2.4).

2.3.2 Hot Pressing

A small sample of the cryoground mixture (approx. 50 mg) was pressed at 5 tons for 30 seconds between two Teflon discs in a 13mm pellet press (figure 2.5). Under no applied pressure and using a band heater the sample was then heated to 80°C. After 4 hours of heating the sample was cooled to 35°C at which point a 2 ton pressure was applied and the sample was allowed to cool to room temperature over night. The films produced were about 1mm thick, but this thickness could be altered by using more or less sample in the first instance.

2.4 Mbraun Glove Box

The Mbraun glove box provides an inert atmosphere for all preparations that require a water and oxygen free atmosphere. Typical water levels are less than 0.05ppm and oxygen levels less than 0.1ppm. The atmosphere of the box is argon which is constantly circulated and replaced by means of a direct line to fresh cylinders of argon. The water and oxygen levels are kept to a minimum by means of sieves and copper catalysts. The sieves and catalysts are regenerated every two weeks and the box is purged with argon. Samples and apparatus entering the box do so through ports that are evacuated and then flushed with argon to remove any residual water and oxygen on their surfaces which also helps to maintain the atmosphere within the box. All polymer electrolyte preparation, including hot pressing is carried out within the box, as is the dissolution of salts for the solution systems. All prepared cells are kept within the box and electrochemical contact with these cells is via leads connected to junctions that are in turn connected to cables outside the box. This allows all electrochemical systems to remain water and oxygen free throughout all investigations.

2.5 Instrumentation

2.5.1 Polymer Cell Design

A two electrode cell was employed for electrochemical measurements on the solid polymer electrolyte (figure 2.6). The working electrode was a platinum disk of 12.5μm radius and the counter electrode a platinum disk of area ca.1.3 cm^2. The

currents measured in these ultramicroelectrode studies were sufficiently small (typically less than 1nA) such that the platinum counter electrode also acts as a very satisfactory reference i.e. there is no need for a third electrode. The cell was then placed inside a Faraday cage before measurements were carried out (figure 2.7).

2.5.2 Liquid Cell Design

2.5.2.1 Three electrode cell configuration

A schematic representation of the cell configuration is shown in figure 2.8. The counter electrode is a platinum gauze (of area $\approx$ 1.3 cm^2) placed directly into the solution. The working electrode is a 2mm diameter platinum disc. The reference electrode consisted of a glass tube closed at the end by a Vicor glass frit attached with heat shrinking Teflon. This glass tube contained a sample of the solution under investigation with a platinum wire placed into this. For equimolar concentrations of the redox species under investigation, the redox couple acts as its own reference with this type of reference electrode. The positioning of the working and reference electrodes within the cell is crucial. Where possible (especially for cyclic voltammetry) the tip of the reference electrode should be placed directly beneath that of the working electrode and in close proximity to it. This reduces the effects of iR drop across the cell.

2.5.2.2 Ultramicroelectrode cell configuration

The cell configuration is the same as for the 3 electrode system, except that the counter electrode also acts as a reference electrode i.e. there is no need for the third electrode as the currents measured in the ultramicroelectrode are sufficiently small (typically less than 1nA). The working electrode is a 25μm diameter platinum wire.

2.5.3 Electrode Polishing

All electrodes were polished with alumina of decreasing sizes (1μm, 0.3μm and 0.05μm) suspended in water on a polishing cloth (Beuhler), followed by rinsing in distilled water and thorough drying.

2.5.4 AC Impedance Spectroscopy

2.5.4.1 At an ultramicroelectrode

Ac measurements were carried out using the apparatus shown in figure 2.9. The cell was enclosed in a Faraday cage (figure 2.7) and the working electrode was connected to the input of an EG&G PAR preamplifier 181 the output of which was connected to the input of a Solatron 1255 Frequency Response Analyser. The generator output of the 1255 was connected to both the voltage input and the counter electrode. Coaxial cables are used to connect the EG&G preamplifier to the 1255 and to the cell, the sheaths of the coaxial cables are grounded, as the currents measured are small and shielding from outside interference is necessary. Measurements were under the

control of an IBM compatible PC. An ac signal of between 5 and 10 mV rms was employed in all measurements . The frequency range was 250kHz to 0.01 Hz. Data were analysed using a modified version of the complex non-linear least squares (CNLS) fitting program written by MacDonald et.al.[3].

2.5.4.2 Standard three electrode system

A Solatron 1255 Frequency Response Analyser and a 1286 Electrochemical interface were employed, under the control of an IBM compatible PC. An ac signal of between 5 and 10 mV rms was applied to the cell and measurements were taken in the frequency range 65kHz to 0.01Hz. The cell was situated inside a Faraday cage and all connections were made by grounded coaxial cables. Data were analysed in the first instance using a non-linear least squares (CNLS) fitting program written by Boukamp [4] and then by a modified version of the CNLS fitting program written by MacDonald et.al.[3]

2.5.5 Cyclic Voltammetry

A Solatron 1286 potentiostat controlled by a PC-486 under software control (*Corrware)* was used to collect and present cyclic voltammetry data.

2.5.6 Differential Scanning Calorimetry

All DSC scans were performed on a Perkin Elmer DSC7 differential scanning calorimeter, a 3700 data station and a TAC 7/3 instrument controller. Cryoground polymer electrolyte samples were sealed into small aluminium sample pans inside the

glove box before being transferred to the calorimeter. A sealed pan containing argon acted as a reference. For sub ambient operations, a liquid nitrogen cooler was used.

2.5.7 Powder X-ray Diffraction

Powder X-ray diffraction data was collected on a Stoe STADI/P high resolution system equipped with a linear position sensitive detector covering ~ 6° in 2θ and employing Ge-monochromatised Cu - $K\alpha_1$ radiation. Data was collected in steps of 0.02° in 2θ. The system was equipped with a furnace for obtaining data at elevated temperatures.

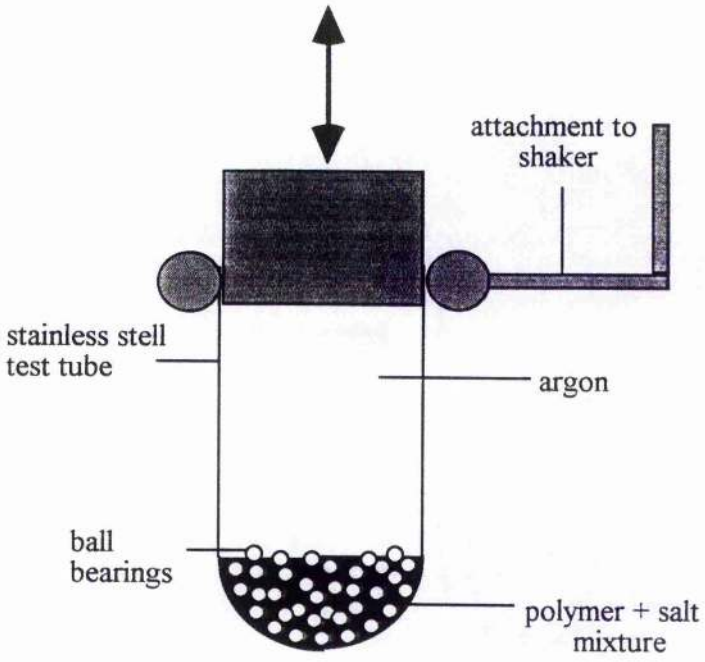

Figure 2.4 Apparatus for cryogrinding

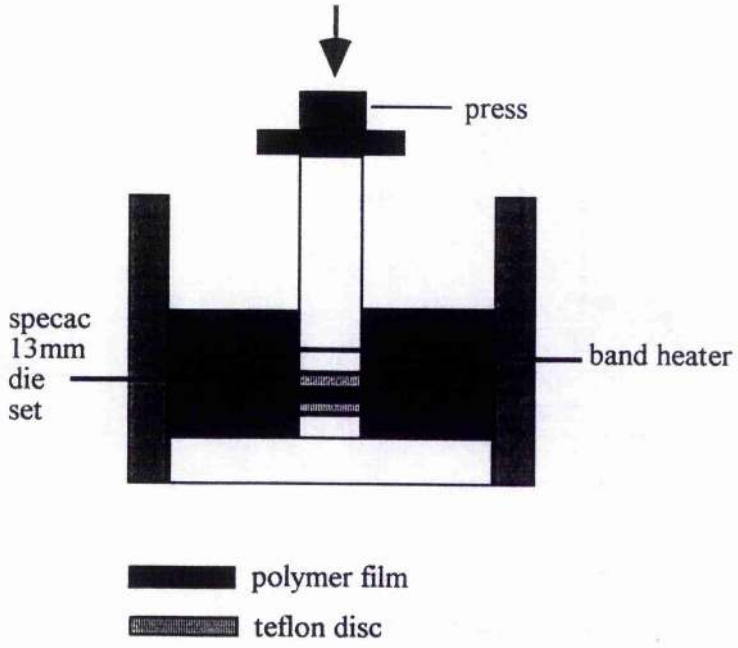

Figure 2.5. Apparatus for hot pressing

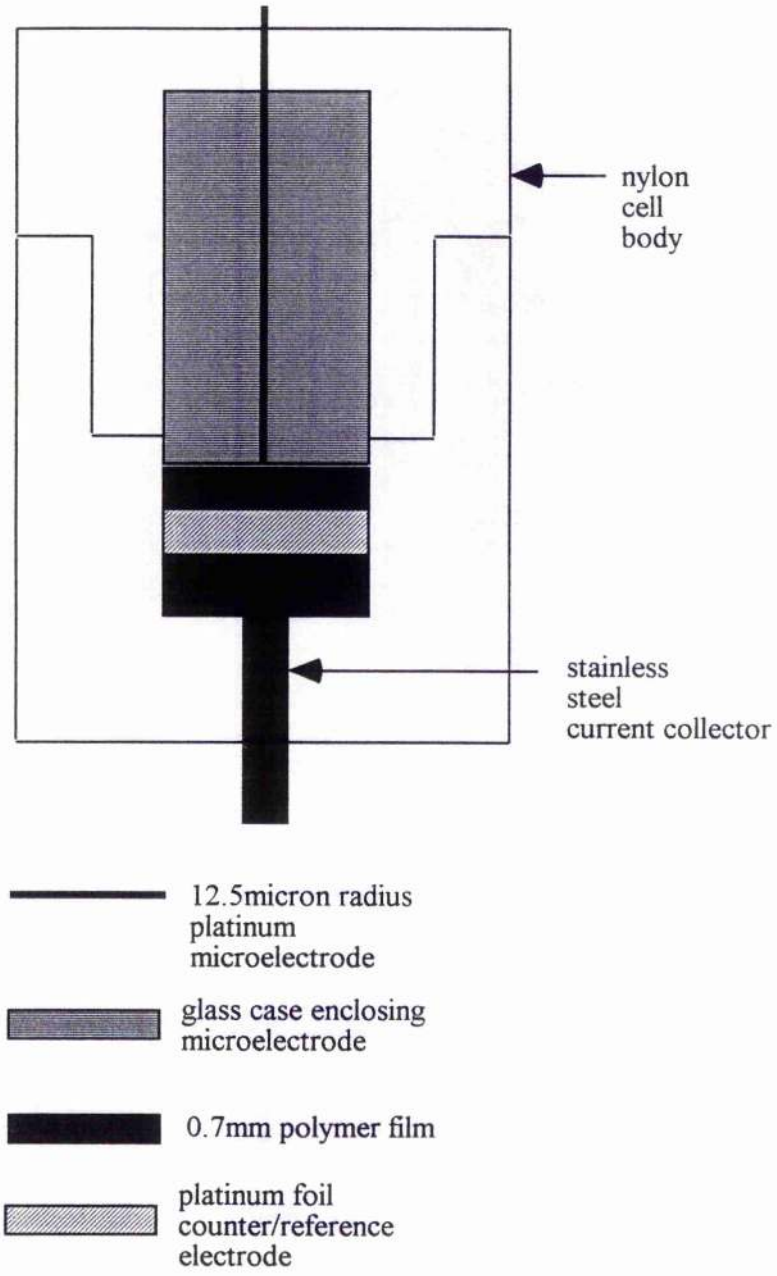

Figure 2.6 Two electrode solid polymer cell

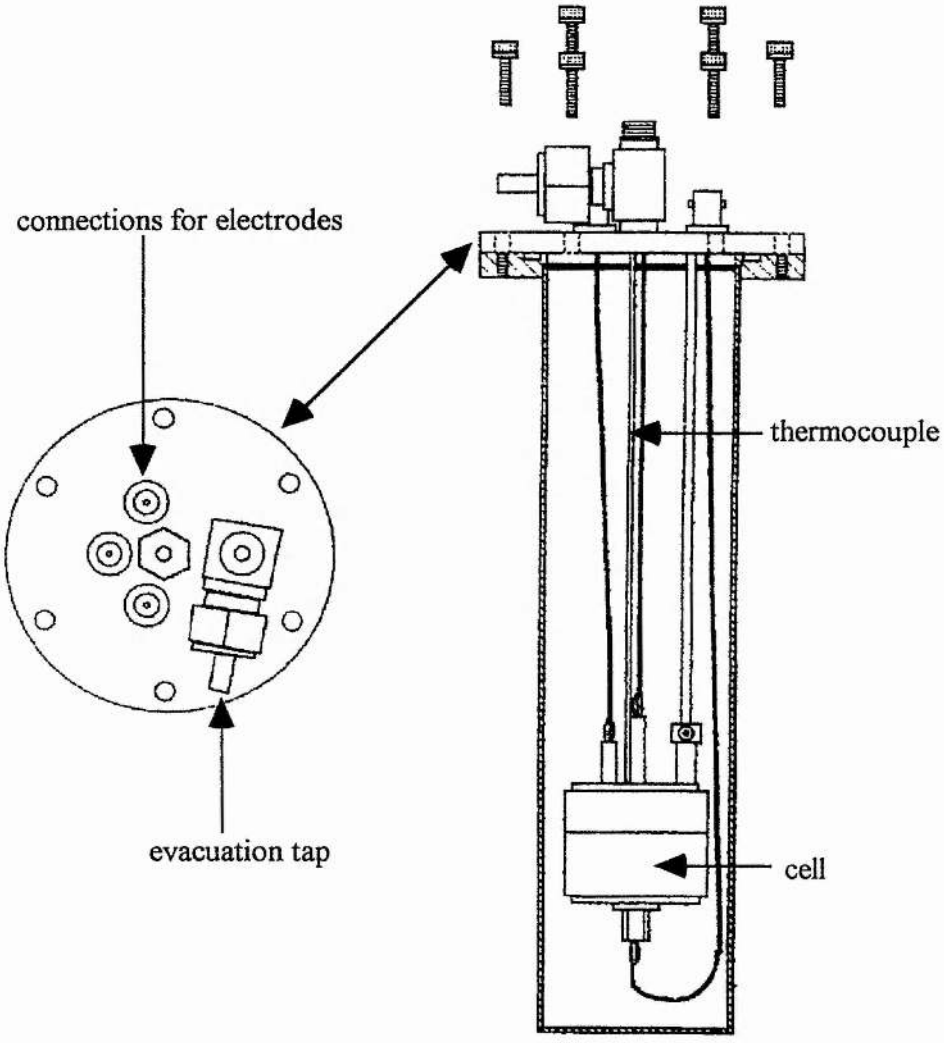

Figure 2.7 Polymer cell inside Faraday cage

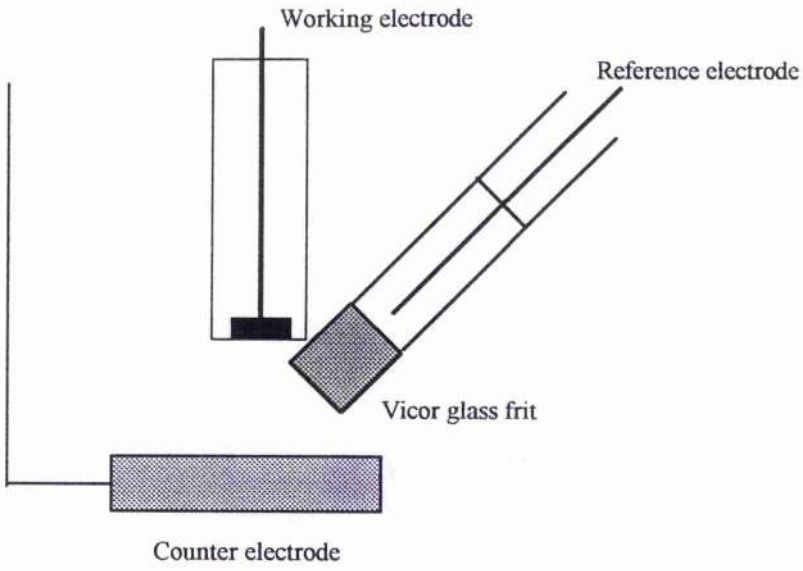

Figure 2.8 Schematic diagram of electrode configuration in liquid cell

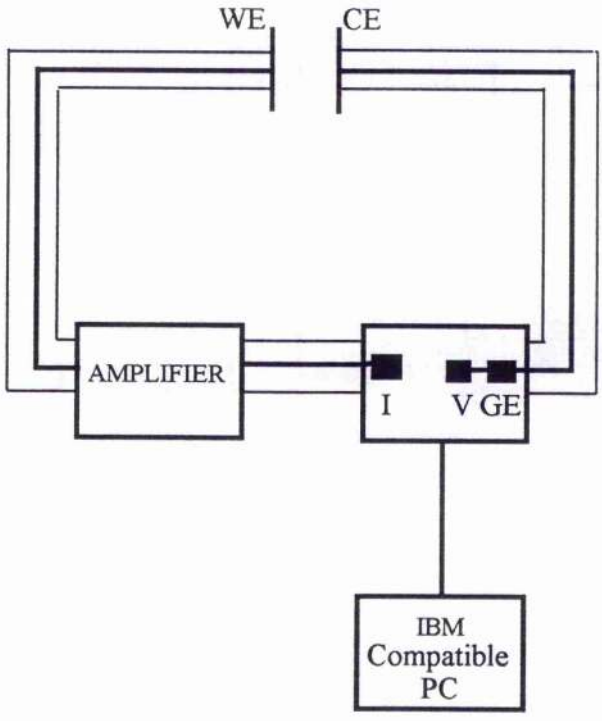

Figure 2.9. Apparatus used for ac impedance at ultramicroelectrodes in solid polymer cells

REFERENCES

1 S.A. Campbell, C. Bowes & R.S. McMillan *J. Electroanal. Chem.*, 284, 195, 1990

2 J.R. MacCallum, F.M. Gray & C.A. Vincent *Solid State Ionics* 18/19, 252, 1986

3 J.R. Macdonald, J. Scoonman & A.P. Lehner, *J. Electroanal. Chem.*, 131, 77, 1982

4 B. Boukamp, *Equivalent Circuit Program*, University of Twente, 1988

CHAPTER 3

Electrochemical Methods

3.1 Cyclic Voltammetry

3.1.1 Introduction

Cyclic voltammetry is often used in the initial study of electroactive species; the data is represented in a form which allows rapid, qualitative interpretation without recourse to detailed calculation. In a typical qualitative study it is usual to record voltammograms over a wide range of sweep rates and potential limits; there may be several peaks and by looking at how these change as the potential limits and sweep rates are varied, and by noting the differences between the first and subsequent cycles, it is possible to determine how the processes represented by the peaks are related. From the sweep rate dependence of the peak height the role of adsorption, diffusion and coupled homogeneous chemical reactions may be identified. Kinetic data however, can only be accurately obtained from an analysis of the first sweep. In a cyclic voltammogram the forward and reverse sweep rates, ν_{anodic} and $\nu_{cathodic}$, are generally chosen to be equal, and this is the case in the present chapter and indeed the entire thesis.

A cyclic voltammogram is a potential - time waveform, and the i(current)-E(potential) response is recorded. The potential is swept through the potential range where an

electrode reaction occurs before the scan direction is reversed in order to define whether the product of the electron transfer is stable, or the reaction intermediates or the final product are electroactive. The variables are the potential limits E_1, E_2 and E_3, the direction of the initial sweep and the potential scan rate, ν. Such a potential - time waveform is shown below:

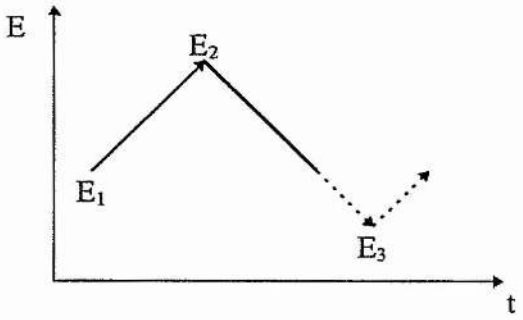

The potential limits define the electrode reactions that are allowed to occur. The experiment is often commenced at a potential where there is no electrode reaction i.e. i=0. To study oxidation reactions the potential is scanned in the positive direction and to study reduction reactions the potential is scanned in the negative direction. The electrode reaction processes observed in a cyclic voltammogram depend on the sweep rate. Slow sweep rates allow slow processes to be observed whilst faster scan rates allow fast processes to be observed.

Several types of systems are studied using cyclic voltammetry:

Reversible systems are ones in which the rate determining step is that of diffusion of the electroactive species to and from the electrode, and the kinetics of the couple O/R

(where O is the oxidised and R the reduced species) are sufficiently fast so that the electron transfer process appears to be in equilibrium at the surface of the electrode;

Irreversible systems are ones where the kinetics of the couple O/R are poor, the rate of electron transfer is insufficient to maintain Nernstian equilibrium at the surface and therefore the rate determining step of the reaction is electron transfer. It is necessary to apply a higher potential than for a reversible reaction in order to overcome the activation barrier and allow the reaction to occur. This additional potential is called the overpotential (η);

It is quite common for a process that is reversible at low sweep rates to become irreversible at higher ones after having passed through a region known as quasi-reversible at intermediate values. In the quasi-reversible systems the kinetics of both the oxidation and reduction reactions make a contribution to the observed currents.

In thermodynamics, however, a reversible change is a change that can be reversed by an infinitesimal modification of a variable; a system is said to be in equilibrium with its surroundings if an infinitesimal change in the conditions in opposite directions results in opposite changes in its state. Each infinitesimal step along a reversible path occurs without dispersing energy chaotically and hence without increasing the entropy. An irreversible process in thermodynamics (for example cooling to the temperature of the surroundings) occurs spontaneously and is therefore accompanied by an increase in entropy.

3.1.2 Reversible Systems

A typical cyclic voltammogram (CV) for a reversible process is shown in figure 3.1, where O and R are soluble species. The ratio of surface concentrations of O and R is given by the Nernst equation, and hence as the potential is swept cathodically the surface concentration of reactant must decrease, and the concentration gradient then increases. From *Fick's first law*:

$$\frac{I}{nF} = -D_O\left(\frac{dc_O}{dx}\right)_{x=0}$$

or

$$\frac{I}{nF} = D_R\left(\frac{dc_R}{dx}\right)_{x=0}$$

it is expected that an increase in cathodic current follows. Due to the relaxation effect of diffusion, the concentration gradient now begins to decrease resulting in a corresponding decrease in current.

On reversing the sweep, the product R continues to be formed until the potential reaches the charge transfer equilibrium and begins to reoxidise back to O, with a corresponding anodic current flowing. The magnitude of the current increases, as before, until the surface concentration of R is depleted and the current becomes diffusion controlled. Solution of Fick's second law for species O and R, with the relevant experimental boundary conditions, reveals the exact form of the CV for a reversible process. The *Randles-Sevcik equation* shows that under planar diffusion control [1-3], the peak current density is

$$|I_P| = 0.4463nF\left(\frac{nF}{RT}\right)^{1/2} c_i^{\infty} D^{1/2} \nu^{1/2}$$

where I_p is the peak current for either the cathodic or anodic process, ν is the sweep rate and c_i^{∞} is the bulk concentration of species i. Thus, it is evident that a plot of I_p against $\nu^{1/2}$ should be linear and pass through the origin for such a reversible process. The reversible region is generally recognised to have [4]: $k_s \geq 0.3\nu^{1/2}$ cm s^{-1} (where k_s is the standard rate constant of the redox couple).

1.	$\Delta E_p = E_p^A - E_p^C = 59/n$ mV
2.	$\lvert E_p - E_{p/2} \rvert = 59/n$ mV
3.	$\lvert I_p^A / I_p^C \rvert = 1$
4.	$I_p \propto \nu^{1/2}$
5.	E_p is independent of ν
6.	At potentials beyond E_p, $\Gamma^2 \propto t$

Table 3.1 Diagnostic tests for cyclic voltammogram of reversible processes at 25°C.

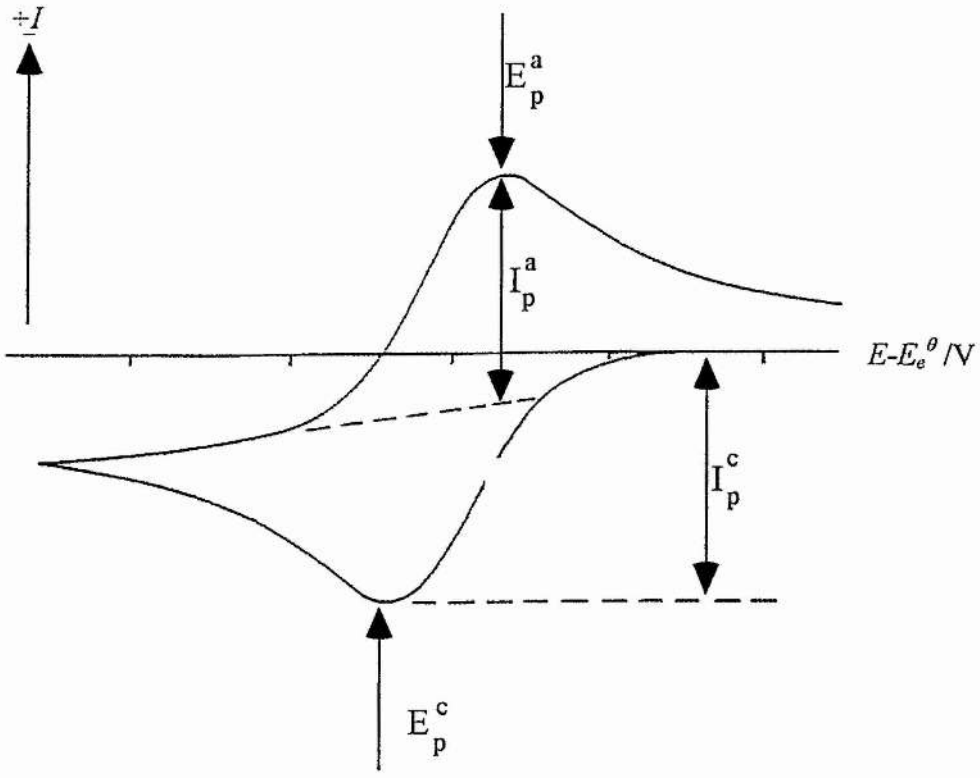

Figure 3.1 Typical cyclic voltammogram for a reversible process, for the reaction $O + e \rightleftharpoons R$. Initially there is only O present in solution before sweeping cathodically.

3.1.3 Irreversible Systems

The solution to Fick's second law for the peak current density of a totally irreversible system is given by [3]

$$| I_p | = 0.282\ [(\pi^{1/2}F^{3/2}) / (RT)^{1/2}]\ n(\alpha_c n_\alpha)^{1/2}\ c_o^{\infty} D_o^{1/2}\ \nu^{1/2}$$

where n_α is the number of electrons transferred up to, and including, the rate determining step. The peak current density is therefore a function of the square root of the sweep rate, as in the reversible case. A reverse peak is absent in a totally irreversible system, although the lack of anodic wave may also be due to a fast following chemical reaction. In the reversible case E_P^C is independent of sweep rate, but for the irreversible case Nicholson & Shain [3] have shown that E_P^C varies with the sweep rate according to:

$$E_P^C = K - \frac{2.3RT}{2\alpha_C n_\alpha F}\log \nu$$

where

$$K = E_e^\theta - \frac{RT}{\alpha_C n_\alpha F}\left\{0.78 - \frac{2.3}{2}\log\left(\frac{\alpha_C n_\alpha FD}{\left(k^\theta\right)^2 RT}\right)\right\}$$

Thus, as the sweep rate increases, the cathodic peak shifts to more negative potentials. The irreversible region is generally recognised to have [4]: $k_s \leq 2 \times 10^{-5}$ $\nu^{1/2}$ cm s^{-1}.

1.	No reverse peak
2.	$I_p^C \propto \nu^{1/2}$
3.	E_p^C shifts $-30/\alpha_C n_\alpha$ mV for each decade increase in ν
4.	$\lvert E_p - E_{p/2} \rvert = (48/\alpha_C n_\alpha)$ mV

Table 3.2 Diagnostic tests for totally irreversible processes at 25°C

3.1.4 Quasi Reversible Systems

Quasi-reversible systems are ones in which the relative rate of the electron transfer with respect to that of mass transport is insufficient to maintain Nernstian equilibrium at the electrode surface. The extent of irreversibilty increases with increasing sweep rate while at the same time there is a decrease in peak current relative to the reversible case and an increasing separation between anodic and cathodic peaks. The quasi-reversible region is generally recognised to have [4] $0.3\nu^{1/2} > k_s > 2 \times 10^{-5}\ \nu^{1/2}$ cm s^{-1}. A plot of I_p as a function of $\nu^{1/2}$ readily shows the change from reversible to quasi reversible and then to irreversible behaviour (figure 3.2).

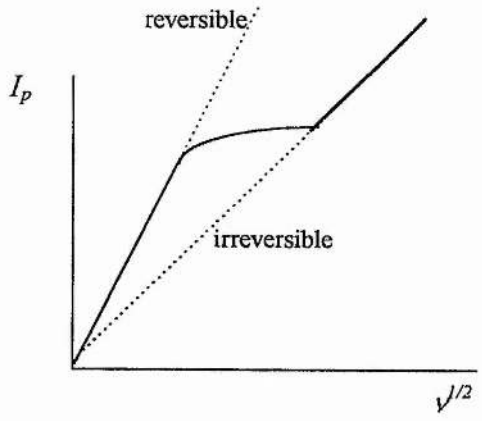

Figure 3.2 Change from reversible, to quasi-reversible, to irreversible behaviour.

Kinetic data such as the rate constant are normally obtained from ΔE_p values [5]. Working curves have been constructed of $n\Delta E_p$ as a function of the variable φ defined by

$$\varphi = \frac{(RT)^{1/2} k^{\theta}}{(nFD\pi v)^{1/2}}$$

By comparing experimental ΔE_p values with the working curve for several sweep rate values the standard rate constant is readily obtained.

1.	$\lvert I_P \rvert$ increases with $v^{1/2}$ but is not proportional to it
2.	$\lvert I_p^A / I_p^C \rvert$ =1 provided $\alpha_C = \alpha_A = 0.5$
3.	ΔE_P is greater than $59/n$ mV and increases with increasing v
4.	E_p^C shifts negatively with increasing v

Table 3.3 Diagnostic tests for quasi-reversible processes at 25°C

3.1.5. Systems with Adsorption

Consider the following reactions for a reversible electron transfer process where both the solution and adsorbed species are electroactive:

$$O_{soln} \rightleftharpoons O_{ads}$$

$$O + ne \rightleftharpoons R$$

$$R_{soln} \rightleftharpoons R_{ads}$$

The voltammogram will exhibit conventionally shaped peaks corresponding to the reaction of the solution species, which may be a simple electron transfer. It will also

exhibit symmetric shaped peaks corresponding to the reactions of the adsorbed species. A strong reactant adsorption gives rise to a post-peak, and a strong product adsorption gives rise to a pre-peak. The separation between the solution and the adsorption peaks reflects the strength of the adsorption, i.e. as the adsorption reduces so to does the peak separation. For weak adsorbates the peak separation is not discernible, but the voltammogram is distorted as shown in figure 3.3 [6].

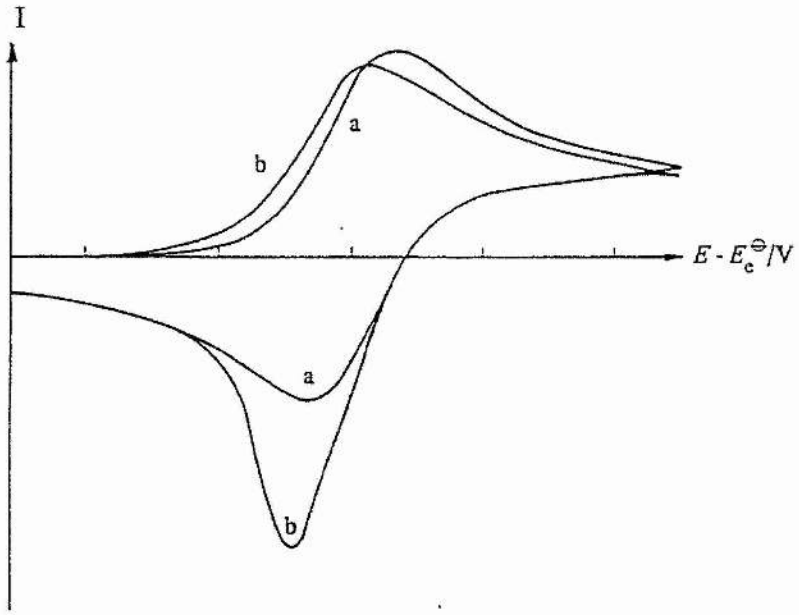

Figure 3.3 Cyclic voltammogram for weakly adsorbed species (b) compared to a cyclic voltammogram where no adsorbed species are present (a)

3.1.6 Experimental Problems Associated with Cyclic Voltammetry

Double Layer Charging Effects

In addition to the Faradaic current (the current due to the electrochemical reaction), there is a double layer charging current contribution given by $I_{dl} = C_{dl}\nu$ where $I_{total} = I_{Faradaic} + I_{dl}$, ν is the sweep rate and C_{dl} is the double layer capacitance. Whilst $I_{Faradaic}$ is proportional to $\nu^{1/2}$, I_{dl} is proportional to ν. C_{dl} is usually between 20 and 40μF cm^{-2}, therefore at 100 mV s^{-1} I_{dl} will be between 2 and 4 μA cm^{-2} and this is usually small by comparison with the Faradaic current. However, at 100 Vs^{-1}, I_{dl} increases to between 2 and 4 mA cm^{-2} and is no longer negligible. Thus, the double layer charging current distorts the voltammograms at high sweep rates, and if C_{dl} varies over the potential range the effect is worse. This effect imposes one of the major limitations on the maximum value of the sweep rate. A good approach to eliminate the problem of the double layer charging current is to use an ultramicroelectrode (discussed later). Another method is to subtract the double layer charging current from the I-E curve for the test solution without the electroactive species (assuming the double layer/potential curve is unchanged by the presence of the electroactive species).

Uncompensated Solution Resistance

The voltage observed at the working electrode is changed from the applied voltage E to E - iR_u, where R_u is the uncompensated solution resistance, and since i varies during a scan, the sweep is no longer linear. This decreases peak heights and increases peak separation. The behaviour is very similar to that expected for a slow electron transfer step, so the iR_u drop problem is often mistaken for this. Great care must

therefore be taken to ensure iR_u drop is not affecting the system under study, or is at least minimised, before performing the experiment. This may be done by incorporating a Luggin capillary or an ultramicroelectrode into the cell or by electronically applying iR_u compensation during the experiment.

3.2. AC Impedance Spectroscopy

3.2.1 Introduction

Alternating current techniques have a long and well documented history within electrochemistry and several reviews have appeared over the years [7-10].

In this section a description of the ac experiment will be given as well as the definition of the impedance of a cell. This will be followed by a discussion of the ac response of some simple circuits which lead directly to an understanding of the ac response of cells.

3.2.2 The Experiment

A small amplitude, sinusoidal voltage is applied to the cell, and the sinusoidal current passing through the cell as a result is determined. To measure the impedance of a cell, two parameters are required to relate the flowing current to the applied potential. One of these parameters is analogous to the resistance in dc measurements, and equal to V_{max}/I_{max}.

The other parameter is θ, the phase difference between the voltage and the current. If these two parameters are combined, it defines the impedance, Z, of the cell. The magnitudes of the impedance and θ are functions of the applied frequency. Measuring the impedance of a cell is done as a function of the frequency of the applied signal over a wide frequency range, usually between 1mHz and 1MHz. As the impedance is frequency dependant, it is possible to extract information about the different electrochemical properties of the cell .

The impedance of a cell may be displayed on a vector diagram. The magnitude of the impedance is represented by a point at a distance from the origin. The angle between the line joining this point to the origin and the x-axis represents the phase difference between the voltage and the current.

The impedance vector is represented by its x and y components:

$$x = |Z| \cos\theta \qquad y = |Z| \sin\theta$$

These components are analogous to the components of a complex number, hence the impedance is referred to as the complex impedance.

A typical ac experiment consists of determining the complex impedance of a cell as a function of the signal frequency, representing the results in the form of a complex impedance plot or Argand diagram (figure. 3.4).

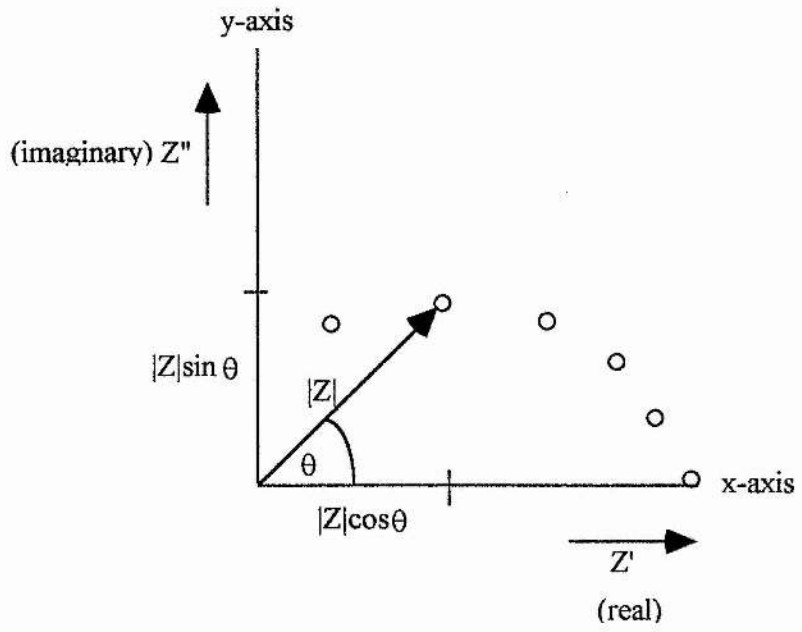

Figure 3.4 Representation of the impedance of a cell on a vector or Argand diagram

The problem with an ac experiment lies in the interpretation of the complex impedance plot in terms of electrical processes occurring within the cell. The response of any ac signal can be represented by an equivalent circuit made up of resistors and capacitors representing charge migration and polarisation occurring within the cell. The resistors and capacitors are connected in the same order as that of their corresponding physical processes, i.e. either in series or in parallel.

Resistor: The sinusoidal voltage applied across a resistor is in phase with the current i.e. $\theta=0$. The impedance, Z, is equal to the resistance: $Z = R$. This is shown as a point at a distance R along the real axis (figure 3.5).

Capacitor: The capacitance C of a capacitor is given by the charge q stored per unit potential difference E across the plates: $C = q/E$. Thus the current that passes through it is given by: $I = dq / dt = CdE / dt$

A sinusoidal voltage of amplitude E_{max} can be represented as

$$E = E_{max}\sin\omega t$$

thus

$$C(dE/dt) = I = E_{max}\omega C\cos\omega t$$

$$I = E_{max}\omega C\sin(\omega t + \pi/2)$$

Thus it can be seen that the voltage lags behind the current with phase angle $\theta = -\pi/2$. The impedance of a capacitor (E_{max}/I_{max}) is therefore frequency dependent and will have a magnitude of $1/C\omega$.

The complex impedance plot for a capacitor defines a vertical spike parallel to the imaginary axis and is shown in figure 3.6.

3.2.3 Simple Systems

The impedance of systems containing combinations of resistors and capacitors can be calculated if the impedances of individual components are known. The total impedance of components connected in series is obtained by the summation of the individual impedances :

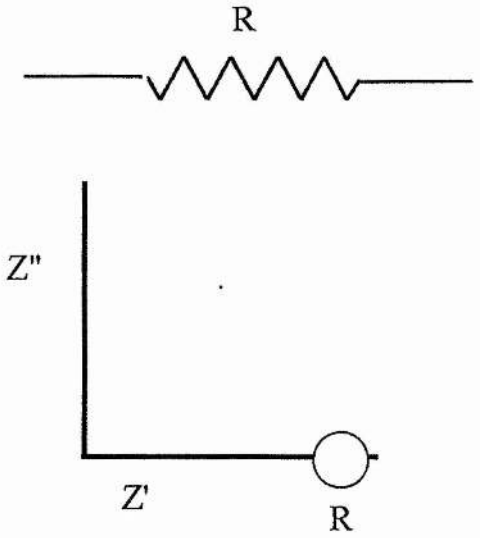

Figure 3.5 Complex impedance plot for a resistor.

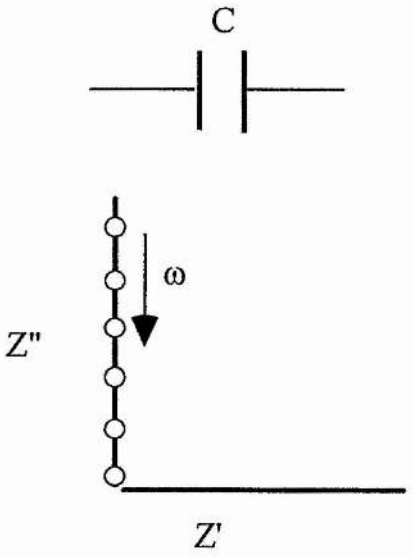

Figure 3.6 Complex impedance plot for a capacitor.

$$Z_{total} = Z_1 + Z_2 + Z_3 + ...$$

The total impedance of components in parallel is found by the summation of the individual reciprocal impedances :-

$$\frac{1}{Z_{total}} = \frac{1}{Z_1} + \frac{1}{Z_2} + ..$$

The reciprocal of the impedance is known as the admittance i.e. 1/Z =Y, and this is additive for components in parallel

$$Y_{total} = Y_1 + Y_2 + ...$$

Therefore it is possible to predict the complex impedance plots that result from a number of RC combinations.

3.2.3.1 A Resistor and Capacitor Connected Together in Series

When components are connected together in series the individual impedances are directly additive and for a resistor and capacitor in series $Z_{total} = R - j(\omega C)^{-1}$ This defines a vertical spike at a distance R along the real-axis. As frequency increases the impedance of the capacitor reduces therefore the contribution of the imaginary component to the impedance falls (figure 3.7).

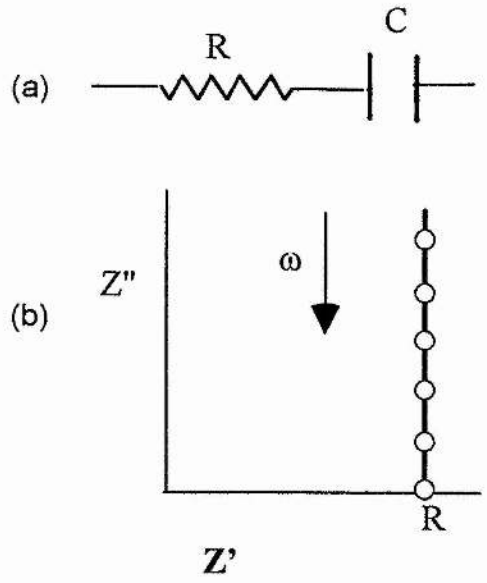

Figure 3.7 The equivalent circuit (a) and complex impedance plot (b) for a series RC combination

3.2.3.2 RC Connected Together in Parallel

In this situation it is not the impedances that are directly additive, but the admittances:

$$Y_{total} = R^{-1} + j\omega C$$

$$Z_{total} = (R+j\omega C)^{-1}$$

multiplying the top and bottom by the complex conjugate (1/R – jωC) gives

$$Z_{total} = \frac{\frac{1}{R} - j\omega C}{\frac{1}{R^2} + (\omega C)^2}$$

which rearranges to

$$Z_{total} = \frac{R - j\omega CR^2}{1+(\omega CR)^2} = \frac{R}{1+(\omega CR)^2} - \frac{j\omega CR^2}{1+(\omega CR)^2}$$

$$= Z' - jZ''$$

This defines a semicircle with a diameter equal to R, extending along the real axis (figure 3.8).

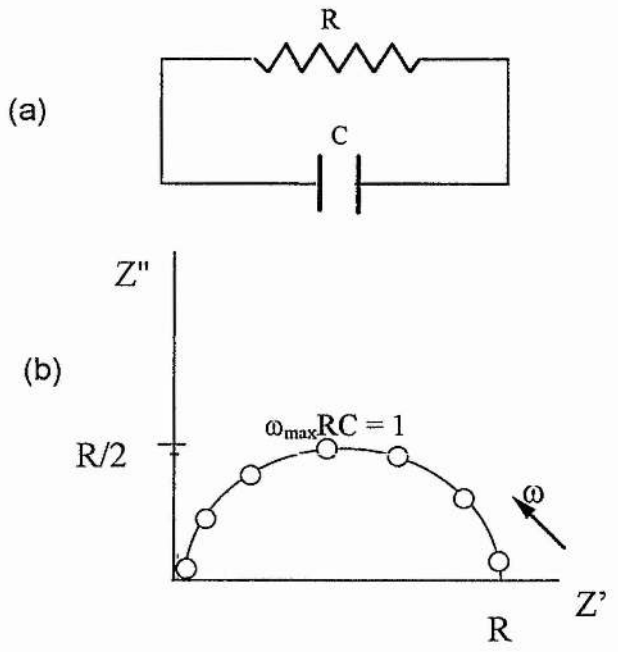

Figure 3.8 The equivalent circuit (a) and complex impedance plot (b) for a parallel RC combination

At the frequency representing the maximum of the semicircle-circle, ω_{max}, the magnitude of the impedance of the resistor is equal to that of the capacitor i.e. $R = (\omega_{max}C)^{-1}$ thus $\omega_{max}RC=1$

3.2.4 AC Response of Cells

3.2.4.1 Blocking Electrodes

When an electrode is said to be blocking, there is no finite electrode reaction. Consider the simplest case of a cell consisting of an electrolyte sandwiched between two blocking electrodes. When an ac voltage is applied to the cell and the frequency varied, the electrode becomes alternatively positively and negatively charged and the alternating field across the electrolyte causes the ions to migrate back and forth in phase with the voltage. The ion migration is represented by the resistor R_b. The immobile solvent becomes polarised in the alternating field. This dielectric polarisation may be represented as the capacitor C_b. As the ions move in the field they are alternatively accumulated and depleted at each electrode, building up ionic charge near the electrode. This is balanced by an opposite electronic charge on the electrodes. Each electrode/electrolyte interface is similar to a parallel plate capacitor and is represented by the capacitance C_e. Most electrolytes, of interest, are of high ionic concentration. The bulk polarisation and ionic migration are in parallel, therefore R_b and C_b are in parallel, and both of which are in series with C_e, the equivalent circuit for this is given in figure 3.9. As the cells contain identical electrodes we combine the capacitors into one overall electrode response:

$$1/C_e = 1/C_{e1} + 1/C_{e2}$$

C_b is related to the dielectric constant of the polymer; $C_b = \varepsilon\varepsilon_0(l/A)^{-1}$ where ε is the dielectric constant (or relative permittivity) of the polymer, ε_0 is the vacuum permittivity and (l/A) is the cell constant, R_b is proportional to temperature and the polymer.

We can now determine the complex impedance plot arising from this situation (figure 3.9). C_e is in series with the parallel combination of R_bC_b, therefore the total impedance equation is obtained by adding the impedance of C_e to that of the parallel R_bC_b combination :

$$Z^*_{tot} = R_b\left\{\frac{1}{1+(\omega R_b C_b)^2}\right\} - j\left(R_b\left\{\frac{\omega R_b C_b}{1+(\omega R_b C_b)^2}\right\} + \frac{1}{\omega C_e}\right)$$

At high frequencies, when the impedance of both R_b and C_b are of the same magnitude $(C_b\omega)^{-1} \approx R_b$ and R_bC_b contribute greatly to the overall impedance, but C_e is insignificant. The circuit therefore reduces to the parallel R_bC_b circuit dominates and defines a semicircle (figure 3.9). At low frequencies, when the impedance of both R_bC_b are not of the same magnitude, $(C_b\omega)^{-1} >> R_b$ and the R_bC_e series circuit dominates, which defines a vertical spike at distance R_b along the real axis.

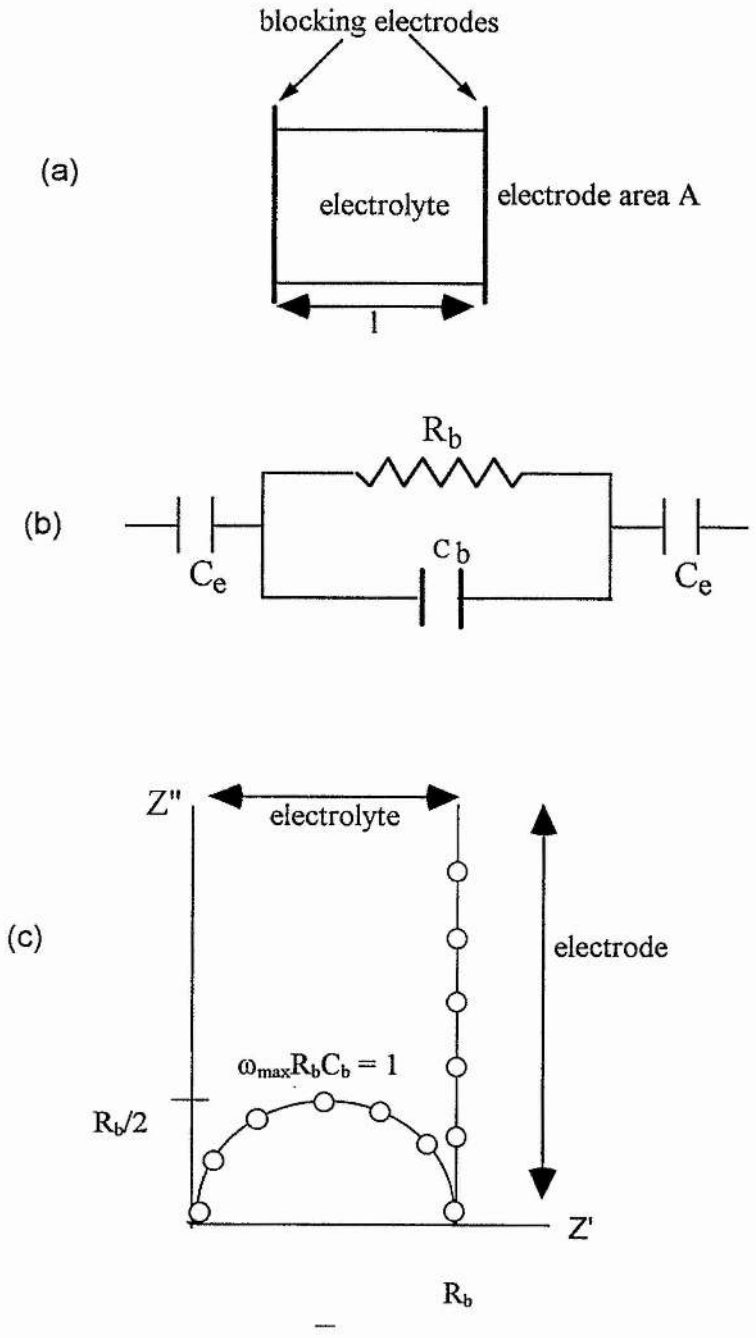

Figure 3.9 The blocking electrode cell (a), the equivalent circuit (b) and complex impedance plot (c)

At very low frequencies, only C_e dominates. High frequencies yield the value of R_b, and hence C_b can be calculated. Low frequencies yield information about the electrode/electrolyte interface. There is no electrode charge transfer reaction.

3.2.4.2 Non - Blocking electrodes

This term is used to imply the presence of any finite electrode reaction. Consider a system where a solid electrolyte containing mobile cations and anions (a polymer electrolyte could serve as a good example), is sandwiched between two electrodes which are non blocking to one of the mobile ions. The ac response of the cell shows three distinct regions: at low frequencies a skewed semicircle with a linear region inclined at 45° to the real axis, at high and intermediate frequencies two semicircles are observed. In practice only some of these features may be observed.

The high frequency semicircle is the ac response of the bulk electrolyte (c.f. a blocking electrode cell) and is defined by the parallel R_bC_b combination in the equivalent circuit figure, which is identical to that proposed by Randles for solution electrolytes [11]. The intermediate frequency semicircle is the ac response of the electrode reaction defined by the parallel R_eC_e combination. C_e is the capacitance arising from the charging/discharging of the electrode/electrolyte interface. R_e is the resistance due to the reaction of the electroactive ions at the electrode, i.e. the electrode reaction. The low frequency region is caused by diffusion arising from the presence of concentration gradients within the electrolyte, represented by the Warburg impedance Z_w in the equivalent circuit (figure 3.10).

The Classical Warburg Impedance

This impedance can occur if solvents contain more than one mobile ionic species where one reacts with the electrode and the other species is inert and in considerable excess (10^2-10^3 times greater concentration than the electroactive ion). The electroactive species is transported to and from the electrode by diffusion. This occurs with no assistance from an electric field due to the large excess of inert (supporting) electrolyte which carries nearly all the current. This diffusion is represented by the Warburg element W, the impedance of which is given by

$$Z_w = A\omega^{-1/2} - j\omega^{-1/2}$$

where A is a constant depending on a number of factors including the diffusion coefficient of the electroactive species: $A = RT[n^2F^2(2D_0^{1/2})c]^{-1}$ where R is the gas constant (J K^{-1} mol^{-1}), T is the temperature (K), n is the number of electrons transferred, F is the Faraday constant (C mol^{-1}), D_O is the diffusion coefficient of the electroactive species (cm^2 s^{-1}) and c is the concentration of the electroactive species (mol cm^{-3}).

The Warburg impedance gives rise to a line inclined at 45° to the real axis as the real and imaginary components are equal. At very low frequencies the theory predicts that the impedance must curve over and reach the real axis in the zero frequency limit. The point at which it intercepts the real axis gives a value for the dc resistance of the entire cell.

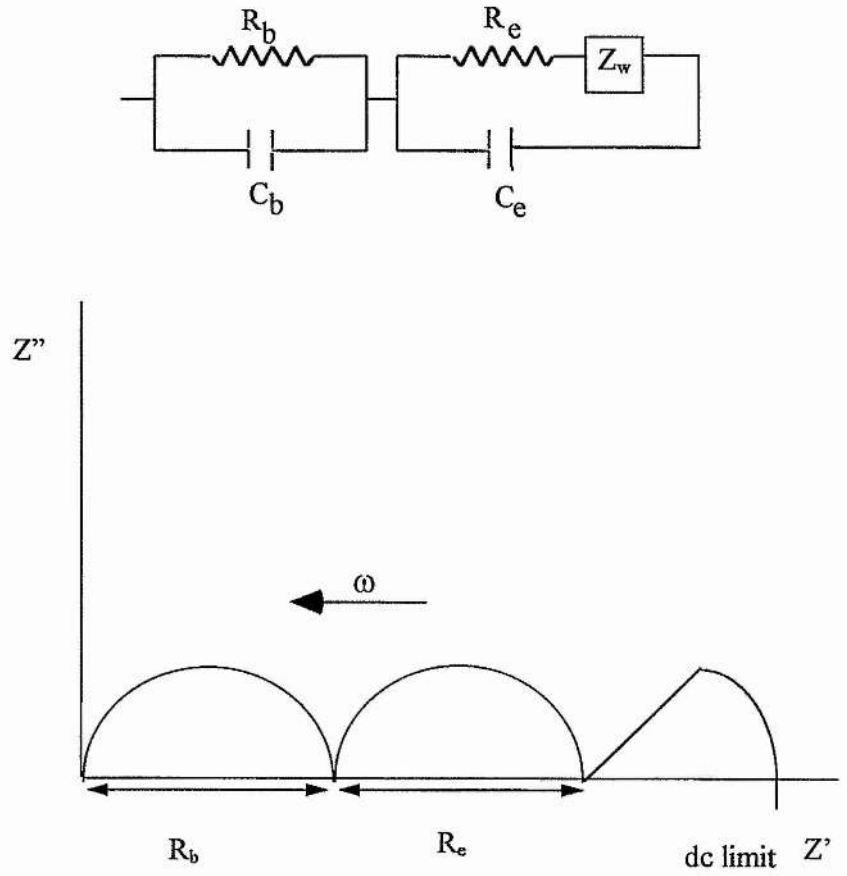

Figure 3.10 The equivalent circuit (a) and complex impedance plot (b) for a cell with non-blocking electrodes

By plotting $|Z_w|$ vs. $\omega^{-1/2}$, a straight is seen (figure 3.11) in the frequency range where diffusion is observed, where the slope of the line is given by A, defined earlier.

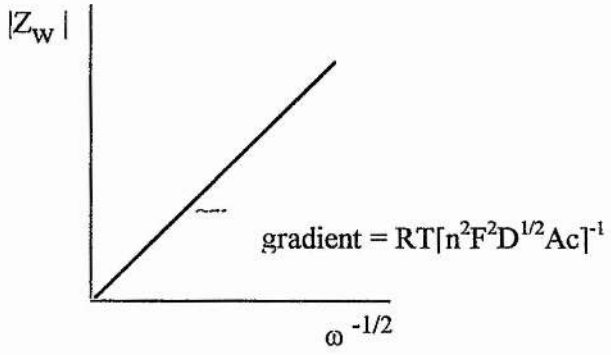

Figure 3.11 Calculation of the diffusion coefficient from ac impedance data

3.2.5 Three Electrode Cells

All of the above discussions are for two electrode symmetric cells where both electrode/electrolyte interfaces contribute to the ac response of the cell. If the aim of the investigation is to study interfaces then it is better to look at one interface at a time, this can be achieved by the use of a third electrode called the reference electrode. The reference electrode must be electroactive to one of the constituents of the electrolyte and must form a stable potential with the ion. It must be placed as close as possible to the interface under investigation, i.e. the working electrode. The potential of the working electrode is then measured with respect to the reference electrode.

Measuring the voltage of the working electrode with respect to the reference electrode during an ac experiment, allows both the impedance of the working electrode/electrolyte interface and the iR_u drop between the working electrode and

the reference electrode to be determined in isolation. The ac response of such a cell will exhibit well defined characteristics. The electrode reaction is represented by a semicircle defined by an RC parallel combination of the charge transfer resistance R_{ct}, and the interfacial capacitance C_{dl}. The uncompensated solution resistance R_u is the displacement of the semicircle along the real axis from the origin. The diffusion of the electroactive species to or from the electrode is represented by the Warburg impedance Z_W, which is observed as a straight line at 45° from the real axis, as described earlier. A typical plot is shown in figure 3.12.

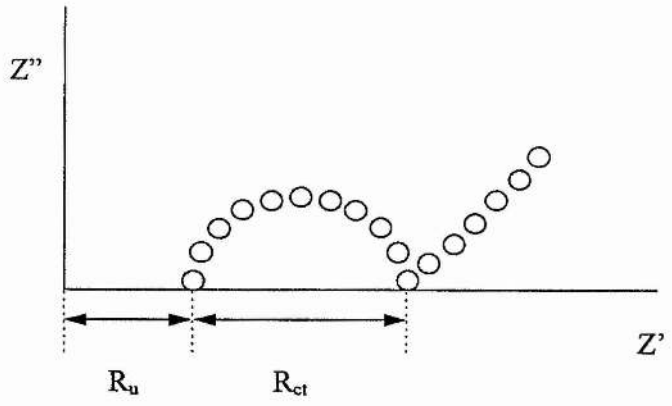

Figure 3.12 Complex impedance plot, at the equilibrium potential, for a redox couple in solution .

3.2.6 Application of AC Impedance Spectroscopy to Determine the Standard Apparent Rate Constant k_{sh}

One of the simplest electrochemical systems to analyse is that of a simple one step reaction at its equilibrium potential E_e, i.e. no net current flowing. The ac impedance plot obtained for such a system, using three electrodes, can also be represented by figure 3.12.

The variation of current density with exchange current density I_0, over potential η and transfer coefficients α_A and α_C is described by the Butler-Volmer equation (derived in Chapter 4):

$$I = \vec{I} + \overleftarrow{I} = I_0 \{exp\ [(\alpha_A nF\eta)/RT] - exp\ [(-\alpha_C nF\eta)/RT]\}$$

At low overpotentials, where $(\alpha_{A\ or\ C} nF)/RT << \eta$, the Butler-Volmer equation reduces to

$$I = I_0 \{(\alpha_A nF\eta)/RT + (\alpha_C nF\eta)/RT\}$$

and since $\alpha_A + \alpha_C = 1$, it can be reduced further to $I = I_0 nF\eta/RT$.

From Ohm's law, the charge transfer resistance is defined by rearrangement of this to give

$$R_{ct} = \eta/I = RT/I_0 nF \qquad \text{eqn 3.1}$$

This is a linear approximation and can be used for systems where the ac perturbation $|\eta|$ is less than or equal to $10/n$ mV.

From the Butler-Volmer equation the exchange current density I_0 is defined as

$$I_0 = k_s nF(c_O^{\infty})^{\alpha A}(c_R^{\infty})^{\alpha C} \qquad \text{eqn. 3.2}$$

Combining the equations for the charge transfer resistance (eqn.3.1 above) and that for the exchange current density (eqn.3.2) gives

$$= RT/[n^2F^2R_{ct}(c_R^{\infty})^{\alpha c}(c_O^{\infty})^{1-\alpha c}] = k_s$$

where k_s is the standard rate constant.

3.3 Ultramicroelectrodes

3.3.1 Introduction

The implementation of ultramicroelectrodes in research first began in the late 1960's at the University of Southampton and was carried out by Martin Fleischmann and co-workers [12]. Other research groups began utilizing ultramicroelectrodes in the early 1980's demonstrating their utility in electroanalytical and bioelectrochemical studies (e.g. Wightman, Osteryoung and others) [13-20].

An ultramicroelectrode is an electrode with at least one dimension small enough that its properties are a function of its size. Most ultramicroelectrodes have radii in the range 0.5-25μm. It may be manufactured in many different forms, for example disk, hemisphere, band or ring.

Three major consequences arise from the reduction in size of the electrode:

i) mass transport rates to and from the electrode are increased due to non-planar diffusion;

ii) ohmic losses, which are the product of electrode current and solution resistance (iR), are reduced due to the greatly diminished current, often in the order of nA. The current is proportional to a^2 (where a is the radius of the electrode surface) so when the radius decreases so does the current.

iii) the double layer capacitance is reduced due to the reduction in surface area (see electrical properties later in the present chapter), resulting in an improved ratio of Faradaic/non Faradaic currents.

When very small electrodes are employed for conventional electrochemical techniques, dramatic changes are encountered in the responses. These changes arise due to a reduction in the transient diffusion response with a tendency towards steady-state mass transport. For example in cyclic voltammetry the conventional response is transformed into a 'polagraphic type wave' which is much easier to analyse.

Additional advantages offered by ultramicroelectrodes include the investigation of electrochemical responses in media without the presence of supporting electrolyte; experiments being carried out in highly resistive media, frozen solutions and the gas phase, providing media for new grounds of investigation in physical and analytical chemistry.

3.3.2 Theoretical Aspects

3.3.2.1 Mass Transport

Consider the simple electron transfer reaction

$$O + ne \rightleftharpoons R$$

where both the reactants and products are soluble, and the reaction is diffusion controlled. With a large planar electrode mass transport is described by semicircle-infinite planar diffusion, given by *Fick's second law*,

$$\partial c_j(x,t)/\partial t = D_j\{\partial^2 c_j(x,t)/\partial x^2\}$$

where $c_{j\,(x,t)}$ are the concentrations of species j at a distance x from the electrode at a time t, and the D_j are the diffusion coefficients. Applying the Laplace transform [21] to this equation with respect to t leads to the Cottrell equation [22]:

$$I = nFD^{1/2}c/(\pi t)^{1/2} \qquad \text{eqn. 3.3}$$

where I is the current density, c is the bulk concentration of reactant and nF is the molar charge transferred.

At a spherical ultramicroelectrode of radius r_0, the relevant diffusion equation is

$$\partial c_i/\partial t = D_i \{(\partial^2 c_i/\partial r^2) + (2\partial c_i / r\partial r)\} \qquad \text{eqn 3.4}$$

Applying the Laplace transform [21] with respect to t leads to

$$I(t) = nFD^{1/2}c_0^{\infty}/(\pi t)^{1/2} + nFD\, c_0^{\infty}/r_0 \qquad \text{eqn 3.5}$$

This is the Cottrell equation plus a spherical correction term. At short times the spherical contribution is negligible (eqn 3.5 reduces to eqn 3.3) and diffusion to a sphere can be treated as linear diffusion. At long times the spherical term becomes dominant leading to a time-independent steady-state current. Due to the effects of natural convection the steady-state is never reached at conventional sized electrodes, but the smaller the electrode radius, the more easily and faster the steady-state is achieved.

The limiting diffusion current for spherical and hemispherical ultramicroelectrodes follows directly from eqn 3.5. Thus, after a certain time depending on the electrode size, a steady state is reached, and the current is given by

$$i = 2\pi nFD\, c_0^{\infty} r_0$$

In general for ultramicroelectrodes, the current density is sufficiently high, due to a high rate of diffusion, that interference from natural, or even forced, convection is negligible.

For a micro-disk electrode, the effects of radial diffusion must be considered due to the non-uniform accessibility of the surface. The relevant equation is

$$\partial c_i/\partial t = D_i \{(\partial^2 c_i/\partial r^2) + (\partial c_i/r\partial r) + (\partial^2 c_i/\partial x^2)\} \qquad \text{eqn 3.6}$$

which does not have an exact solution. Numerical analysis, however, shows that at long times the current is equal to that of a hemisphere of a radius $a = \pi r_0/2$, such that

$$i = 4nFaD\, c_0^{\infty}$$

Here, the current is the same as that of the hemispherical electrode. This, and the similarity between eqns. 3.4 and 3.6 indicates that the simpler model of the hemisphere can be applied to the more easily manufacture disc, without significant error.

Another important aspect about mass transport is that the true steady state of diffusion is achieved with an ultramicroelectrode as long as the dimensions of its surface is less than the length of the natural convection layer i.e. less than 20μm. The composition of the electrolyte solution is perturbed only within a small distance from the ultramicroelectrode and the response is practically unaffected by movements in

solution. The time to reach a new steady state of diffusion after perturbation is of the order of $a^2/4D$, which is usually less than 10ms for a disk of radius 5μm. Therefore, during voltammetry of moderate sweep rates, steady state conditions are maintained, and the voltammogram does not develop characteristic peaks associated with conventional sized electrodes.

3.3.2.2 Electrical Properties

Two important electrical properties of ultramicroelectrodes arise due to their small size:. The first of these is electrical resistance: both the resistance within the electronic conductor (body of the ultramicroelectrode) R_m and the resistance of the electrolyte R_S need to be considered.

The resistance of the ultramicroelectrode is given by $R_m = l_1 / \sigma A$, where l_1 is the length of the wire, A is the cross sectional area and σ is the specific conductivity. For a microscopic hemispherical electrode, with a second electrode placed an almost infinite distance away the resistance of the electrolyte is found to be [23-25] $R_s = l_2 / 2\pi\kappa r_0^2$, where κ is the specific conductivity of the electrolyte and l_2 is the electrode separation.

The resistances per unit area are low and become lower with decreasing radius of the ultramicroelectrode, and are smaller than the uncompensated resistances between the Luggin capillary reference and the working electrode in conventional three electrode cells.

The second property is the reduction in double layer capacitance. This is proportional to the electrode area and determines the shortest time at which meaningful measurements of Faradaic currents can be made. The cell resistance has an approximately inverse dependence on the electrode radius but C_{dl} depends directly on the radius, the net result being a decrease in the relaxation time for double layer charging.

3.3.3 Applications

3.3.3.1 Measurement of Kinetics with Fast Transients.

At short times, and very high scan rates, after the onset of electron transfer processes at the ultramicroelectrode / electrolyte interface planar diffusion dominates. At such high scan rates techniques already developed to analyse data from conventional sized electrodes can therefore be applied to the data obtained from ultramicroelectrodes [22].

Despite the difficulties associated with obtaining kinetic data from high scan rate cyclic voltammograms, this has been by far the most preferred technique used for the study of fast reactions at ultramicroelectrodes [19]. This technique has also proved useful in the determination of thermodynamic data related to electrode processes [26].

3.3.3.2 Electrochemistry in Highly Resistive Media

The minimisation of iR effects with ultramicroelectrodes allows measurements to be made without the presence of an added supporting electrolyte. This reduces the likelihood of ion-ion interactions, an important factor when measuring the kinetics of reactions, and reduces the possibility of added impurities to the solution.

The tolerance of ultramicroelectrodes for low conductivity has also allowed studies to be carried out in highly resistive media:

$$iR_s = nFDc^{\infty}\kappa \qquad \text{eqn. 3.7}$$

Equation 3.7 has been shown to apply to ultramicroelectrodes [27]. However, there are also double layer effects to be taken into account; the Debye length is large for a solution with low ionic content and can be comparable to the size of the ultramicroelectrode and the diffusion layer around it [28]. Hence it seems unlikely that the simple analysis that leads to equation 3.7 can be applied to ultramicroelectrodes of small radii in solutions sparsely populated with ions.

In spite of these difficulties, steady state measurements at ultramicroelectrodes have proven useful for analytical determinations of charged and uncharged species in the absence of supporting electrolyte in highly resistive solvents, or in the exploration of systems in unusual situations.

REFERENCES

1 J.E.B. Randles, *Trans.Faraday Soc.*, 44 , 327, 1948

2 A. Sevcik, *Coll. Czech. Chem. Comm.*, 13, 349, 1958

3 R.S. Nicholson & I. Shain, *Anal. Chem.*, 36, 706, 1964

4 H. Matsuda & Y.Ayabe, *Z. Electrochem.*,59, 494, 1955

5 R.S. Nicholson, *Anal. Chem., 37*, 1351, 1965

6 R.H. Wopschall & I. Shain, *Anal. Chem..*, 39, 1514, 1527, 1535, 1967

7 D.C. Grahame, *J. Electrochem. Soc.*, 99, 3700, 1952

8 M. Sluyters-Rehbach & J.H. Sluyters in *Electroanal. Chem.*, Vol.4. A.J. Bard (ed).

9 J. Ross Macdonald, *J. Chem. Phys.*, 61, 3977, 1974

10 W.I. Archer & R.D. Armstrong in *Electrochemistry*, Vol.7. The Roy.Soc. London

11 J.E.B. Randles, *Dis. Faraday Soc.*, 1 11 1947

12 M. Fleischmann, S. Pons, D.R. Rolison & P.P, Schmidt eds., *Ultramicroelectrodes*, Datatech Systems, Inc., 1987

13 R.M. Wightmann, *Anal. Chem.*, 53, 1125R, 1125A, 1981

14 M.I. Montenegro, *Portugaliae Electrochim. Acta.*, 3, 165, 1985

15 *Ultramicroelectrodes*, (Edited by M. Fleischmann, S. Pons, D.R. Robinson & P. Schmidt), 1987

16 S. Pons & M. Fleischmann, *Anal. Chem.*, 59, 1391A, 1987

17 J.O. Howell, *Current Separations*, 8, 2, 1987

18 J. Robinson, *Chemical Kinetics*, 29, 1989

19 R.M. Wightmann & D.O. Wipf, *Electroanal. Chem.*, 15, 267, 1989

20 A.M. Bond, K.B. Oldham & C.G. Zoski, *Anal. Chim. Acta.*, 216, 177, 1989

21 Instumental Methods in Electrochemistry, Southampton Electrochemistry Group, Ellis Harwood, Chichester 1990

22 A,J, Bard & L.J. Faulkener, *Electrochemical Methods*, Wiley, New York 1980

23 B.Scharifker & G. Hills, *J. Electroanal. Chem.*, 130, 81, 1981

24 D. Ilkovic, *Coll.,Czech. Chem. Comm.*, 8, 13, 1936

25 J. Newman, *J. Electrochem. Soc.*, 113, 501, 1966

26 J.O. Howell, J.M. Goncales, C. Amatore, L. Klasinic, R.M. Wightmann & J.K. Kochi, *J. Am. Chem. Soc.*, 106, 3968, 1984

27 S. Bruckenstein, *Anal. Chem.*, 59, 2098, 1987

28 K.B. Oldham in *Ultramicroelectrodes*, (Edited by M. Fleischmann, S. Pons, D.R. Robinson & P. Schmidt), page 276, 1987.

CHAPTER 4

Theory of Electron Transfer at Electrode/Electrolyte Interfaces

4.1 Introduction

Electron transfer is the foundation of all electrochemistry, it can be either homogeneous or heterogeneous. Homogeneous electron transfer occurs when two ions meet in the interior of the solution and an electron transfers from one ion to the other, for example $Fe^{2+} + Ti^{4+} \rightarrow Fe^{3+} + Ti^{3+}$. Heterogeneous electron transfer is the transfer of electrons between an electronically conducting phase and localised energy levels on molecules or ions in an adjacent phase. The simplest electrochemical reaction that can take place is the transfer of a single electron at an electrode surface which takes place via electron tunnelling, for example:

$$Fe^{3+}(H_2O)_6 + e^- \rightleftharpoons Fe^{2+}(H_2O)_6$$

The electron moves from occupied orbitals on one side of the interface to vacant electronic states on the other side. This movement is governed by the Franck-Condon principle: During the timescale of electron transfer, the adjustment of the charge cloud is much faster (10^{-16}s) than the movement of the atomic nuclei (10^{-14}s). On the timescale of 10^{-16} s the nuclei do not have time to alter their positions, they are 'frozen' and appear to be stationary. This process occurs with no emission or

absorption of energy, i.e. with no change in energy and so electron transfer is a non-radiative process that takes place at the isoenergetic point where the initial and final electronic states have the same energy. If the initial and final states have different energies, transfer is accompanied by absorption or emission of thermal energy and the probability of electron transfer is much reduced.

Electron transfer and its activation has been the subject of many investigations for decades. These investigations have spawned many models, but before looking at specific models in detail it is necessary to give a brief historical background into their development as progress towards a satisfactory theory of heterogeneous electron transfer has been slow and is so far incomplete.

Historical Background of the Theory of Heterogeneous Electron Transfer

In 1931 Gurney [1], considering the discharge of a proton at an interface, postulated that heterogeneous electron transfer between an electrode and a solution phase occurred by electrons tunnelling through a potential barrier at the interface, the height of which is dependent on the interaction between the reactant and the surface. The next major advance occurred in 1934 when Fowler [2] pointed out the importance of the Franck-Condon principle in electron transfer processes accompanying proton discharge. 1935 saw the development of a theory for the discharge step of the hydrogen electrode reaction by Horiuti and Polanyi [3]. This theory was developed within the framework of the activated complex theory and used the concepts put forward by Gurney. Based on the same concepts of the activated complex theory R.J. Marcus, Zwolinski and Eyring [4,5], as well as Sacher and Laidler [6,7], developed a

theory for the outer sphere electron transfer reaction treating the solution as a static dielectric, which represented one pole in the controversy concerning the theoretical aspects of charge transfer reactions. The other pole emerged from a suggestion by Libby [8] that for homogeneous outer sphere electron transfer reactions a considerable part of the activation barrier arose from non-equilibrium solvent polarization fluctuations. In 1954, Platzmann and Franck [9] used the same idea to describe homogeneous charge transfer within the structure of radiationless transition theory using the polaron concept, originally developed by Pekar [10] for polar crystals in and extended to polar solvents by Davydov [11].

The next major group of advances was split into two camps, that of R.A. Marcus [12-19] and Hush [20-22] and the other of the LDK group i.e. Levich, Dogonadze and Kuznetsov [23-37]. Most of today's research follows one of these models, as they represent most of the theoretical effort made towards the understanding of electrode processes within the last 20-30 years. At first, both camps developed the same model, where the metal ion with its inner coordination sphere could be treated as a conducting sphere with an activation barrier associated with solvent polarization fluctuations. Marcus [12-19] developed his model using classical statistical mechanics to describe the solvent, whereas the LDK group [23-37] developed their model via a quantum statistical mechanics approach. Marcus [12-19] and other authors [8,20-22] then pointed out that the neglect of the bond stretching contribution from the inner sphere was a serious mistake and thus Marcus [12-19] and Hush [20-22] modified their models to take this fact into account. The LDK group [23-37], however, continue to omit the inner sphere contributions. The basis for their decision was that

the vibrational modes of the inner sphere have hω >>kT and these bonds require multiple phonon interactions involving far too many phonons to have a reasonable probability of being excited. This reasoning has been greatly questioned by many scientists, including Bockris [38].

The most recent advances in the theory have not brought forward new models, but have further advanced the solvent fluctuation model by firstly presenting a more generalised non-equilibrium statistical mechanical picture [39,40] and secondly by considering more specifically the effect of the inner co-ordination sphere [41,42].

4.2 Basic Physical Picture of Electron Transfer

For ions in solution, the electrons are localised in discrete orbitals: Consider the redox couple $Fe^{2+}/Fe^{3+}(H_2O)_6$ ($3d^6$)

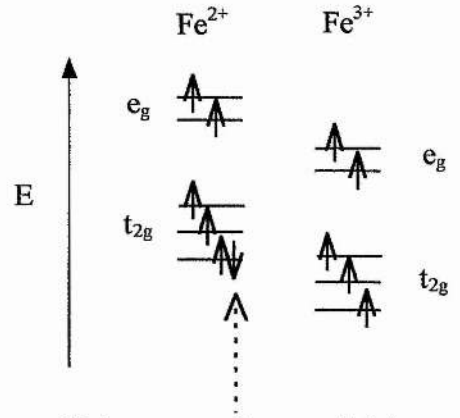

Figure 4.1 Diagram of orbital energy levels on ions in solution

The structure of the electrode is very different to that of the electrolyte. The electronic energy levels are closely spaced; the valence electrons being delocalised over the whole lattice. To a first approximation the electrons can be considered to form a 'gas' constrained inside the 'box' formed by the metallic lattice. The electrons fill up the closely spaced levels up to the Fermi level which, by definition is the highest occupied level.

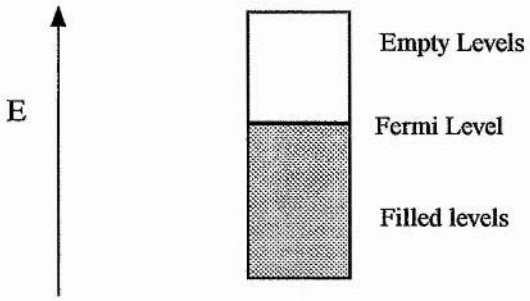

Figure 4.2. Diagram of energy levels for electrons in the metal

When the electrode is introduced into the electrolyte the reactants diffuse to the electrode where electron transfer can take place from the ions in solution to the electrode or from the electrode to the ions in solution. This is an outer sphere reaction in which no bonds are broken or formed. If the electron transfer process is fast then the diffusion of the reactants to the electrode will be the rate determining step, but for this chapter it is assumed that transport processes are in equilibrium and electron transfer is the rate determining step.

In figure 4.3 electron transfer can be represented as a horizontal movement, with the actual transfer occurring via electron tunnelling.

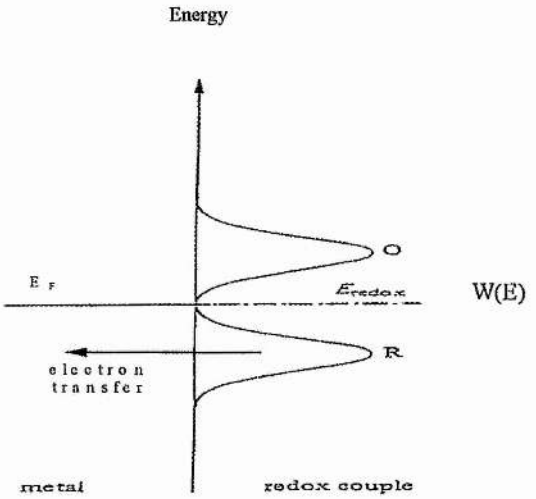

Figure 4.3 Horizontal representation of electron transfer

The true electron tunnelling condition is that the ionization potential of the ion in solution must be equal to the energy of the Fermi level in the electrode. Achieving this ionisation potential presents an energy barrier for electron transfer. However, electrode reactions in solution often do not take place in one smooth process over the energy barrier, they are multistep reactions proceeding through the following stages:

1. Diffusion of reactants to electrode
2. Arrangement of the ionic atmosphere suitable for transition state
3. Orientation of solvent suitable for transition state
4. electron transfer.

The process of electron transfer must go through a transition state; the reactants and products do not have the same ionic atmosphere, ligand-ion bond distances or solvent co-ordination and the timescales for each of these alterations vary greatly.

1. Electron transfer	10^{-16} s
2. Alteration to ligand-ion bond distances	10^{-14} s
3. Re-orientation of solvent dipoles	10^{-11} s
4. Reorientation of ionic atmosphere	10^{-9} s

Figure 4.4 shows schematically a plot of a reactant changing to a product in which two features A and B must be altered. If process A takes place much faster than process B the reaction cannot proceed along the dotted line, as the time taken for the A co-ordinate to change is far to small for any change in the B co-ordinate.

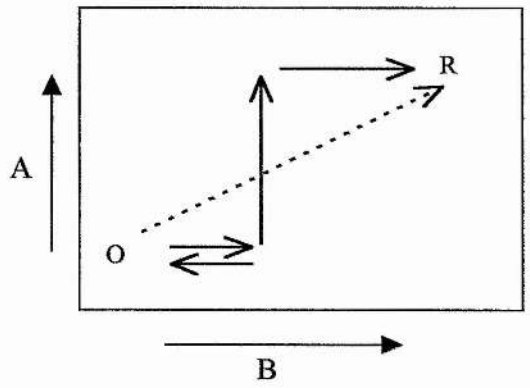

Figure 4.4 Separation of steps for multistep reactions due to differing time scales

The reaction must follow the solid lines through one or more transition states. This is also the basis for the Franck-Condon principle in which electron transfer occurs on too fast a timescale for other nuclei to move, and so they are 'frozen' in position and electron transfer occurs with no emission or absorption of energy at the isoenergetic point.

The energy of the electronic state involved in electron transfer will change rapidly with time due to fluctuations in the solvent, and can be represented by a normal distribution function centred on the 'most probable' energy. As the reactants and products have different electronic charges they have different energies due to solvent interactions, and this is shown in figure 4.5. The vertical scale (y-axis) of the diagram represents electronic energy, referred to the energy required to remove an electron to infinity. On the electrode side of the interface the horizontal axis describes distance, and the highest filled energy level, the Fermi level, is also shown. On the electrolyte side of the interface, the horizontal coordinate describes the number of states existing in solution, close to the electrode surface, with the particular electronic energy given by the vertical coordinate.

The energy of the electronic state involved in electron transfer changes until the ionisation potential is reached. If the ionisation potential is equal to the Fermi level energy then electron transfer occurs. Many factors can alter the energy of the electronic state of the ion: the metal-ligand bonds can vibrate, the surrounding solvent molecules can translate and vibrate, or the solvent dipoles can rotate or reorientate.

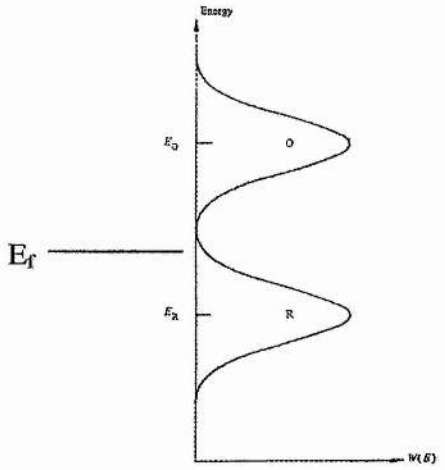

Figure 4.5 Energies of the electronic states for the oxidised and reduced species

All of these factors can occur in any given system where electron transfer takes place, so which of the different possible contributions is the main factor in attaining the ionisation potential and hence overcoming the activation energy barrier to electron transfer? Many models have been put forward to try and explain the activation of electron transfer. The Russian group of Levich, Dogonadze and Kuznetsov (LDK) [23-37] promote the solvent dielectric fluctuation or solvent reorganisation theory. Bockris [38] promotes the metal-ligand bond vibration theory; while Marcus [12-19] and Hush [20-22] have developed models that consider both theories, as they believe one cannot be mutually exclusive of the other.

4.3 Rate Constant for the Electrode Reaction

Consider the reaction where electron transfer occurs between the electrode and two solvated cations forming the redox couple $M^{n+/(n-1)+}$. The energy of each of these ions is different due to the different polarisation of the solvent molecules by ions of different charge. Therefore, for example, when M^{n+} accepts an electron the solvent polarisation should change, the solvent dipoles should change their orientation leading in general to solvent reorganisation. The energy associated with this reorganisation can be expressed by means of the expression for the energy of a simple harmonic oscillator, as the solvent dipoles oscillate around their equilibrium position r_0, with a definite frequency:

$$U = U_0 + 0.5h\omega(r - r_0)^2 \qquad \text{eqn. 4.1}$$

where U_0 is the minimum energy of the system and occurs when $r = r_0$ and r is a dimensionless coordinate of the system

As the system coordinate r changes so does the energy of the oxidised and reduced states and this is shown diagramatically in figure 4.6. Figure 4.6 is a much simplified two dimensional diagram of the more complex system that involves the intersection of two parabolas.

According to the Franck-Condon principle, electron transfer occurs at a fixed position of the ions and molecules in the system. However, at the equilibrium coordinate of the

oxidised system, the energies of the initial and final states are different and so electron transfer is not possible. If the energy ΔU (see figure 4.6) could be supplied to the electrons in a very short space of time from an external source then electron transfer would become possible.

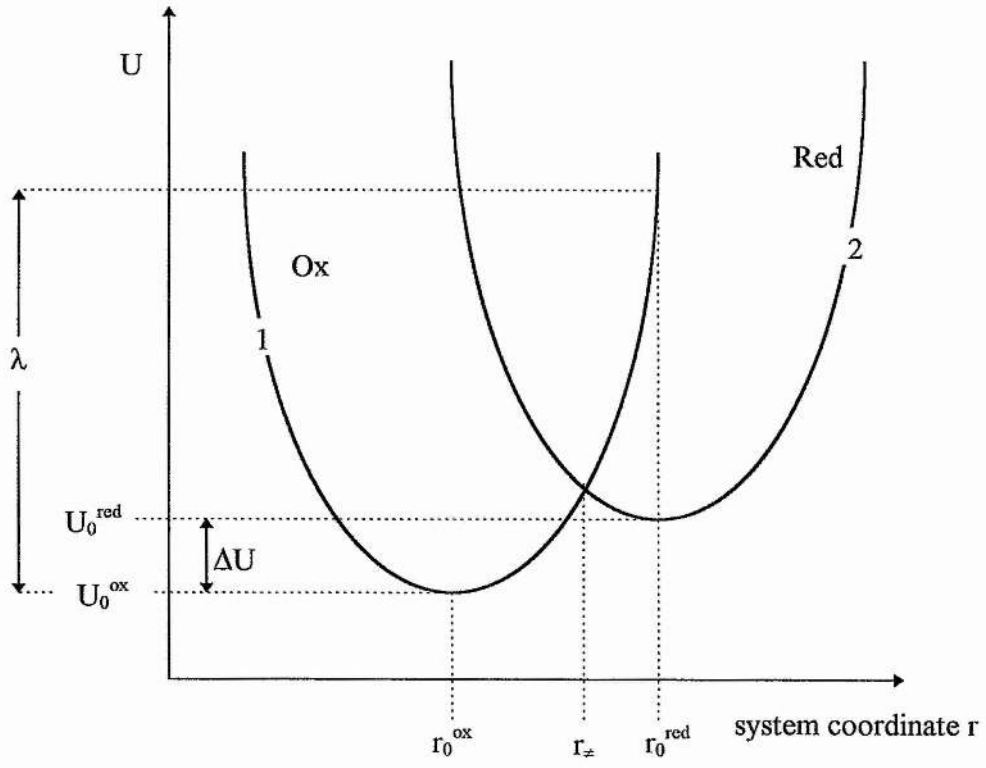

Figure 4.6 Change in energy with system coordinate

Electron transfer is possible when the energies of the oxidised and reduced states are equal and this occurs at the coordinate $r_{\neq}$. The rate of the reaction is determined by

the probability of such a situation and this is higher when the equilibrium coordinate of the oxidised and reduced species are similar.

According to the theory of electron transfer reactions at an electrode [12-19] the standard rate constant (k_s) can be given as

$$k_s = \kappa Z \exp(-\Delta G^*/RT) \qquad \text{eqn. 4.2}$$

where κ is the electronic transmission coefficient, G^* is the free activation energy and Z is the collisional frequency. Z can be given as $(RT/2\pi M)^{1/2}$ where M is the mass of the reactant, and G^* can be given as

$$G^* = \frac{\lambda}{4} + (w^{red} + w^{ox})/2 + nF[(E-E_f^0)/2] + [nF(E - E_f^0) + (w^{red} - w^{ox})]^2/4\lambda$$

eqn 4.3

where w^{ox}, w^{red} is the electrical work needed to transfer one mole of the oxidised and reduced species respectively, from the bulk solution to the *OHP* which is regarded as identical with the charge transfer plane, E is the electrode potential, E_f^0 is the formal potential of the system and λ is the reorganisation energy i.e. the work expended in the reorganisation of atoms and molecules in the environment of the oxidised species from their equilibrium positions to the positions occupied about the reduced species when it is at equilibrium. From figure 4.6 and from equation 4.1 (the equation for the energy of the harmonic oscillator in 2d space) λ can be given as

$$\lambda = 0.5h\omega\,(r_0^{red} - r_0^{ox}) \qquad \text{eqn. 4.4}$$

When specific adsorption of the oxidised and reduced species is absent

$$w^{ox} = z_{ox} F \phi_2 \qquad \text{eqn. 4.5}$$

and

$$w^{red} = z_{red} F \phi_2 \qquad \text{eqn. 4.6}$$

but $z_{ox} = z_{red} + n$

so $$w^{red} = (z_{ox} - n) F \phi_2 \qquad \text{eqn. 4.7}$$

When ϕ_2 is equal to zero and $E = E_f^0$ then equation 4.3 reduces to

$$\Delta G^* = \lambda/4 \qquad \text{eqn. 4.8}$$

Marcus separated λ into two components $\lambda = \lambda_o + \lambda_i$, i.e. an outer sphere contribution, λ_o, and an inner sphere contribution, λ_i. The outer sphere contribution λ_o depends on the size and shape of the reacting substance and the strength of interaction between the ion and the solvent in the outer sphere via the Pekar factor $\varepsilon_{op}^{-1} - \varepsilon_s^{-1}$. For a spherical molecule involved in the electrode reaction λ_o can be defined as

$$\lambda_o = 0.5(ne)^2 (a^{-1} - R_e^{-1}) (\varepsilon_{op}^{-1} - \varepsilon_s^{-1}) \qquad \text{eqn. 4.9}$$

where a is the radius of the reacting molecule, R_e is twice the distance from the centre of the molecule to the electrode surface and ε_{op}, ε_s are the optical and static permittivities respectively for the surrounding solvent

The inner sphere contribution to λ, λ_i [12-19], is dependent on the vibration of the inner sphere coordination bond and is given by

$$\lambda_i = \sum_j \frac{f_j f_j^p}{f_j + f_j^p} (\Delta q_j)^2 \qquad \text{eqn. 4.10}$$

where Δq_j is the difference between lengths of a given bond in the oxidised and reduced species and k_j and k_j^p denote the force constant of the jth vibrational coordinate in a species involved in the reaction when that species is a reactant and when it is a product respectively.

Marcus theory [12-19] therefore includes contributions to G* from both the inner sphere and the outer sphere, and it assumes that the dielectric polarization of the solvent is at equilibrium. and the transition state is reached by translational energy. However, the transition state can also be reached by the transfer of the oscillation energy of the bulk solvent molecules to the solvent molecules interacting with the reactant. In the encounter preequilibrium model [43-45]

$$Z = K_p \nu_n \qquad \text{eqn. 4.11}$$

where K_p is the equilibrium constant for the precursor complex and ν_n is the effective frequency of formation of the configuration which participates in the electron transfer process

This model (developed by Calef & Wolynes and also Zusman [43-45]) points out the importance of the role of the dynamics of solvent reorganisation in the electron transfer process, a view also held by the LDK group [23-37]. If the frequency of the reorientation of the solvent molecules is slow, i.e. less than the frequency of the change of the electrical field, then the process of solvent reorientation limits the change of dielectric polarization of the solvent, and hence determines the rate of electron transfer. By considering the influence of the solvent dynamics, the effective frequency of reorganisation of the reactant is determined by the frequency of reorganisation of the solvent molecules around the reactant. If it is assumed that the free energy of the reaction is equal to zero and the reorientation of the solvent molecules is not inhibited by their thermal motion, then the nuclear frequency factor ν_n is given by [43,44]

$$\nu_n = \tau_L^{-1} [\lambda / 16\pi RT]^{1/2} \qquad \text{eqn. 4.12}$$

where τ_L is the longitudinal relaxation time of the solvent which can be given by

$$\tau_L = \tau_D \varepsilon_\infty / \varepsilon_s$$

and τ_D is the Debye relaxation time and ε_∞ is the dielectric constant of the solvent. Equation 4.9 is valid when $\lambda_0 >> \lambda_i$.

The preexponential factor is now dependent on both τ_L and on λ and using equations 4.2, 4.8, 4.11 and 4.12 the equation for the standard rate constant (k_s) can be written as:

$$k_s = \kappa K_p \tau_L^{-1} [\lambda/16\pi RT]^{1/2} exp [-\lambda/4RT] \quad \text{eqn. 4.15}$$

As in the Marcus model, the standard rate constant k_s depends on the activation energy determined by $\lambda/4$, but it also depends on the reorientation of the bulk solvent molecules.

If a system with fast electrode kinetics and low reorganisation energy is studied in several solvents, a linear relationship between k_s and τ_L^{-1} should be seen. If the system has a higher reorganisation energy that is dominated by the outer sphere contribution to λ, then k_s should be linear with $\varepsilon_{op}^{-1} - \varepsilon_s^{-1}$. However, for systems that are dominated by the inner sphere contribution to λ, k_s should be linear with the square of the change in bond length between the reduced and oxidised species, i.e. k_s should be linear with Δq_i^2.

4.4 Derivation of the Butler-Volmer Equation

Looking at one of the contributions to electron transfer, metal-ligand bond vibration, in more detail leads to an expression for ΔU, the change in energy required to achieve electron transfer: For the $Fe^{3+/2+}$ redox couple in water, the ionization potential at any given bond length is the difference between the electronic energy of $Fe^{2+}(H_2O)_6$ and the $Fe^{3+}(H_2O)_6$ at the same bond length, as shown in figure 4.7. The change in energy of the Fe^{2+} required to achieve electron transfer is ΔU, but the change in energy of the electron is

$$\Delta E = E_{IP} - E_F$$

therefore

$$\Delta U = \beta \Delta E$$

where β is the transfer coefficient with a value of $0<\beta<1$, and is equal to α_A for an anodic reaction or α_C for a cathodic reaction.

ΔU is the work which must be done to excite the ion into the transition state, i.e. the activation energy barrier for electron transfer.

If j_a is the flux of electrons across the interface due to the anodic (oxidation) reaction then

$$j_a = C_{Fe}^{2+} k_s \exp(-\Delta U/RT)$$

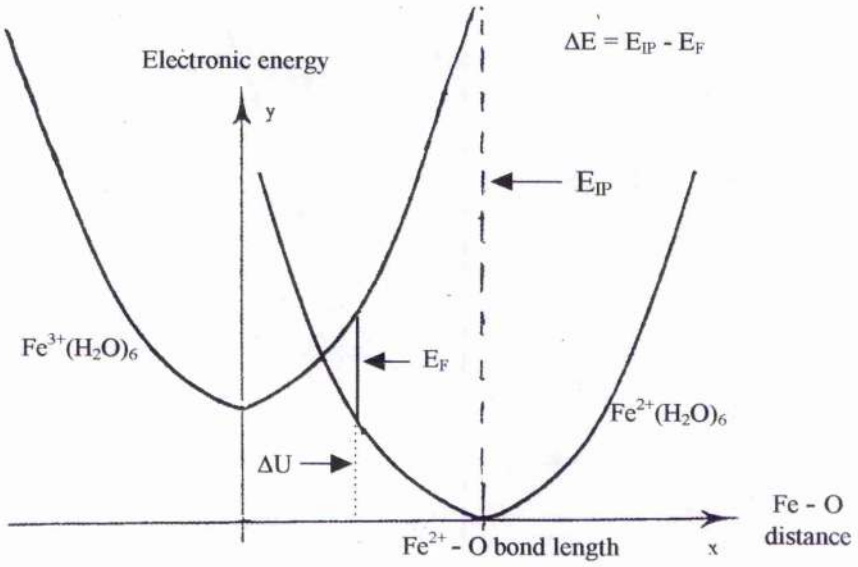

Figure 4.7 Representation of the ionisation potential for the Fe^{2+}/Fe^{3+} redox couple

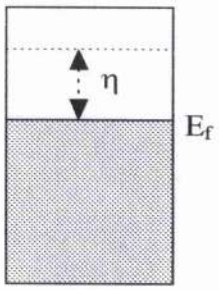

Figure 4.8 Alteration of the electrode potential by a value η

where C_{Fe}^{2+} is the concentration of the Fe(II) species and k_s is the standard rate constant.

Since $\Delta U = \alpha_A \Delta E = \alpha_A(E_{IP} - E_p)$

then $j_a = C_{Fe}^{2+} k_{sh} \exp [-(\alpha_A \Delta E)/RT]$

On changing the electrode potential by η, the overpotential (see figure 4.8)

$$\Delta E' = E_{ip} - (E_F + F\eta)$$

$$-\Delta U = -\alpha_A (E_{IP} - E_F - F\eta)$$

$$= -\alpha_A \Delta E + \alpha_A F\eta$$

giving

$$j_a = C_{Fe}^{2+} k_s \exp \{(-\alpha_A \Delta E + \alpha_A F\eta) / RT\}$$

$$j_a = C_{Fe}^{2+} k_s \exp \{-\alpha_A \Delta E / RT\} \exp \{\alpha_A F\eta / RT\}$$

Similarly,

$$j_c = C_{Fe}^{3+} k_s \exp \{\alpha_C \Delta E / RT\} \exp \{-\alpha_C F\eta / RT\}$$

At equilibrium $\eta = 0$ and $j_a = j_c = j_0$

For a one electron transfer, the current density is defined as $I = Fj$ and the exchange current density is given by $I_0 = Fj_0$

Thus,

$$I_a = FC_{Fe}^{2+} k_s \exp \{-\alpha_A \Delta E / RT\} \exp \{\alpha_A F\eta / RT\} \quad \text{eqn. 4.16}$$

and

$$I_0 = FC_{Fe}^{2+} k_s \exp \{-\alpha_A \Delta E / RT\}$$

$$I_0 = FC_{Fe}^{3+} k_s \exp \{\alpha_C \Delta E / RT\} \qquad \text{eqn. 4.17}$$

Substituting equation 4.17 into equation 4.16 gives

$$I_a = I_0 \exp \{\alpha_A F\eta / RT\}$$

similarly,

$$I_c = I_0 \exp \{-\alpha_C F\eta / RT\}$$

The net current density is given by $I = I_a - I_c$

$$I = I_0 [\exp \{\alpha_A F\eta / RT\} - \exp \{-\alpha_C F\eta / RT\}]$$

which defines the empirical Butler-Volmer equation.

REFERENCES

1 R.W. Gurney, *Proc. Roy. Soc.*, London A 134, 137, 1931

2 R.H. Fowler, *Electrolytes*, ed. H. Falkenhagen (transl. R. Bell), Appendix. London: Oxford Univ. Press, 1934

3 J. Horiuti and M. Polanyi, *Acta Physicochim.*, URSS 2, 505, 1935

4 R.J. Marcus, B.J. Zwolinski and H. Eyring, *J. Phys. Chem.*, 58, 432, 1954

5 R.J. Marcus, B.J. Zwolinski and H. Eyring, *Chem. Rev.*, 55, 157, 1955

6 E. Sacher and K.J. Laidler, *Trans. Faraday Soc.*, 59, 396, 1963

7 E. Sacher and K.J. Laidler, *Mod. Aspects Electrochem.*, 3, Chap 1, 1964

8 W. Libby, *J. Phys. Chem.*, 56, 863, 1952

9 R. Platzmann and J. Franck, *Z. Physik*, 138, 411, 1954

10 S.I. Pekar, *Investigation of the Electronic Theory of Crystals*, Moscow, 1951

11 A.S. Davydov, *Zh. Eksp. Teor. Fiz.*, 18, 913, 1948

12 R.A. Marcus, *J. Chem. Phys.*, 24, 966, 1956

13 R.A. Marcus, *J. Chem. Phys.*, 26, 867, 1957

14 R.A. Marcus, *Can. J. Chem.*, 37, 155, 1959

15 R.A. Marcus, *Discuss. Faraday Soc.*, 29, 21, 1960

16 R.A. Marcus, *J. Phys. Chem.*, 67, 853, 2889, 1963

17 R.A. Marcus, *Ann. Rev. Phys. Chem.*, 15, 155, 1964

18 R.A. Marcus, *J. Chem. Phys.*, 43, 679, 1965

19 R.A. Marcus, *Electrochim. Acta*, 13, 995, 1968

20 N.S. Hush, *Z. Elektrochem.*, 61, 734, 1957

21 N.S. Hush, *J. Chem. Phys.*, 28, 962, 1958

22 N.S. Hush, *Trans. Faraday Soc.* 57, 557, 1961

23 V.G. Levich and R.R. Dogonadze, *Dokl. Acad. Nauk SSSR*, 124, 123, 1959

24 V.G. Levich and R.R. Dogonadze, *Coll. Czech. Chem. Commun.*, 29, 193, 1961

25 R.R. Dogonadze and Y.A. Chizmadshecv, *Dokl. Acad. Nauk SSSR*, 144, 1077, 1962

26 R.R. Dogonadze, A.M. Kuznetsov and Y.A. Chizmadshecv, *Zh. Fiz. Khim.*, 38, 1195, 1964

27 R.R. Dogonadze & A.M. Kuznetsov, *Izv. Akad. Nauk. SSSR, SER. Khim.*, 1884, 2140, 1964

28 R.R. Dogonadze, *Elecktrokhimiya,* 1, 1434, 1965

29 R.R. Dogonadze & A.M. Kuznetsov, *Elecktrokhimiya,* 1, 742, 1965

30 V.G. Levich, *Itogi nauki, Elecktrokhimiya* 1965

31 V.G. Levich, *Advanc. Electrochem. Eng.*, 4, Chap5, 1966

32 R.R. Dogonadze & A.M. Kuznetsov, *Itogi nauki, Elektrokhimiya* 1967

33 R.R. Dogonadze, A.M. Kuznetsov & V.G. Levich, *Electrochim. Acta,* 13, 1025, 1968

34 R.R. Dogonadze & A.M. Kuznetsov *Elektrokhimiya,* 6, 562, 1970

35 V.G. Levich & Y.I. Kharakats, *Elecktrokhimiya,* 6, 562, 1970

36 R.R. Dogonadze, and A.M. Kuznetsov, Proceedings of the Symposium on Electrocatalysis, ed. M.W. Breiter. The Electrochemical Society. pp195, 1974

37 R.R. Dogonadze & A.M. Kuznetsov, *Progress Surf. Sci.,* 6, 1, 1975

38 J.O'M. Bockris, *Modern Electrochemistry*, vol.2 1970

39 P.P. Schmidt, *J. Chem. Phys.*, 56, 2775, 1972

40 P.P. Schmidt, *J. Chem. Phys.*, 58, 4290, 1973

41 W. Schmickler and W. Vielstich, *Electrochim. Acta*, 18, 883, 1973

42 W. Schmickler, *Ber. Bunsenges. Phys. Chem.*, 77, 991, 1973

43 D.F. Calef & P.G. Wolynes, *J. Phys. Chem.*, 87, 3387, 1983

44 D.F. Calef P.G. Wolynes, *J. Chem. Phys.*, 78, 470, 1983

45 L.D. Zusman, *Elektrokhimiya*, 21, 621, 1985

CHAPTER 5

The $Fe^{3+/2+}$ Redox Couple in Aprotic Solvents

5.1 Aims of chapter

The aim of this investigation is to establish the influence of the solvent on the electrode kinetics of the $Fe^{3+/2+}$ redox couple and by so doing to better understand the role that the solvent characteristics (e.g. dielectric constant, longitudinal relaxation time etc.) and the solute-solvent vibrations play in determining electron transfer processes in general.

5.2 Experimental

All salts and solvents were purified as in chapter 2. Equimolar concentrations of the Fe^{2+} and Fe^{3+} salts from 1 to 20mM were dissolved in a series of solvents along with 0.1M supporting electrolyte. A three electrode cell (described in chapter 2) was used with a platinum working electrode of 2mm diameter.

5.3 Techniques

Ac impedance

The electrode reaction was investigated by ac impedance measurements carried out in the frequency range of 80kHz to 0.1Hz at the equilibrium potential of the working

electrode. All of the complex impedance plots produced have similar features. The high frequency section of the plot intercepts the real axis at a point equal to the bulk resistance of the electrolyte, R_u. In the intermediate frequency range a single semicircle is observed with a capacitance corresponding to 20-50μFcm^{-2} indicating that the semicircle corresponds to the electrode reaction which is the one step process of electron transfer. The low frequency end of the plot exhibits a linear region which can be ascribed to a Warburg impedance, i.e. the diffusion of the electroactive species to and from the electrode. All these features are exhibited in the plot shown in figure 5.1a which serves as a typical example. For most systems both the charge transfer semicircle and the Warburg impedance was present, in some the Warburg impedance was not seen and in a few systems, for example ACN with $LiAsF_6$ as the supporting electrolyte, the Warburg impedance and the semicircle due to the electrode reaction could not be distinguished from each other. The real and imaginary components, Z' and Z'', obtained for all frequencies were analysed using a CNLS program written by MacDonald [1].This program provides a value for the standard apparent rate constant k_{sh}, and also, from this semicircle, the value of the charge transfer resistance R_{ct} and the interfacial capacitance C_{dl} . The equivalent circuit used in the fitting program is illustrated in figure 5.1b.

5.4 Results

Determination of equilibrium potential

Because the reference and the working electrodes were identical except for their size the measured equilibrium potential should be 0V. This was checked by measuring the

Figure 5.1 Typical complex impedance plot for a liquid solvent system (A), and equivalent circuit used to fit the data (B).

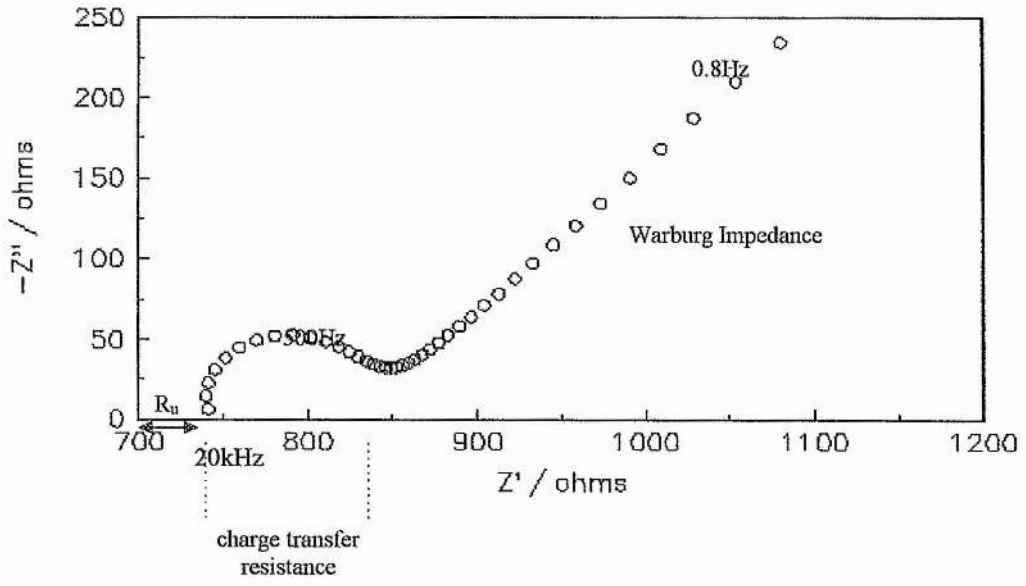

(A)

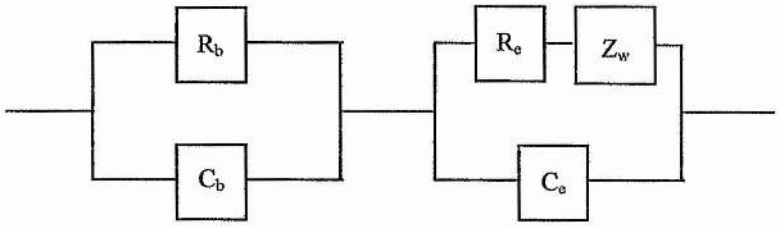

(B)

R_b is the bulk resistance, R_e is the electrode resistance, C_b is the bulk capacitance and C_e is the electrode capacitance, Z_w is the diffusional impedance.

open circuit potential of the cell and by carrying out cyclic voltammetry. Cyclic voltammetry was carried out at a working electrode of diameter 2mm in a three electrode cell configuration (chapter 2 section 2.4.2). Figure 5.2 is a typical example

of the results obtained. It shows the cyclic voltammograms for 1,10 and 50mVs^{-1} of 20mM $Fe^{3+/2+}$ in PC with 0.1M TBAP and, as can be seen, the equilibrium potential of the redox couple was 0V.

5.4.1 Supporting Electrolyte Dependence

Before studying the effects of the solvent parameters on electron transfer, it is necessary to check that the supporting electrolyte has no effect on the kinetics of the reaction The supporting electrolyte must be inert in the potential range of the experiment and it must not react with the electrode or with the products of the electrode reaction. The supporting electrolyte ions can also ion pair with the ions of the redox couple which could lead to the kinetics of the ion pairs being measured instead of the kinetics of the redox couple. All of these possibilities must be ruled out and to achieve this different supporting electrolytes are studied. In any electrochemical system the supporting electrolyte should be completely inert allowing only the required redox system to be studied. To be confident that the supporting electrolyte does not influence the kinetics and does not interact with the system as described above, the standard apparent rate constants obtained for each supporting electrolyte should be in reasonable agreement with each other (i.e. differing by a factor of 3-4). In the supporting electrolytes studies the size of the anion and cation were varied.

The following supporting electrolytes were investigated; tetrabutylammonium perchlorate (TBAP), lithium perchlorate ($LiClO_4$), lithium hexafluoroarsenate ($LiAsF_6$), tetraethylammonium hexafluorophosphate ($TEAPF_6$) and

tetraethylammonium tetrafluoroborate ($TEABF_4$) The studies were carried out using solutions of 10mM iron (II) triflate and 10mM iron (III) triflate in the five solvents with 0.1M solution of the supporting electrolytes. All of these supporting electrolytes dissolve fully in ACN, DMSO, PC and DMF. However, in THF only $LiClO_4$ and TBAP dissolve, $TEABF_4$ is completely insoluble, $LiAsF_6$ and $TEAPF_6$ dissolve initially but the entire solution solidifies after 45 minutes of stirring.

Ac impedance spectroscopy was used to measure the electrode kinetics in the different supporting electrolytes and the data were fitted using the CNLS fitting program written by MacDonald [1]. Figures 5.3-5.24 are the fitted plots for each supporting electrolyte in all five solvents. The fitted curves were in excellent agreement with the original data collected. Tables 5.1-5.5 tabulate these results. It can be assumed that a correction for the diffuse double layer is unnecessary at this concentration of supporting electrolyte [5] and so the rate constants calculated can be regarded as true rate constants.

Figure 5.2 Cyclic voltammogram for 20mM $Fe^{3+/2+}$ in PC with 0.1M TBAP at sweep rates of 1,10 and 50mVs^{-1}

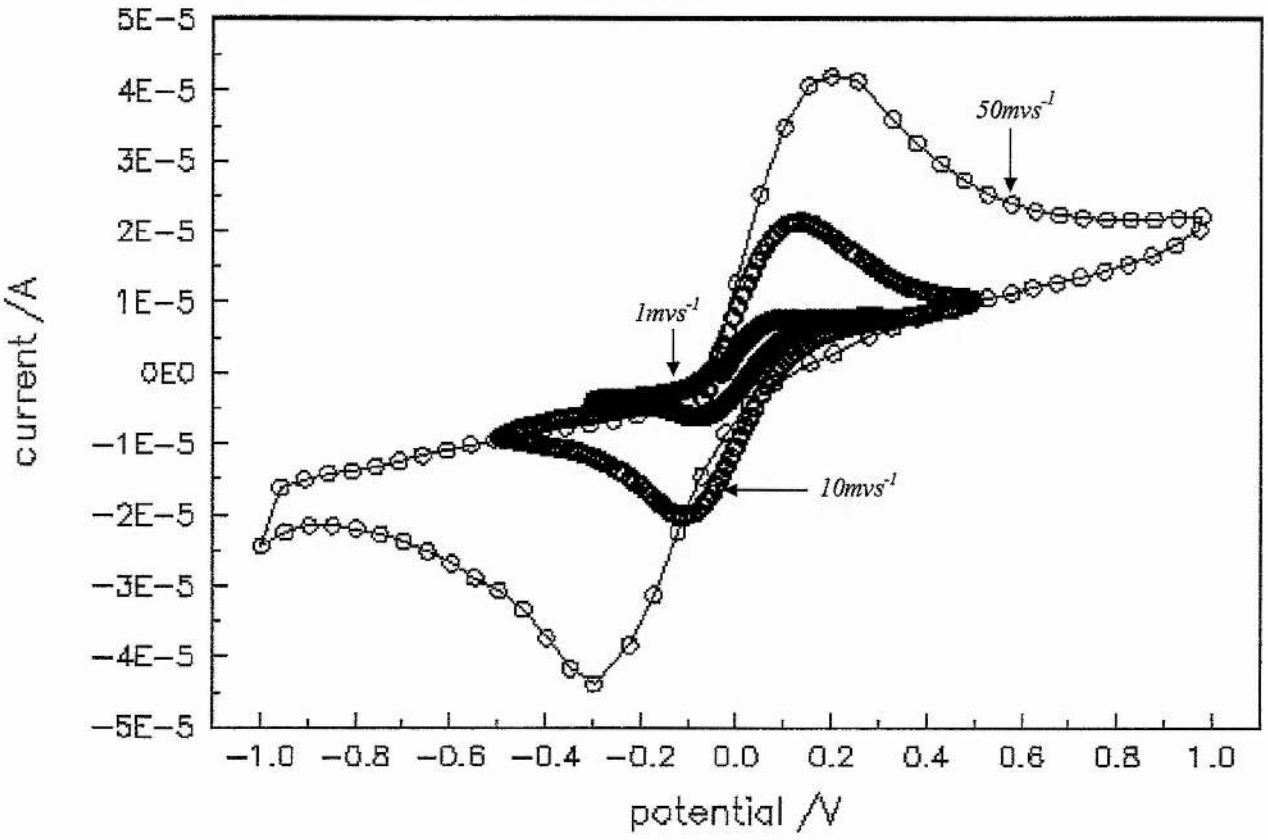

Figure 5.3 Complex impedance plot for 10.02mM Fe (II) / Fe (III) in DMSO with 0.1M TBAP; O representing data and — representing fit

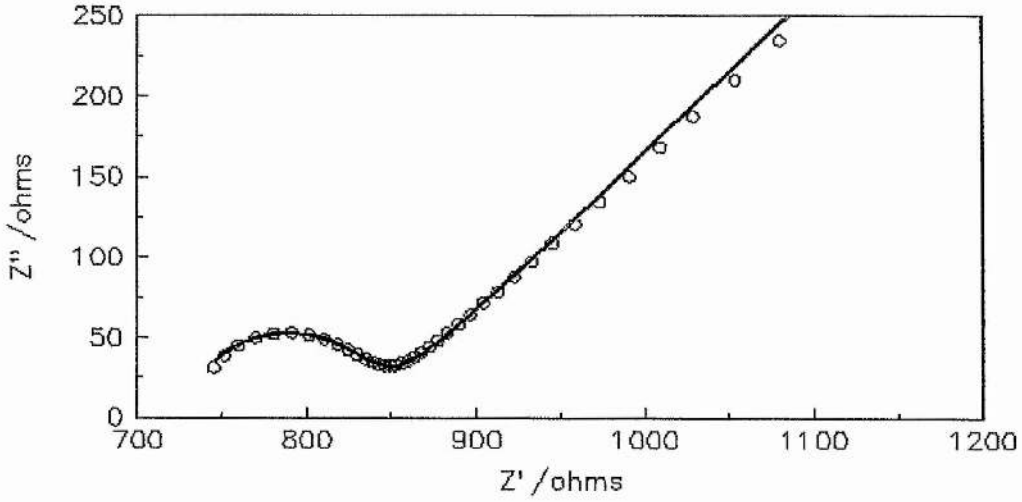

Figure 5.4 Complex impedance plot for 10.02mM Fe (II) / Fe (III) in DMSO with 0.1M $LiClO_4$; O representing data and — representing fit

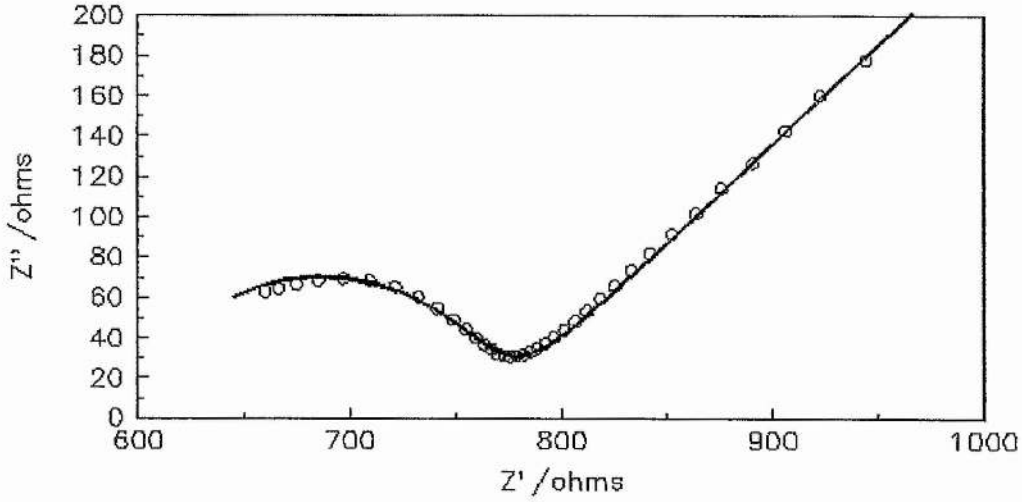

Figure 5.5 Complex impedance plot for 10.02mM Fe (II) / Fe (III) in DMSO with 0.1M $LiAsF_6$; O representing data and — representing fit.

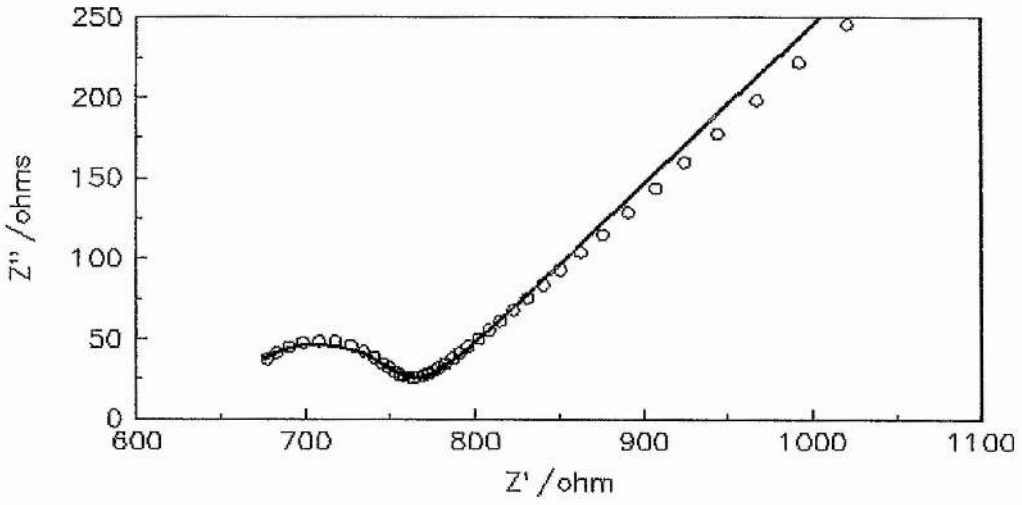

Figure 5.6 Complex impedance plot for 10.11mM Fe (II) / Fe (III) in DMSO with 0.1M $TEAPF_6$; O representing data and — representing fit.

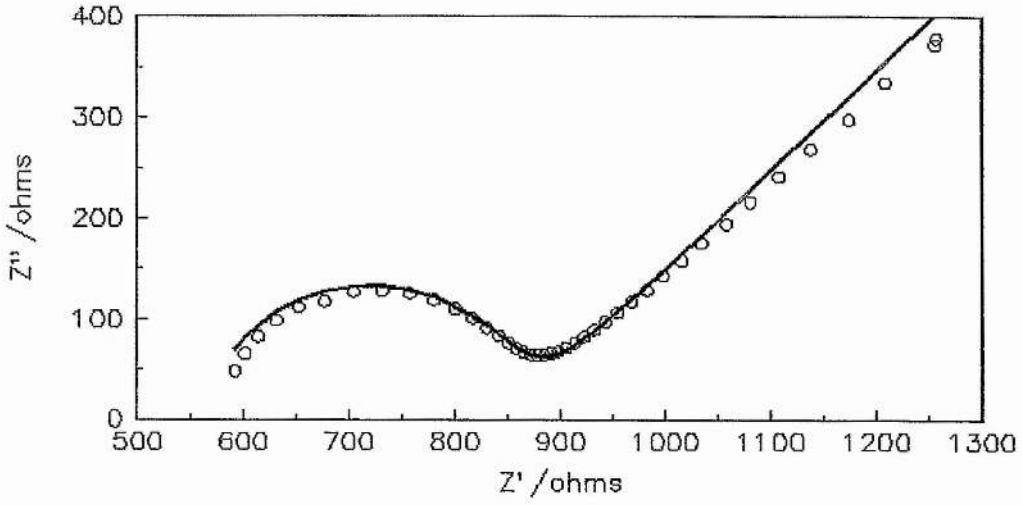

Figure 5.7 Complex impedance plot for 10.11mM Fe (II) / Fe (III) in DMSO with 0.1M $TEABF_4$; O representing data and — representing fit.

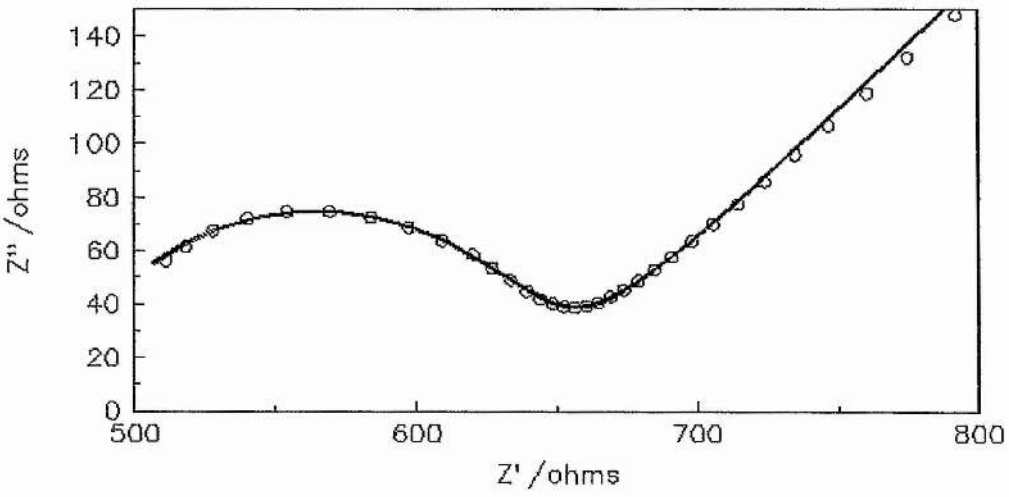

Table 5.1 Results for 10mM Fe (II) / Fe (III) triflate in DMSO

	TBAP	$TEAPF_6$	$LiClO_4$	$LiAsF_6$	$TEABF_4$
C_{dl} (μFcm^{-2})	16	19	18	21	19
D_0 ($10^{-6}cm^2s^{-1}$)	1.52	1.39	2.24	2.0	1.60
R_u (ohms)	729	547	599	649	475
k_{sh} ($10^{-3}cms^{-1}$)	7.99	2.91	5.13	8.05	5.11

Figure 5.8 Complex impedance plot for 10.02mM Fe (II) / Fe (III) in DMF with 0.1M TBAP; O representing data and — representing fit.

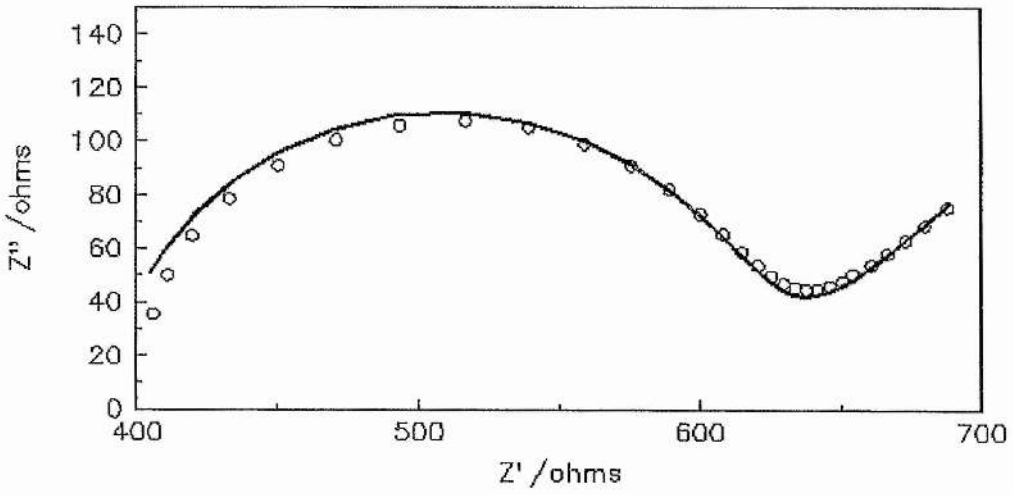

Figure 5.9 Complex impedance plot for 10.02mM Fe (II) / Fe (III) in DMF with 0.1M $LiClO_4$; O representing data and — representing fit.

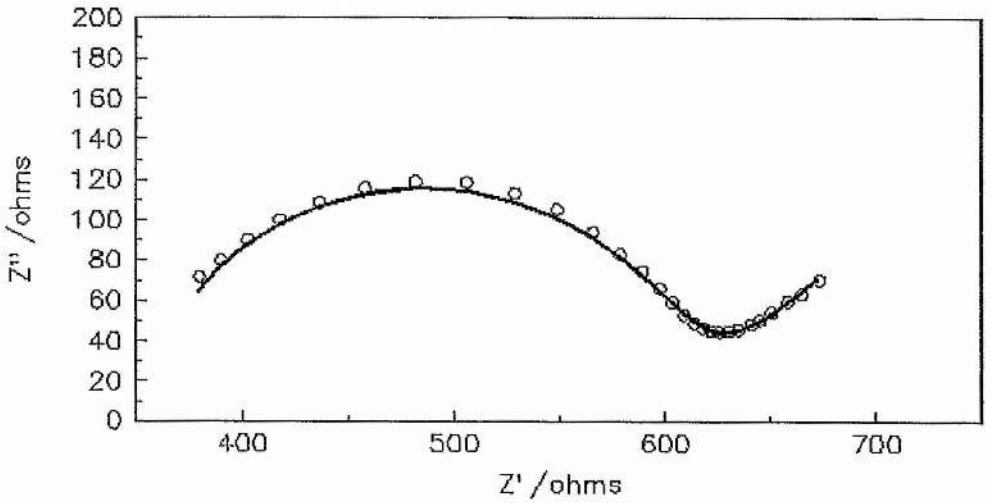

Figure 5.10 Complex impedance plot for 10.02mM Fe (II) / Fe (III) in DMF with 0.1M $LiAsF_6$; O representing data and — representing fit.

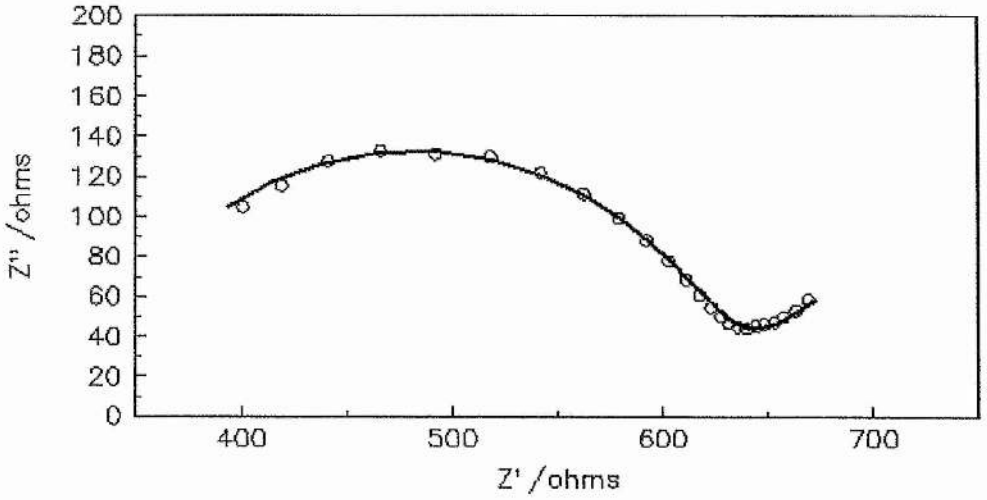

Figure 5.11 Complex impedance plot for 10.04mM Fe (II) / Fe (III) in DMF with 0.1M $TEAPF_6$; O representing data and — representing fit.

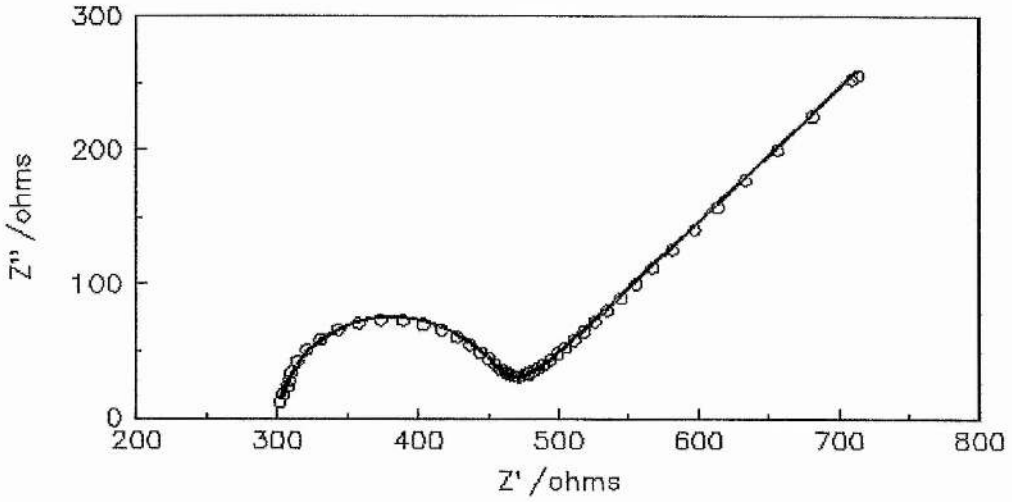

Figure 5.12 Complex impedance plot for 10.04mM Fe (II) / Fe (III) in DMF with 0.1M $TEABF_4$; O representing data and — representing fit.

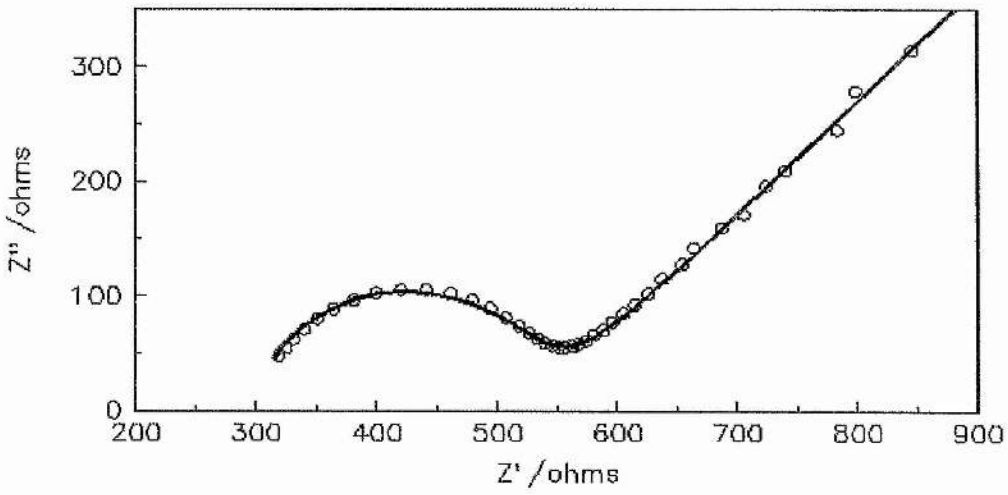

Table 5.2 Results for 10mM Fe (II) / Fe (III) triflate in DMF

	TBAP	$TEAPF_6$	$LiClO_4$	$LiAsF_6$	$TEABF_4$
C_{dl} (μFcm^{-2})	13	14	20	18	28
D_0 ($10^{-6}cm^2s^{-1}$)	2.64	3.18	3.23	4.12	1.51
R_u (ohms)	390	301	352	331	297
k_{sh} ($10^{-3}cms^{-1}$)	3.78	5.57	3.35	2.94	3.59

Figure 5.13 Complex impedance plot for 10.01mM Fe (II) / Fe (III) in PC with 0.1M TBAP; O representing data and — representing fit.

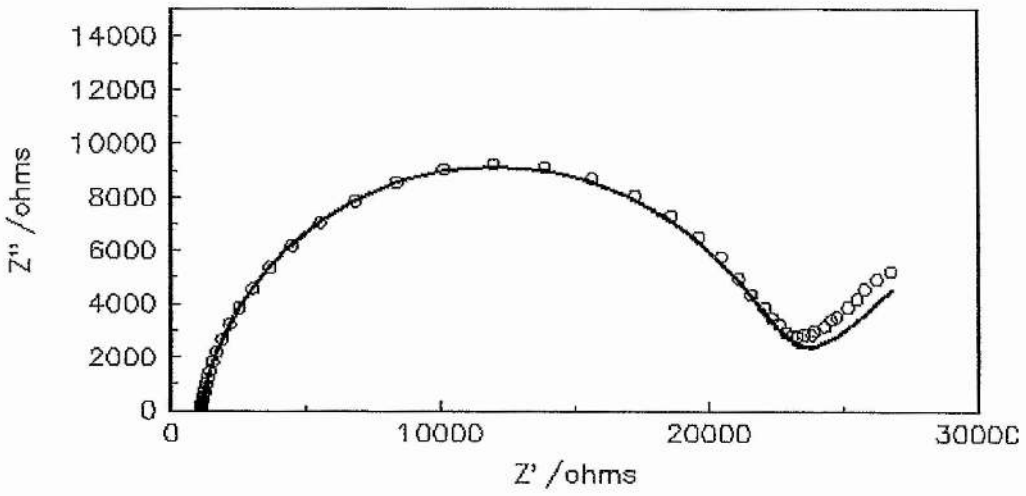

Figure 5.14 Complex impedance plot for 10.01mM Fe (II) / Fe (III) in PC with 0.1M $LiClO_4$; O representing data and — representing fit.

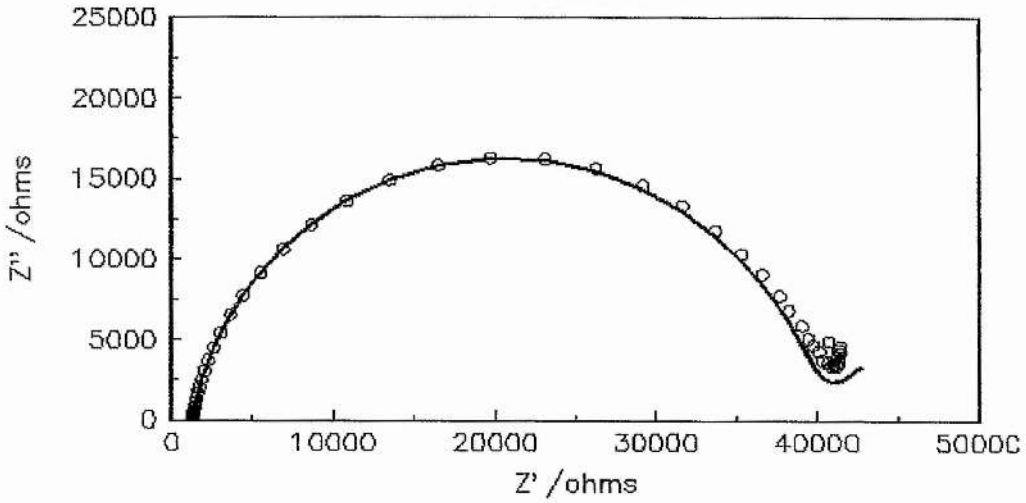

Figure 5.15 Complex impedance plot for 10.01mM Fe (II) / Fe (III) in PC with 0.1M $LiAsF_6$; O representing data and — representing fit.

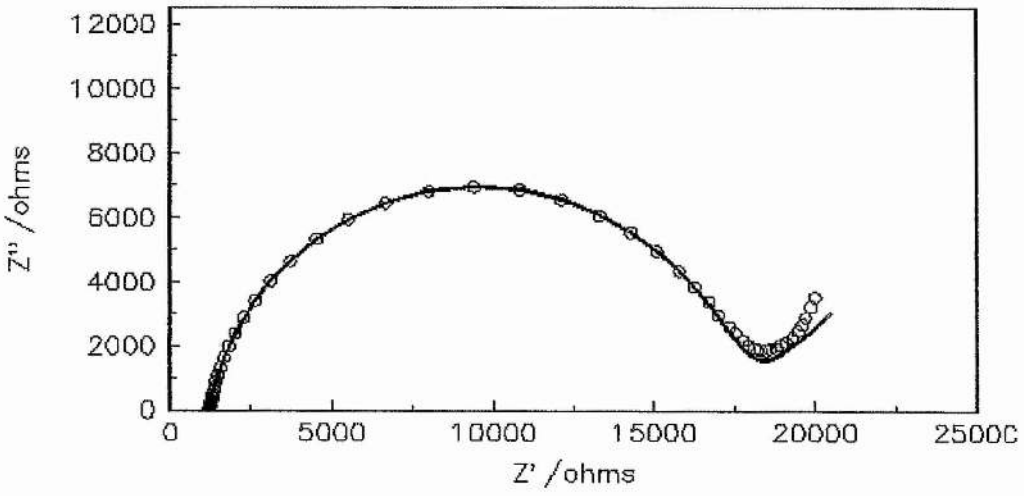

Figure 5.16 Complex impedance plot for 10.02mM Fe (II) / Fe (III) in PC with 0.1M $TEAPF_6$; O representing data and — representing fit.

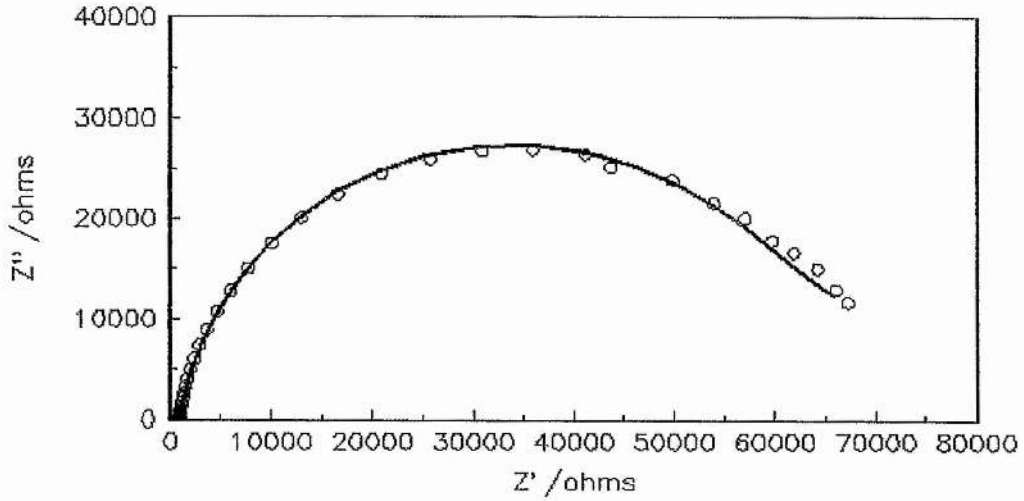

Figure 5.17 Complex impedance plot for 10.02mM Fe (II) / Fe (III) in PC with 0.1M $TEABF_4$; O representing data and — representing fit.

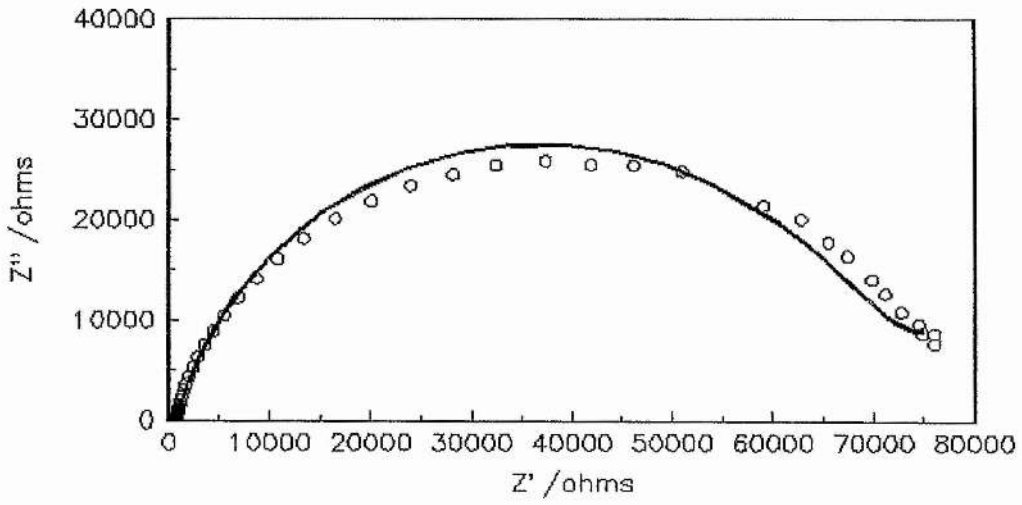

Table 5.3 Results for Fe (II) / Fe (III) triflate in PC

	TBAP	$TEAPF_6$	$LiClO_4$	$LiAsF_6$	$TEABF_4$
C_{dl} (μFcm^{-2})	28	23	25	32	39
D_0 ($10^{-7}cm^{-2}s^{-1}$)	3.02	1.44	9.53	6.65	2.07
R_u (ohms)	1086	827	1279	1210	704
k_{sh} ($10^{-5}cms^{-1}$)	4.00	1.36	2.23	5.23	1.21

Figure 5.18 Complex impedance plot for 9.99mM Fe (II) / Fe (III) in ACN with 0.1M TBAP; O representing data and — representing fit.

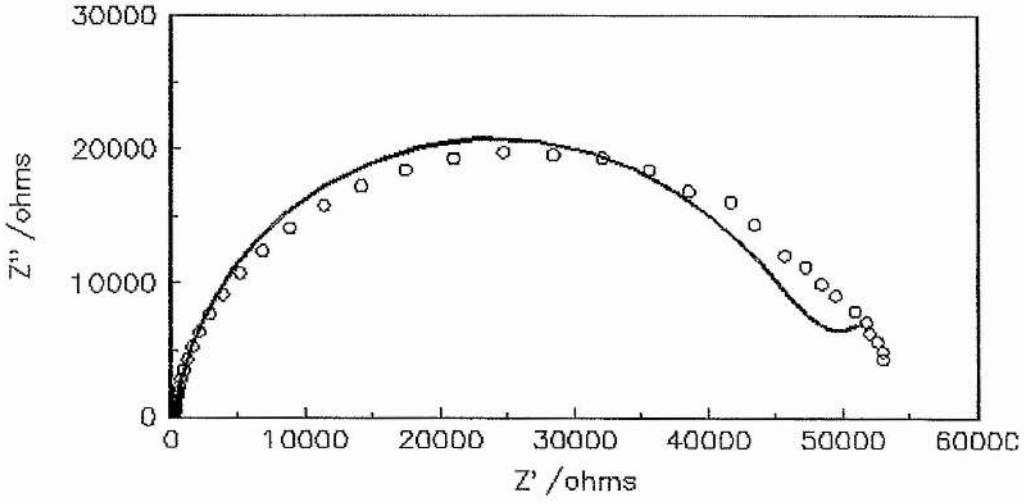

Figure 5.19 Complex impedance plot for 9.99mM Fe (II) / Fe (III) in ACN with 0.1M $LiClO_4$; O representing data and — representing fit.

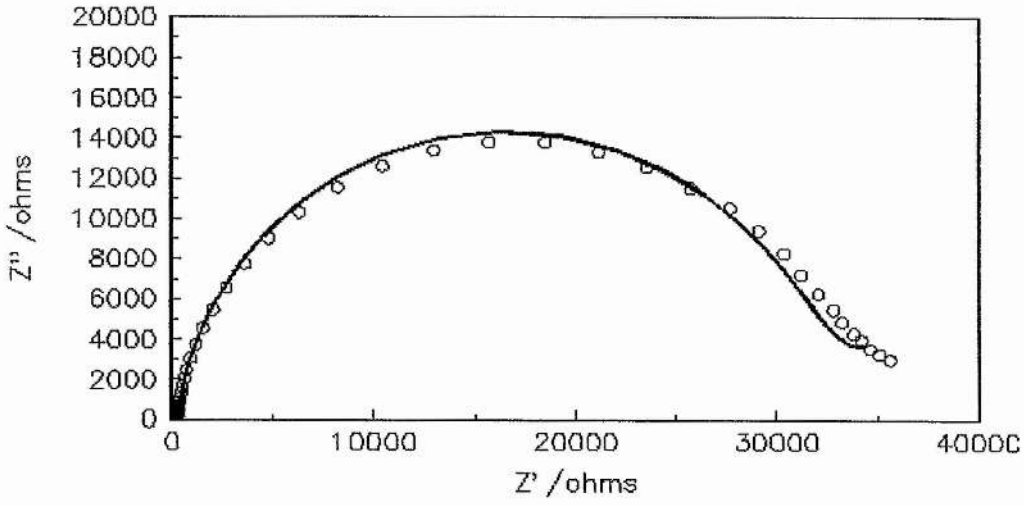

Figure 5.20 Complex impedance plot for 9.99mM Fe (II) / Fe (III) in ACN with 0.1M $LiAsF_6$; O representing data and — representing fit.

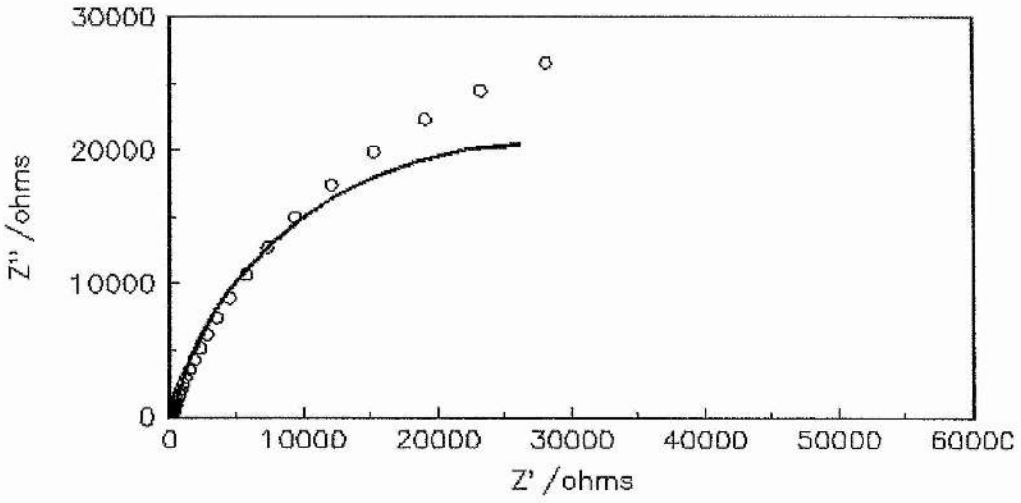

Figure 5.21 Complex impedance plot for 10.01mM Fe (II) / Fe (III) in ACN with 0.1M $TEAPF_6$; O representing data and — representing fit.

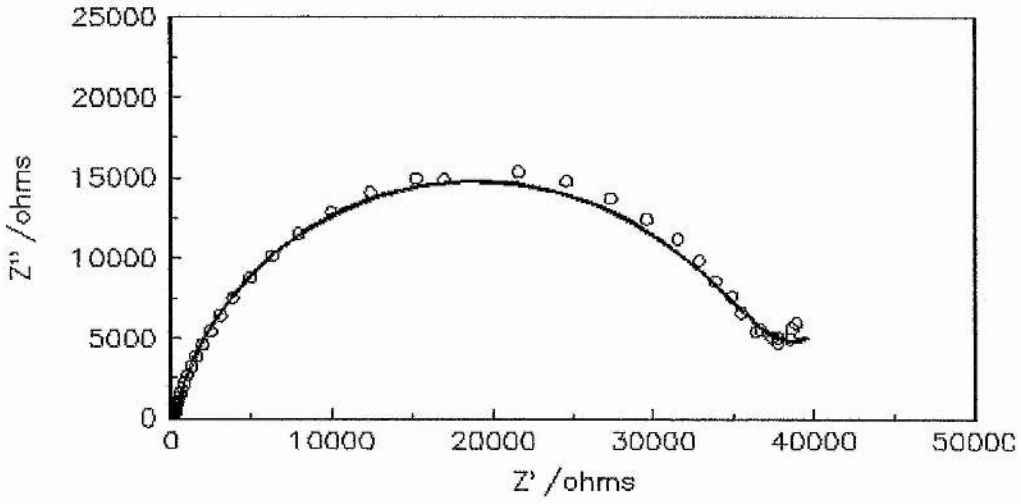

Figure 5.22 Complex impedance plot for 10.01mM Fe (II) / Fe (III) in ACN with 0.1M $TEABF_4$; O representing data and — representing fit.

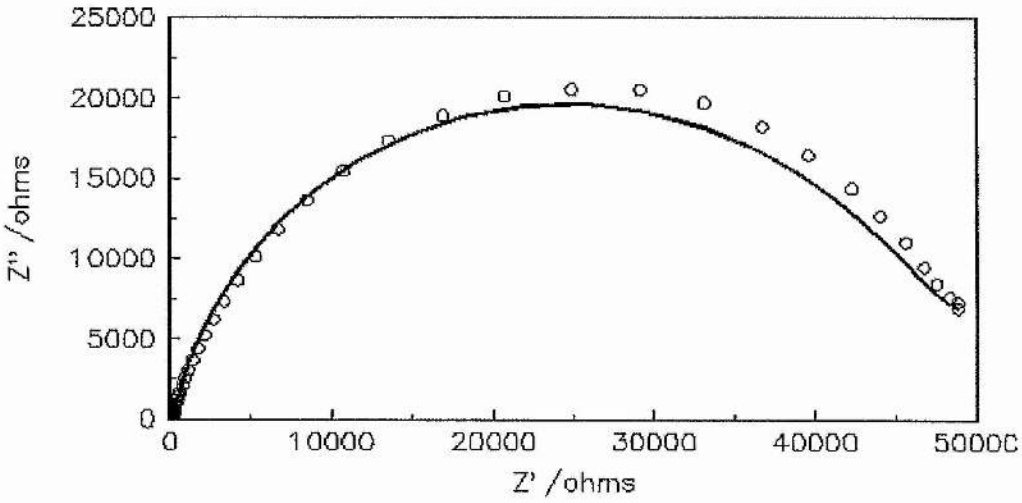

Table 5.4 Results for 10mM Fe (II) / Fe (III) triflate in ACN

	TBAP	$TEAPF_6$	$LiClO_4$	$LiAsF_6$	$TEABF_4$
C_{dl} (μFcm^{-2})	18	39	21	33	36
D_0 ($10^{-7}cm^{-2}s^{-1}$)	0.46	1.34	1.46	0.04	1.01
R_u (ohms)	235	172	259	216	167
k_{sh} ($10^{-5}cms^{-1}$)	1.86	2.36	2.68	1.89	1.81

Figure 5.23 Complex impedance plot for 10mM Fe (II) / Fe (III) in THF with 0.1 M TBAP; O representing data and — representing fit.

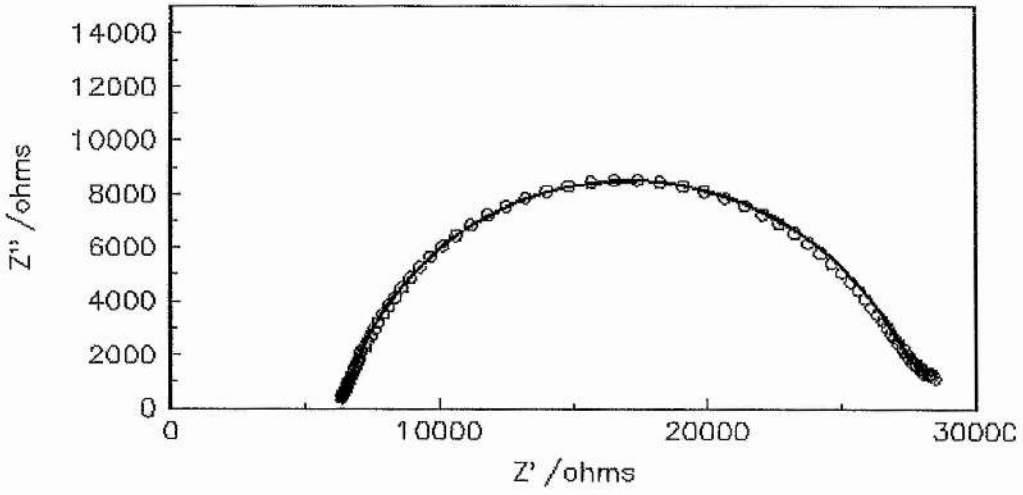

Figure 5.24 Complex impedance plot for 10mM Fe (II) / Fe (III) in THF with 0.1 M $LiClO_4$; O representing data and — representing fit.

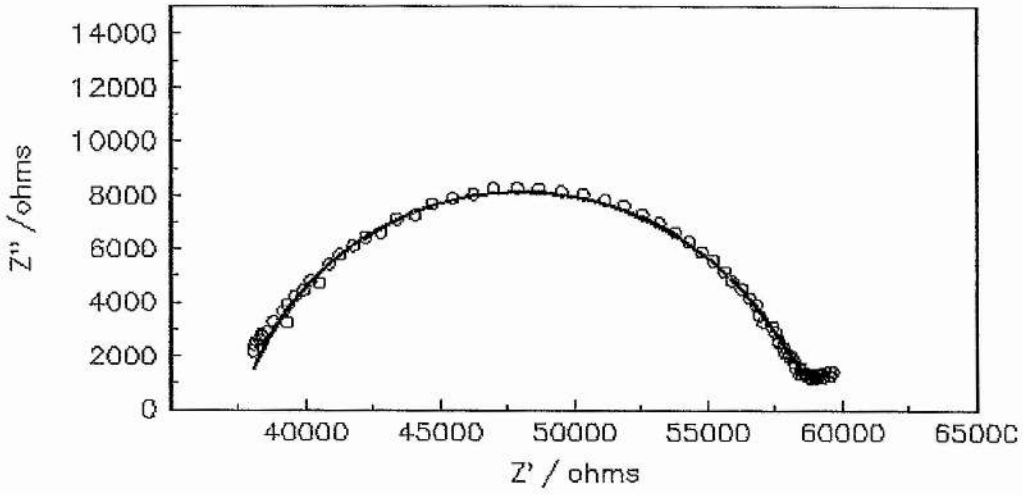

Table 5.5 Results for 10mM Fe (II) / Fe (III) triflate in THF

	TBAP	$LiClO_4$
C_{dl} (μFcm^{-2})	20	24
D_0 ($10^{-6}cm^2s^{-1}$)	1.64	1.54
R_u (ohms)	6343	37551
k_{sh} ($10^{-5}cms^{-1}$)	4.23	4.23

The data obtained for 0.1M LiAsF6 in ACN, and presented in figure 5.20, exhibits a less well defined semicircle than the data for other systems. This was consistently observed and represents the best data that could be obtained.

.

For THF there is no supporting electrolyte dependence, $LiClO_4$ and TBAP give identical results. For DMSO, DMF and ACN the results obtained for all five supporting electrolytes vary by a maximum of a factor of three within each solvent, indicating a slight supporting electrolyte dependence within each solvent. For PC the results obtained for the five supporting electrolytes are somewhat different. The rate constants obtained for TBAP, $LiClO_4$ and $LiAsF_6$ vary a factor of 3, but when all five salts are taken into account the overall variation of k_{sh} with supporting electrolyte is 5; however, the results obtained for $TEAPF_6$ and $TEABF_4$ are equal within

experimental error. The variation within each solvent is relatively small when compared to the results obtained for a specific supporting electrolyte in all five solvents. For example 0.1M TBAP with 10mM $Fe^{3+/2+}$ in DMSO gives a value for the rate constant of 7.99×10^{-3} cms^{-1} whereas in ACN the value decreases to 1.86×10^{-5} cms^{-1}, a difference of a factor of over 400. This factor is obviously more significant than the slight supporting electrolyte dependence indicated in the results.

5.4.2 Concentration Dependence

In view of the high charge of the electroactive species (2+ and 3+), and the low dielectric constant of the solvents association between the iron ions and the anions present in the electrolyte is a distinct possibility. The fact that different supporting electrolytes yield similar k_{sh} values suggests that such ion association between $Fe^{3+/2+}$ and anions from the supporting electrolyte does not influence the kinetics, or is not present. However, $Fe^{3+/2+}$–counter anion ion pairing would be dependent on the concentration of the $Fe^{3+/2+}$ ions present in solution; and if a dependence on concentration of $Fe^{3+/2+}$ is not found for the rate constant then this possibility can be eliminated. A dependence of k_{sh} on concentration indicates possible ion pairing between the iron ions and the triflate anions.

Ac impedance was employed to probe the concentration dependence. 20mM, 10mM and 1mM concentrations of the electroactive species were studied, using 0.1M TBAP as the supporting electrolyte, in all five solvents. Figures 5.25-5.34 are the complex impedance plots obtained in this section of the study. The fitted curves are in

in excellent agreement with the data and the calculated values from the CNLS program [1] are tabulated in tables 5.6-5.10.

Figure 5.25 Complex impedance plot for 20mM Fe (II) / Fe (III) in DMSO with 0.1M TBAP; O representing the data and – representing the fit.

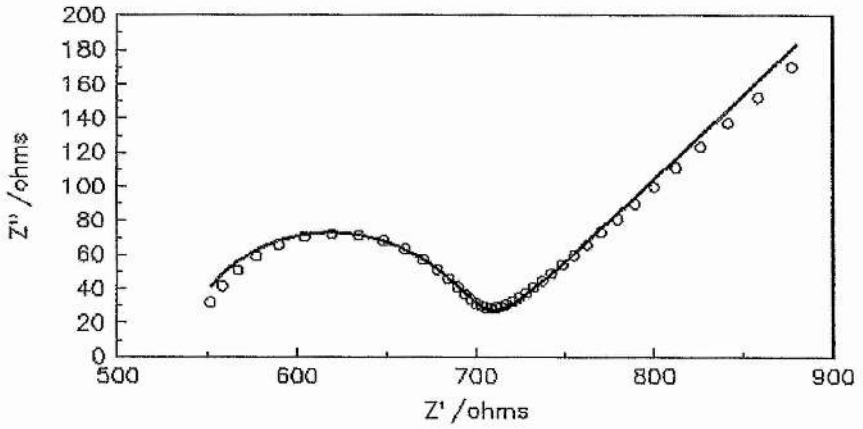

Figure 5.26 Complex impedance plot for 1mM Fe (II) / Fe (III) in DMSO with 0.1M TBAP; O representing the data and – representing the fit.

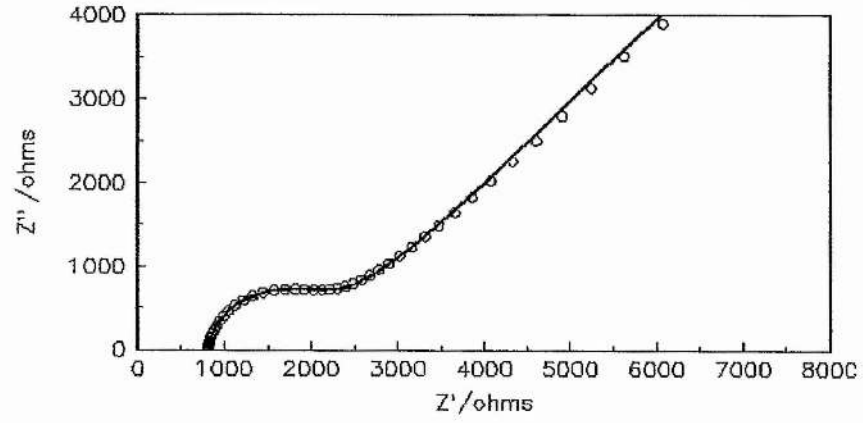

Table 5.6 Summary of results for concentration dependence in DMSO with 0.1M TBAP

	20mM $Fe^{3+/2+}$	10mM $Fe^{3+/2+}$	1mM $Fe^{3+/2+}$
C_{dl} (μFcm^{-2})	16	16	22
D_0 ($10^{-6}cm^2s^{-1}$)	2.01	1.52	1.03
R_u (ohms)	513	729	813
k_{sh} ($10^{-3}cms^{-1}$)	2.69	7.99	5.81

Figure 5.27 Complex impedance plot for 20mM Fe (II) / Fe (III) in DMF with 0.1M TBAP; O representing the data and – representing the fit.

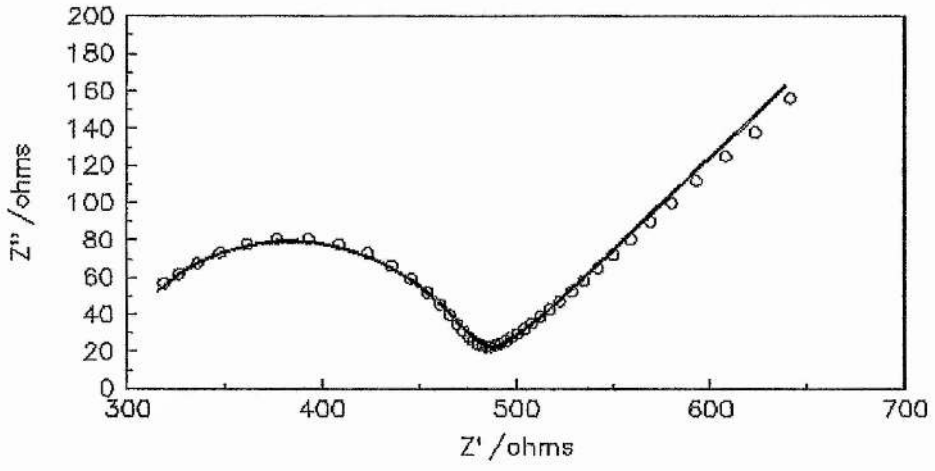

Figure 5.28 Complex impedance plot for 1mM Fe (II) / Fe (III) in DMF with 0.1M TBAP; O representing the data and – representing the fit.

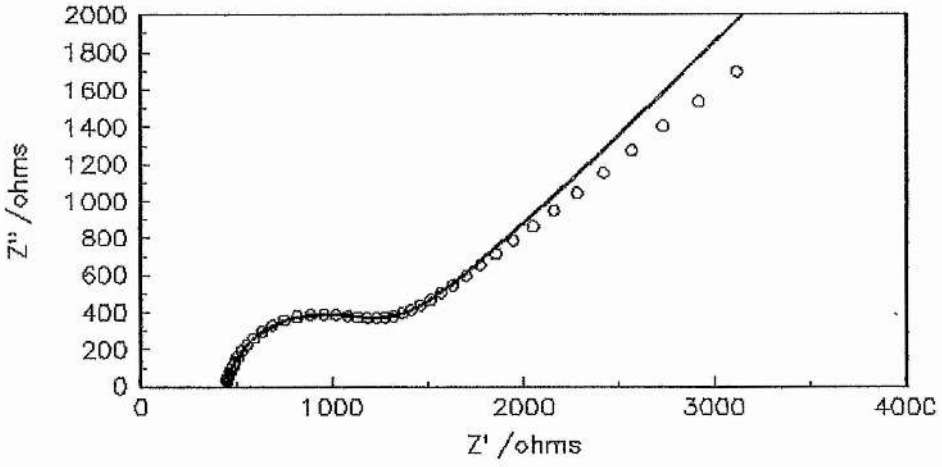

Table 5.7 Summary of results for concentration dependence in DMF with 0.1M TBAP

	20mM $Fe^{3+/2+}$	10mM $Fe^{3+/2+}$	1mM $Fe^{3+/2+}$
C_{dl} (μFcm^{-2})	27	13	29
D_0 ($10^{-6}cm^2s^{-1}$)	2.89	2.64	1.12
R_u (ohms)	329	390	447
k_{sh} ($10^{-3}cms^{-1}$)	2.39	3.78	9.58

Figure 5.29 Complex impedance plot for 20mM Fe (II) / Fe (III) in PC with 0.1M TBAP; O representing the data and – representing the fit.

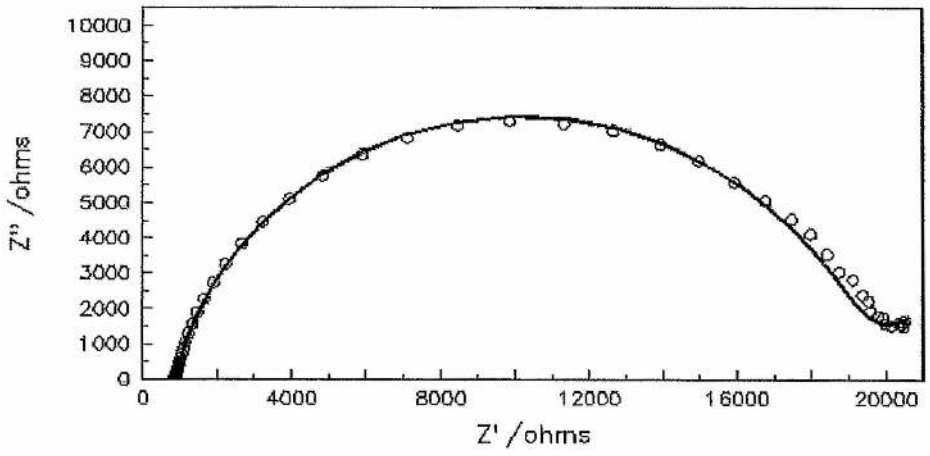

Figure 5.30 Complex impedance plot for 1mM Fe (II) / Fe (III) in PC with 0.1M TBAP; O representing the data and – representing the fit.

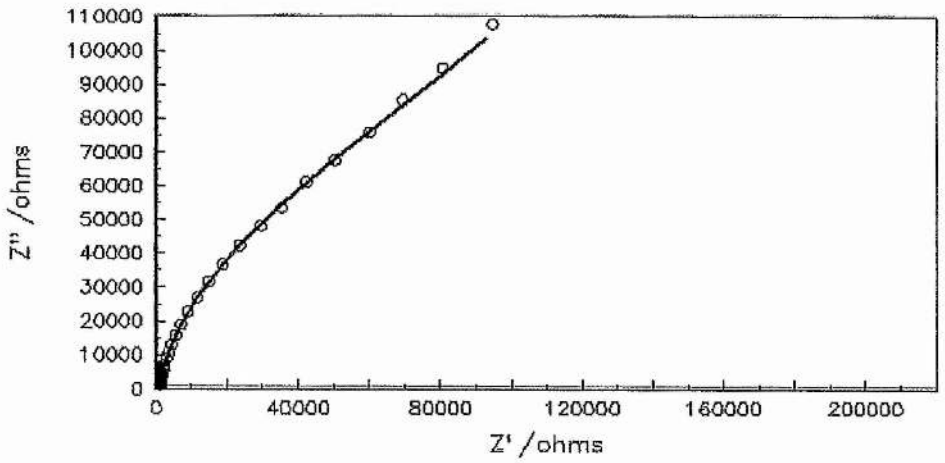

Table 5.8 Summary of results for concentration dependence in PC with 0.1M TBAP

	20mM $Fe^{3+/2+}$	10mM $Fe^{3+/2+}$	1mM $Fe^{3+/2+}$
C_{dl} (μFcm^{-2})	38	29	28
D_0 ($10^{-7}cm^2s^{-1}$)	6.56	3.02	2.22
R_u (ohms)	996	1086	1462
k_{sh} ($10^{-5}cms^{-1}$)	2.35	4.00	9.32

Figure 5.31 Complex impedance plot for 20mM Fe (II) / Fe (III) in ACN with 0.1M TBAP; O representing the data and – representing the fit.

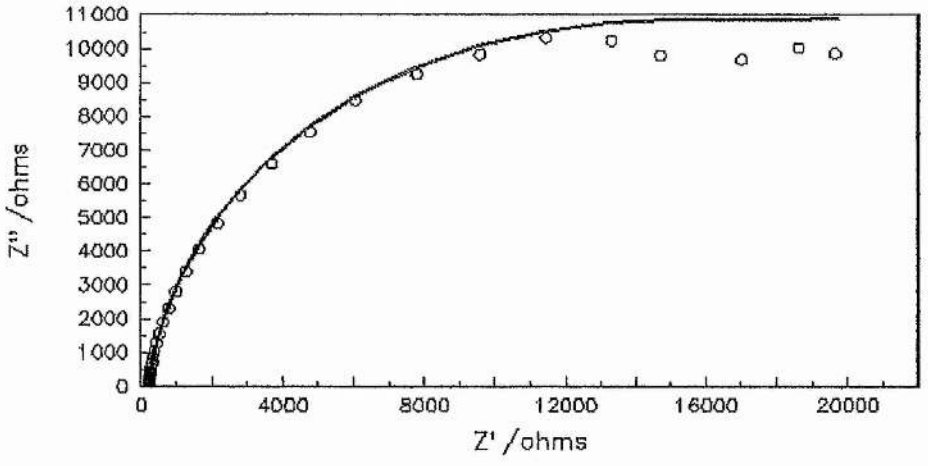

Figure 5.32 Complex impedance plot for 1mM Fe (II) / Fe (III) in ACN with 0.1M TBAP; O representing the data and – representing the fit.

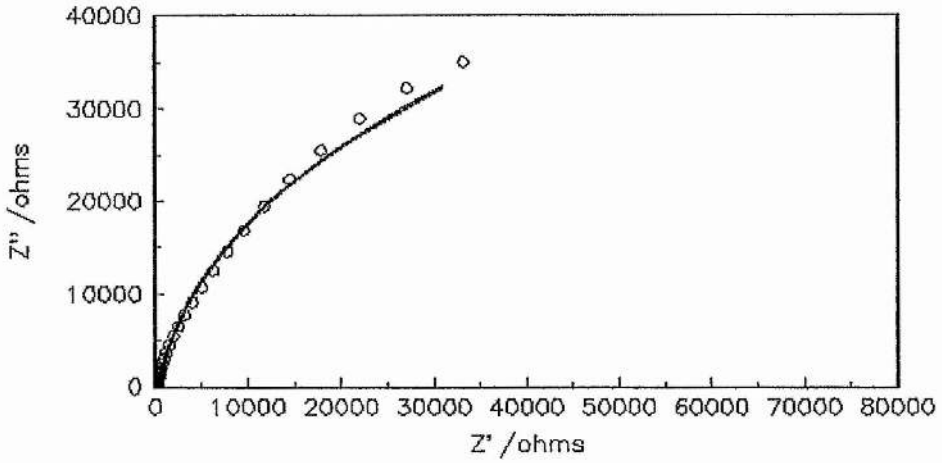

Table 5.9 Summary of results for concentration dependence in ACN with 0.1M TBAP

	20mM $Fe^{3+/2+}$	10mM $Fe^{3+/2+}$	1mM $Fe^{3+/2+}$
C_{dl} (μFcm^{-2})	28	19	14
D_0 ($10^{-8}cm^2s^{-1}$)	36.6	4.64	3.33
R_u (ohms)	221	235	442
k_{sh} ($10^{-5}cms^{-1}$)	2.17	1.86	13.1

Figure 5.33 Complex impedance plot for 20mM Fe (II) / Fe (III) in THF with 0.1M TBAP; O representing the data and – representing the fit.

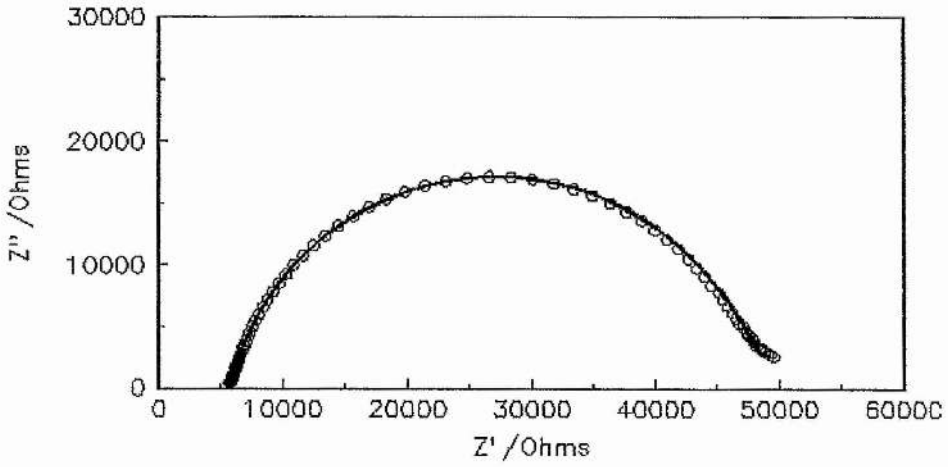

Figure 5.34 Complex impedance plot for 1mM Fe (II) / Fe (III) in THF with 0.1M TBAP; O representing the data and – representing the fit.

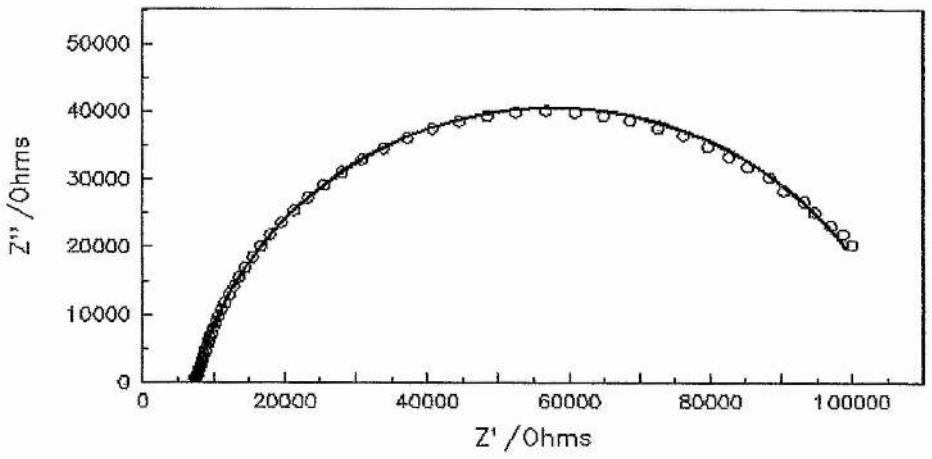

Table 5.10 Summary of results for concentration dependence in THF with 0.1M TBAP

	20mM $Fe^{3+/2+}$	10mM $Fe^{3+/2+}$	1mM $Fe^{3+/2+}$
C_{dl} (μFcm^{-2})	28	20	24
D_0 ($10^{-6}cm^2s^{-1}$)	3.41	1.64	1.01
R_u (ohms)	5742	6343	7442
k_{sh} ($10^{-5}cms^{-1}$)	1.11	4.23	8.88

For all five solvents there seems to be some concentration dependence. In DMSO the rate constants vary by a factor of three, in DMF and PC the rates vary by a factor of 4, in ACN by a factor of 7 and in THF by a factor of 8. The data obtained for the PC and ACN systems are poor which could explain the abnormally high values of k_{sh} for concentrations of 1mM $Fe^{3+/2+}$. For DMF, PC, ACN and THF 1mM $Fe^{3+/2+}$ provides the fastest rate constant. This concentration dependence indicates that there is slight ion pairing between the iron ions and the triflate ions, but this effect is again masked by the solvent dependence of the rate constants.

5.5 Discussion

Influence of Solvent Parameters

The results have established a minimal influence of supporting electrolyte but there is a definite indication of concentration dependence for the rate of electron transfer for the $Fe^{3+/2+}$ redox couple. However, by far the largest variation in k_{sh} came with solvent type, typically two orders of magnitude. The next step is to consider what factors of the solvent influence the kinetics of electron transfer.

The influences of the solvent on the rate of electron transfer arise from a number of sources: alterations in the longer range reactant-solvent interactions in the outer sphere and as metal-ligand bond vibrations in the inner sphere. The $Fe^{3+/2+}$ redox couple is complexed by the solvent and because of this significant inner sphere vibrational activation is expected. However, the extent of this influence is not known and it is possible that there is an influence on the kinetics of the couple from the outer sphere solvent dynamics.

Each of these influences can be identified with a measurable solvent parameter. The solvents were carefully selected to provide a range of values for the different parameters while also being capable of dissolving the redox couple. These are summarized in table 5.11. To investigate the influences of these solvent parameters it is necessary to try and correlate them with the rate constant for the redox couple.

Table 5.11 Solvent parameters for DMSO, DMF, PC, ACN and THF.

	Donor number	$\tau_L^a \times 10^{12}/s$ longitudinal dielectric relaxation time	$\left(\varepsilon_{op}^{-1} - \varepsilon_s^{-1}\right)$ polarity parameter or Pekar Factor
DMSO	29.8	2.4	0.437
DMF	26.6	1.3	0.462
PC	15.1	2.6	0.481
ACN	14.1	0.2	0.526
THF	20.0	3.3	0.372

5.5.1 Outer Sphere Contributions

In the outer sphere the solvent can have an influence in a number of ways, the first of which is via τ_L, *the longitudinal relaxation time.*

τ_L is a measure of the rate at which the solvent dipoles reorientate or relax back to their equilibrium state, around the ion. It indicates the speed at which the solvent sheath alters to allow an incoming electron to the ion the solvent is surrounding or an electron to leave the ion. If τ_L is slow then this can have an effect on the rate of electron transfer as it becomes the rate determining step. Correlation of the rate

constant to this parameter indicates the importance of solvent reorientation in the activation of electron transfer [17-31]. In the 'encounter pre-equilibrium model the rate constant k_{sh} can be expressed by:

$$k_{sh} = \kappa K_p \nu_n \exp(-G^*/RT)$$

where κ is the electronic transmission coefficient

K_p is the equilibrium constant of precursor complex formation

ν_n is the nuclear frequency factor

ν_n can be related to τ_L by the following equation:

$$\nu_n = \tau_L^{-1} (G^*/4\pi RT)^{1/2}$$

If the rate constant is strongly dependent on τ_L then solvent reorientation dynamics play an important role in the kinetics of the reaction: the rather slow reorientation of the solvent molecules gives a significant contribution to the overall activation energy of the electrode process.

If outer sphere solvent reorientation effects predominate in the pre-exponential factor then k_{sh} should vary linearly with τ_L^{-1}. Using values of k_{sh}, determined at a concentration of 10mM for the redox couple and 0.1M TBAP, a plot of k_{sh} vs. τ_L^{-1} can be produced (figure 5.35). As can be seen from figure 5.35 the rate constant does not depend directly on τ_L. Previous investigations [2-7,12,16] into the role of this solvent parameter have suggested conclusions as to its role in electron transfer.

Opallo [4] investigated the correlation between electron transfer rates for PPD $\rightleftharpoons$ PPD^{+} + e using solvents whose τ_L varied by a factor of 40. He concluded that solvent reorientation dynamics has a major influence on the kinetics of the one electron transfer for PPD^{+}/PPD. Fawcett and Foss [6] came to a similar conclusion for the redox reaction between the cobaltacenium cation and cobaltocene.

Figure 5.35 Correlation of k_{sh} with τ_L^{-1}

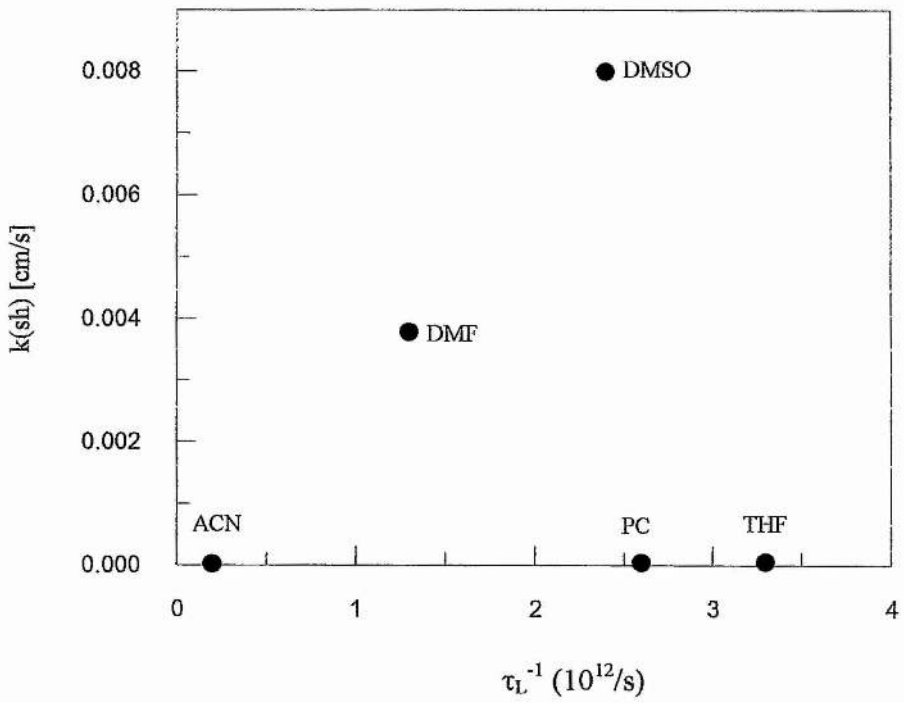

However, in all of these previous investigations the conclusions were drawn from ln k_{sh} vs ln τ_L^{-1} plots. These ln-ln plots only serve to disguise poor fits and if the data presented in figure 5.35 is re-presented in a ln-ln plot (figure 5.36) then a possible linear correlation may be seen, although the data seems to divide into two classes. This sub-division into two groups has no basis as all bar one solvent (PC) are Debye

solvents. If Opallo's data from reference 4 is plotted as k_{sh} vs τ_L^{-1} then no linear correlation is seen.

Figure 5.36 Correlation of ln ksh with ln τ_L^{-1}

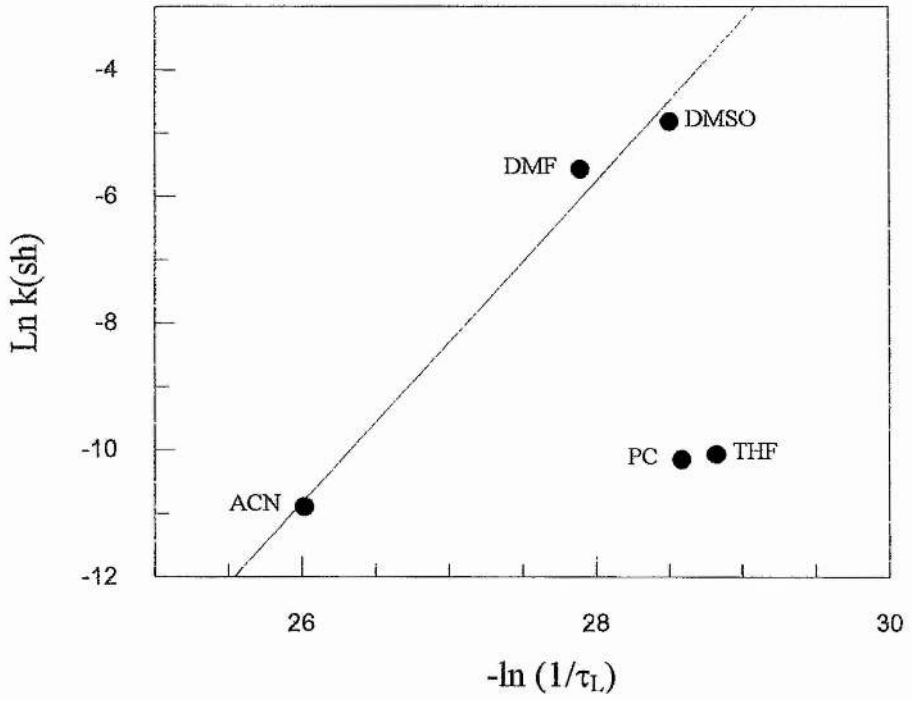

The outer sphere can also have an influence via the *Pekar factor* (or *polarity parameter*).

The Pekar factor is $\varepsilon_{op}^{-1} - \varepsilon_s^{-1}$ where ε_{op} is the optical permittivity and ε_s is the static permittivity. It is a measure of the polarizability of the solvent and a measure of the strength of interaction between the solvent and the ion in the outer sphere. The polarity parameter also reflects the outer solvation shell effects of the solvent. From

Marcus theory [16] the Pekar factor governs G*, the free energy for activation of electron transfer [12], via the outer sphere contribution G*(os) to it.

The outer sphere contribution G*(os) can be calculated from

$$G^*(os) = 0.5(ne)^2 (a^{-1} - R^{-1}) (\varepsilon_{op}^{-1} - \varepsilon_s^{-1})$$

where e is the charge on the electron

a is the radius of the reactant represented as a sphere

R is the distance of the reactant from its image in the conducting electrode

Hence the Pekar factor, $\varepsilon_{op}^{-1} - \varepsilon_s^{-1}$, becomes a major determinant of the free energy of activation. To investigate the effects of the outer solvation shell on the activation of the electrode process, the polarity parameter must be plotted against ln k_{sh}. Using values of k_{sh}, determined at a concentration of 10mM for the redox couple and 0.1M TBAP, a plot of ln k_{sh} vs. $\varepsilon_{op}^{-1} - \varepsilon_s^{-1}$ can be produced (figure 5.37)

As can be seen from figure 5.37 there is no evidence that k_{sh} is dependent on the Pekar factor . From this it can be concluded that the simple Marcus theory [16] which allows outer solvation shell effects to be estimated, does not describe solvent effects in this case, nor can the outer solvation effects of the transition state theory be used to describe the activation of the electrode process for the $Fe^{3+/2+}$ redox couple. This

conclusion has also been reached by other authors [8,9,14,15] for other redox couples.

Figure 5.37 Correlation of log k_{sh} with polarity parameter

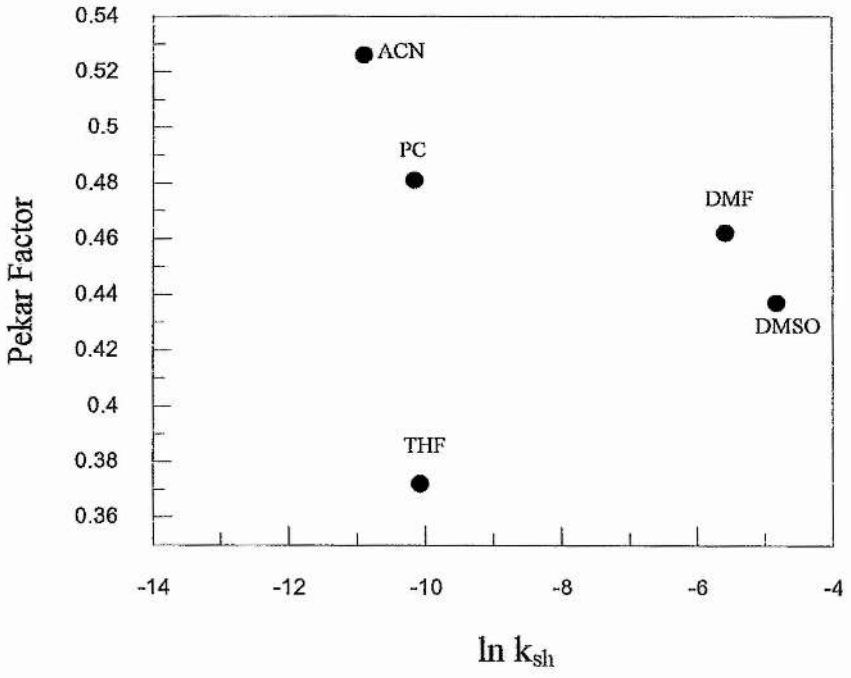

Having found that there is no correlation with either the longitudinal relaxation time, τ_L, or the Pekar factor with the rate of electron transfer, it must be concluded that there is no influence from the outer sphere solvent dynamics on the electrode kinetics of the $Fe^{3+/2+}$ redox couple.

5.5.2 Inner Sphere Contributions

In the inner sphere, there are influences from ion coordination by the solvent. The bonds formed between the Fe^{2+} ion and the solvent ligand and the Fe^{3+} ion and the solvent ligand will vibrate and these inner sphere contributions will have a strong influence on the rate of electron transfer. The extent, however, of this influence is unknown.

In his theory, Marcus [16, 32-36] predicts that there is a contribution to G* arising from inner coordination sphere vibrational activation of electron transfer and this can be related to the force constants and the changes in bond length in going from the oxidised to the reduced species, i.e. $G^* \propto \lambda_i$ where λ_i is given by the following equation:

$$\lambda_i = \Sigma_j k_j k_j^p / k_j + k_j^p (\Delta q_j)^2$$

where k_j and k_j^p denote the force constant of the jth vibrational coordinate in a species involved in the reaction when that species is a reactant and when it is a product respectively and Δq_j is the change in bond distances and bond angles in the inner coordination shell of the reactant:

Table 5.12 lists the changes in bond lengths Δq_j (measured via x-ray crystallography) when going from Fe^{2+} to Fe^{3+} for each of the solvents. As the change in bond length decreases the rate constant increases. Using values of k_{sh} obtained for 10mM $Fe^{3+/2+}$ with 0.1M TBAP the change in k_{sh} with $(\Delta q_j)^2$ is plotted in figure 5.38.

Table 5.12 Summary of metal-solvent bond lengths.

SOLVENT	Change in bond length for $Fe^{2+} \rightarrow Fe^{3+}$ (Å)	Rate constant k_{sh} (cms^{-1})
ACN	0.2121	1.86×10^{-5}
THF	0.1976	4.23×10^{-5}
DMSO	0.1093	7.99×10^{-3}
DMF	0.1064	3.78×10^{-3}

Figure 5.38 Variation of k_{sh} with $(\Delta q_j)^2$

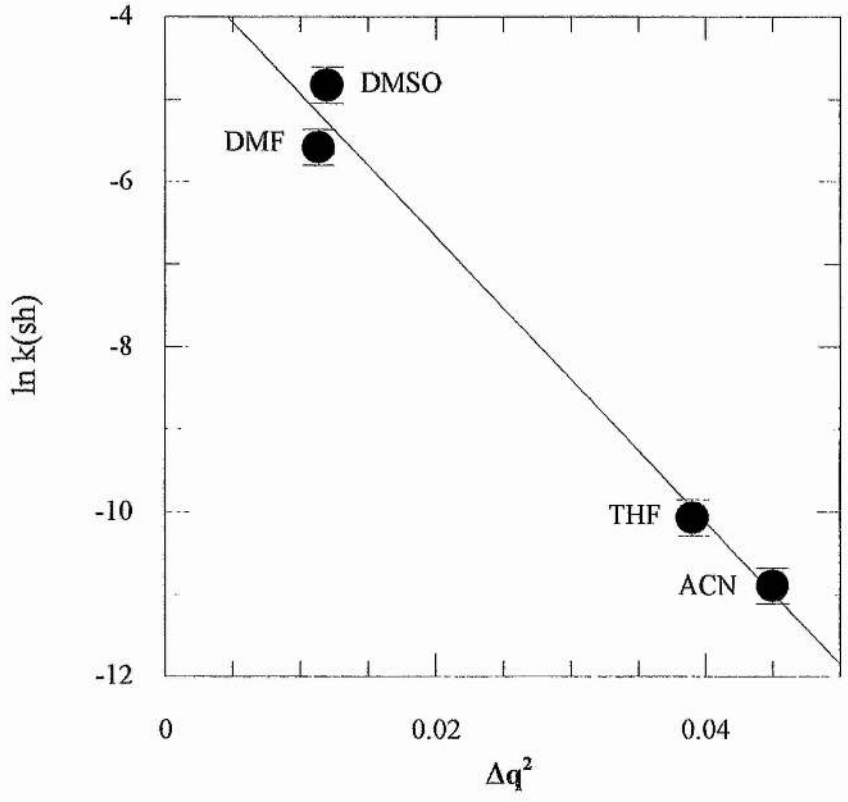

The correlation between k_{sh} and $(\Delta q_j)^2$ indicates significant inner coordination sphere activation of electron transfer. However, the correlation is not as good as was hoped for, which may be due to the fact that the force constants of the systems are unknown. If the force constants were known then λ_i could be fully calculated and the correlation of this with k_{sh} might prove to be excellent.

As electron transfer appears to be activated via inner coordination sphere contributions to G* a plot of ln k_{sh} vs. donor number has been produced (figure 5.39). The values of k_{sh} were determined at a concentration of 10mM for the redox couple and 0.1M TBAP supporting electrolyte.

Figure 5.39 Correlation of ln k_{sh} with donor number

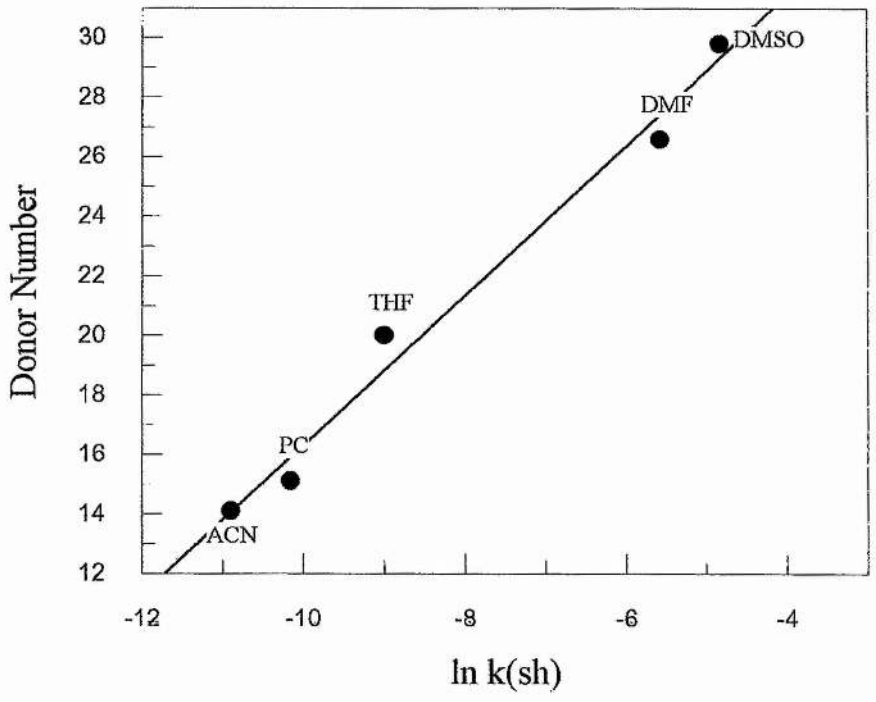

The donor number [10,11] is a measure of the -ΔH value for the interaction of the solvent with $SbCl_5$ in highly diluted dichloroethane i.e.DN ≡ -ΔH($SbCl_5$). The donor number allows the properties of the solvents to be compared from the viewpoint of their ability to coordinate ions. As can be seen in figure 5.39, there is an excellent linear correlation between the donor numbers and the values of the rate constants obtained for each of the solvents.

The donor number of a solvent is a measure of its electron donation to the metal, i.e. it is a measure of the covalency of the bond formed between the solvent ligand (S) and the metal cation (M) in the complex MS_x. It appears that the standard apparent rate constant increases with increasing covalency of the bond indicated by an increase in donor number of the solvent. This can be further understood by looking at ferrocene ($FeCp_2$). Ferrocene can be regarded as a highly covalent reaction between an Fe^{2+} cation and two cyclopentadiene rings. The rate of electron transfer for $FeCp_2$ has been reported as being very fast [5,6], indicating a low activation energy, G*, for electron transfer and high inner sphere contributions to this activation.

5.5.3 Other Possibilities

The investigation into the concentration dependence of k_{sh} yielded a dependence that was greater than expected suggesting a possible alternative to all of the above discussion. It is possible that the investigation has not been measuring electron transfer for an isolated fully dissociated system. The concentration dependence suggests the presence of iron ion - triflate anion pairing. As k_{sh} increases with

decreasing concentration it indicates that the free ions have a faster rate of electron transfer than the ion pairs. The rate of electron transfer also increases with increasing donor number. This can be explained by the fact that the solvent ions and the triflate anions are competing with each to coordinate the iron ions, as the donor number increases the solvent ions win and coordinate the iron ions. This whole argument however, fails when considering the $Fe^{3+/2+}$ redox couple in THF. THF has a low donor number and so it would be expected that there would be strong ion pairing, which would lead to a strong variation with supporting electrolyte. As was reported earlier in this chapter strong variation with supporting electrolyte is not seen, in fact in THF there is no supporting electrolyte dependence.

REFERENCES

1 J.R. Macdonald, J. Scoonman & A.P. Lehner, *J. Electroanal. Chem.*, 131, 77, 1982

2 A. Kapturkiewicz & M. Opallo, *J. Electroanal. Chem.*, 185, 15, 1985

3 A. Kapturkiewicz & M. Opallo, *Electrochimica Acta*, 30, 1301, 1985

4 M. Opallo, *J. Chem. Soc., Faraday Trans.*, 82, 339, 1986

5 W.R. Fawcett & C.A Foss, *Electrochimica Acta*, 36, 1767, 1991

6 W.R. Fawcett & C.A Foss, *J. Electroanal. Chem.*, 252, 221, 1988

7 M.J. Weaver & T. Gennett, *Chem. Phys. Letters*, 113, 213, 1985

8 S. Sahami & M.J. Weaver, *J. Electroanal. Chem.*, 124, 35, 1981

9 H. Elzanowska, Z. Galus & Z. Borkowska, *J. Electroanal. Chem.*, 157, 251, 1983

10 V. Gutmann, *Coordination Chemistry Reviews*, 18, 225, 1976

11 V. Gutmann, *The Donor-Acceptor Approach to Molecular Interaction*, Plenum Press, New York, 1979

12 M.J. Weaver, *Trends in Interfacial Electrochemistry*, ed. A.J. Silva, D. Reidel Publishing, 281, 1986

13 A. Kapturkiewicz & B. Behr, *J. Electroanal. Chem.*, 179, 187, 1984

14 A. Baranski & W.R. Fawcett, *J. Electroanal. Chem.*, 94, 237, 1978

15 W.R. Fawcett & J.S. Jaworski, *J. Phys. Chem.*, 87, 2972, 1983

16 R.A. Marcus *J. Chem. Phys.*, 43, 679, 1963

17 V.G. Levich and R.R. Dogonadze, *Dokl. Acad. Nauk SSSR*, 124, 123, 1959

18 R.R. Dogonadze and Y.A. Chizmadshecv, *Dokl. Acad. Nauk SSSR*, 144, 1077,1962

19 R.R. Dogonadze, A.M. Kuznetsov and Y.A. Chizmadshecv, *Zh. Fiz. Khim.*, 38, 1195, 1964

20 V.G. Levich and R.R. Dogonadze, *Coll. Czech. Chem. Commun.*, 29, 193, 1961

21 V.G. Levich, *Advanc. Electrochem. Eng.*, 4, Chap5, 1966

22 R.R. Dogonadze, and A.M. Kuznetsov, Proceedings of the Symposium on Electrocatalysis, ed. M.W. Breiter. The Electrochemical Society. pp195, 1974

23 R.R. Dogonadze, *Elecktrokhimiya*, 1, 1434, 1965

24 R.R. Dogonadze & A.M. Kuznetsov, *Elecktrokhimiya*, 1, 742, 1965

25 R.R. Dogonadze & A.M. Kuznetsov, *Izv. Akad. Nauk. SSSR, SER. Khim.*, 1884, 2140, 1964

26 R.R. Dogonadze & A.M. Kuznetsov *Elektrokhimiya*, 6, 562, 1970

27 R.R. Dogonadze, A.M. Kuznetsov & V.G. Levich, *Electrochim. Acta*, 13, 1025, 1968

28 V.G. Levich & Y.I. Kharakats, *Elecktrokhimiya*, 6, 562, 1970

29 V.G. Levich, *Itogi nauki, Elecktrokhimiya* 1965

30 R.R. Dogonadze & A.M. Kuznetsov, *Itogi nauki, Elektrokhimiya* 1967

31 R.R. Dogonadze & A.M. Kuznetsov, *Progress Surf. Sci.*, 6, 1, 1975

32 R.A. Marcus, *Ann. Rev. Phys. Chem.*, 15, 155, 1964

33 R.A. Marcus, *J. Chem. Phys.*, 24, 966, 1956

34 R.A. Marcus, *J. Chem. Phys.*, 26, 867, 1957

35 R.A. Marcus, *Can. J. Chem.*, 37, 155, 1959

36 R.A. Marcus, *Discuss. Faraday Soc.*, 29, 21, 1960

37 R.A. Marcus, *J. Phys. Chem.*, 67, 853, 2889, 1963

38 R.A. Marcus, *Electrochim. Acta*, 13, 995, 1968

CHAPTER 6

Redox Couples in Tetraethyleneglycol-dimethylether (Tetramer)

6.1 Introduction

The work reported in chapter 5 confirms that the $Fe^{3+/2+}$ couple in liquid solvents is dominated by the local coordination of the ions by the solvent. In order to study the influences of solvent dynamics on the rate of electron transfer it is desirable to find a range of solvents in which the dynamics varies by the greatest possible extent. This may be achieved by comparing electron transfer in liquid and solid polyethers, therefore, it is necessary to find a suitable redox couple that can be studied in both systems. The aim of this chapter is to investigate the electrochemistry of couples that are potentially attractive for studying solvent dynamics in tetramer (liquid polyether) and poly(ethyleneoxide) (solid polyether). In particular it is necessary to establish if the electrochemistry of the redox couple exhibits simple one electron transfer behaviour, and to investigate the influence of supporting electrolyte and concentration dependence on k_{sh} to eliminate the possibility of ion pairing etc.

Investigations of three redox couple are reported in this chapter: two are molecular, one organometallic and the other an organic species, the final one is a simple ionic couple.

(i) the $CoCp_2^+/CoCp_2$ (cobaltocene/cobaltocenium) redox couple

(ii) the Fe^{3+}/Fe^{2+} redox couple

(iii) the PPD^+/PPD redox couple (where PPD is 1,4 phenylenediamine).

6.2 The Cobaltocene/Cobaltocenium Redox Couple ($CoCp_2^+/CoCp_2$)

The electrochemistry of this couple was measured in the tetramer (liquid polymer). Supporting electrolyte dependence and concentration dependence were studied using a three electrode cell described in chapter 2.

6.2.1 Supporting Electrolyte Dependence

Four different supporting electrolytes were investigated for this couple in tetramer: sodium triflate ($NaCF_3SO_3$), potassium triflate (KCF_3SO_3), sodium perchlorate ($NaClO_4$) and potassium perchlorate ($KClO_4$). Due to the nature of the solvent used here it was not possible to study supporting electrolytes with larger cations as they would not dissolve in the solvent medium, however the size of the anion was altered. The sodium and potassium triflates were prepared as described in chapter 2 and the sodium and potassium perchlorates (Aldrich 99%) were dried as for lithium perchlorate (chapter 2). An equimolar concentration of 1mM $CoCp_2^+/CoCp_2$ was used for all the solutions and the supporting electrolyte concentration was 0.2M. A three electrode cell with a 2mm diameter platinum working electrode and a 2cm square platinum gauze counter electrode was employed. The $CoCp_2^+/CoCp_2$ couple

acted as its own reference electrode by placing a coiled platinum wire directly into the solution

Ac impedance spectroscopy was carried out at the open circuit potential (0V ± 4mV) in the frequency range 65kHz to 0.1Hz. All plots produced had similar features, i.e. an intermediate frequency semicircle, corresponding to the electrode reaction, and a low frequency Warburg impedance, corresponding to the diffusion of the electroactive species to and from the electrode (figure 6.1 below).

Figure 6.1 Typical complex impedance plot for a liquid solvent system.

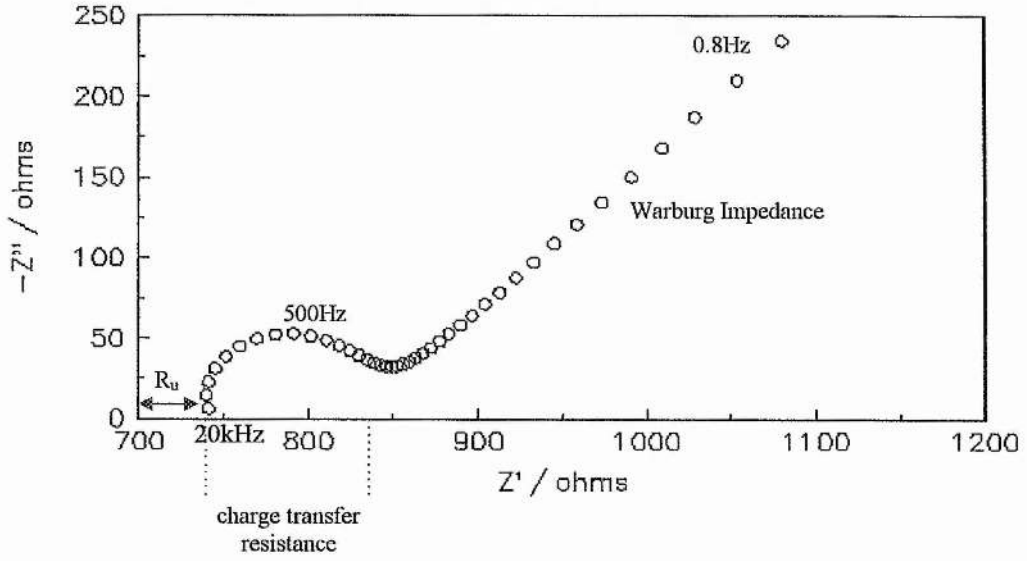

The data obtained were analysed using three methods:

(i) estimated by hand: a perfect semicircle was assumed to represent the electrode process and the diameter was measured by hand to give a value of the charge transfer resistance which was then used to calculate k_{sh} using the equations

(ii) using Boukamp [1]: a non-linear least squares program was used to calculate the charge transfer resistance by fitting an equivalent circuit to the data, this value of R_{ct} was again used in conjunction with the equations given in chapter 3 section 3.2.6 to give a value for k_{sh}. The double layer capacitance was calculated as above.

(iii) using the MacDonald program [2]: this program was used to produce a fit over the full frequency range for a simple equivalent circuit (shown in figure 6.2). The program fit provided a value for k_{sh}, and C_{dl} .

Figure 6.2 Equivalent circuit for simple liquid systems used in the MacDonald program [2].

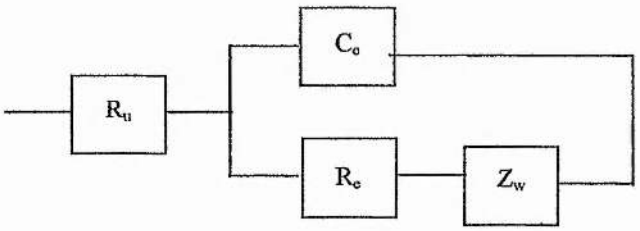

Table 6.1 summarises all the values obtained from each of the three methods listed above for the four supporting electrolytes investigated. As can be seen from the table three conclusions can be drawn: firstly the two least squares methods give values which differ by more than the esd's but are in reasonable agreement with each other (i.e. variation of less than $\pm 40\%$), second the manually estimated values are in reasonable agreement (k_{sh} values vary by a factor of 2) with the fitted values and third that there is no significant supporting electrolyte dependence.

6.2.2 Concentration Dependence

The experiments were carried out using the same cell set up as for the supporting electrolyte study. Potassium perchlorate was used as the supporting electrolyte at a concentration of 0.2M. Equimolar concentrations of the electroactive species of 0.05, 0.075, 1, 2, , 4, 6, 8, 10 and 25mM were studied. Again three methods were employed to calculate values for k_{sh}; analysis by hand, using Boukamp [1] and thirdly using MacDonald [2].

Table 6.1 Summary of values for k_{sh} obtained from the three different methods of calculation employed and summary of supporting electrolyte dependence.

	Fitting by hand (10^{-3} k_{sh} cms^{-1})	**Boukamp [1]** (10^{-3} k_{sh} cms^{-1})	**MacDonald [2]** (10^{-3} k_{sh} cms^{-1})
$NaClO_4$	8.5 ± 1.7	7.7 ± 0.35	6.1 ± 0.21
$KClO_4$	10.8 ± 2.2	5.6 ± 0.25	4.3 ± 0.15
$NaCF_3SO_3$	11.6 ± 2.3	8.1 ± 0.36	5.9 ± 0.21
KCF_3SO_3	9.2 ± 1.8	6.5 ± 0.29	4.7 ± 0.16

Figure 6.3 depicts a typical complex impedance plot obtained for these studies and incorporates the fit obtained using the MacDonald program [2]. As can be seen the fit is in excellent agreement with the data.

Figure 6.4 shows graphically the concentration dependence obtained for each of the three methods employed in the calculation of k_{sh}. As can be seen from figure 6.4 there seems to be some concentration dependence at the lower concentration end. Table 6.2 summarizes the values obtained, at each concentration, for the k_{sh}, D_0, C_{dl} and R_u using the MacDonald program.

Figure 6.3 Complex impedance plot for 25mM $CoCp_2^+/CoCp_2$ in tetramer with 0.2M $KClO_4$; O representing data and — representing fit.

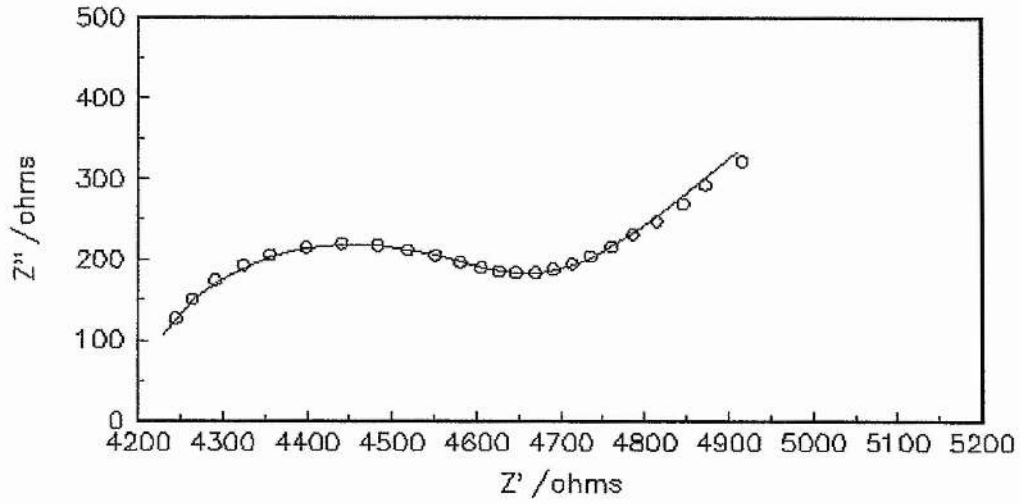

Figure 6.4 Concentration dependence of the $CoCp_2^+/CoCp_2$ redox couple in tetramer with 0.2M $KClO_4$; (a) k_{sh} vs. concentration and (b) log k_{sh} vs. concentration.

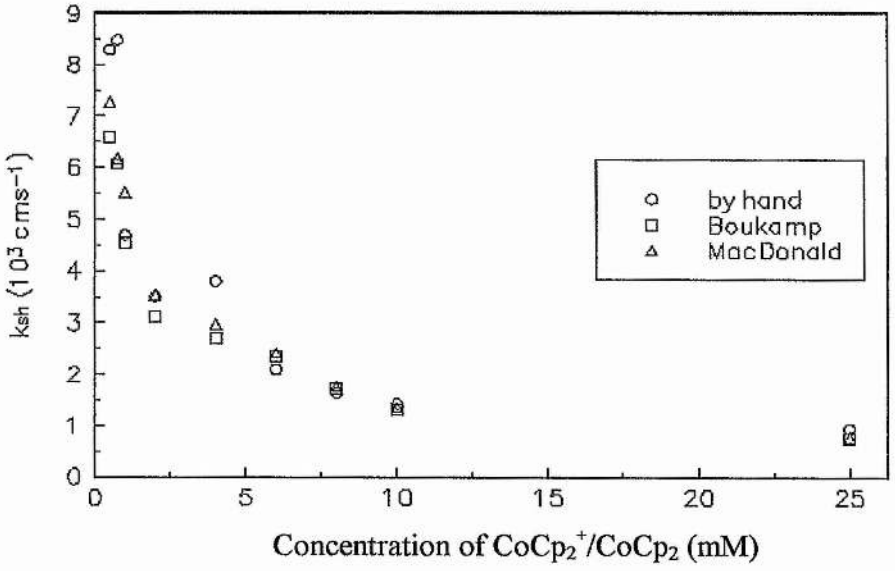

(a)

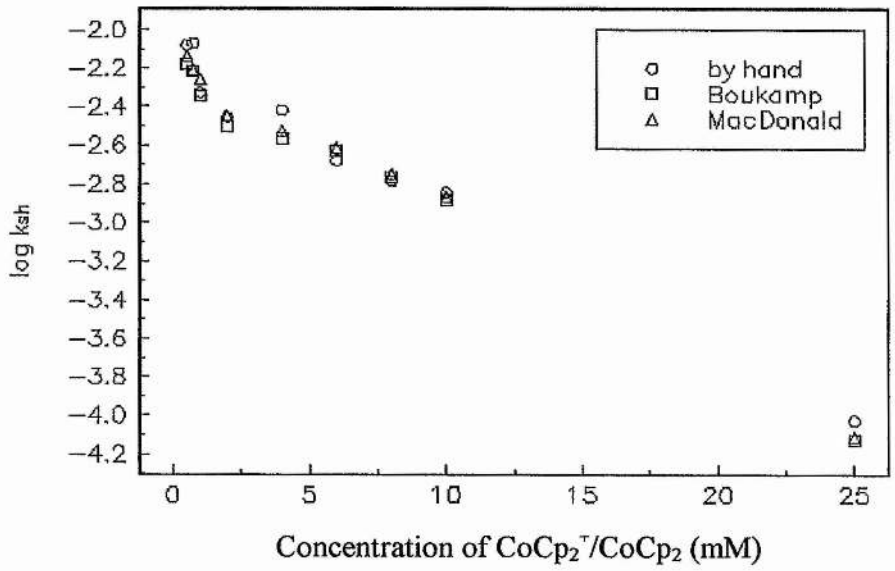

(b)

Table 6.2 Summary of results obtained in the investigation of concentration dependence of the $CoCp_2^+/CoCp_2$ redox couple in tetramer with 0.2M $KClO_4$ using the MacDonald fitting program [2].

Concentration (mM)	**C_{dl} (μFcm^{-2})**	**D_0 ($10^{-8}cm^2s^{-1}$)**	**R_u (ohms)**	**k_{sh} ($10^{-3}cms^{-1}$)**
0.5	19	7.21	11302	8.1
0.75	21	6.87	11003	7.6
1	22	5.01	10005	4
2	17	3.02	9690	3.05
4	27	4.04	8779	2.98
5	24	3.64	8235	3
6	20	3.91	7798	2.09
8	27	4.85	7417	2.63
10	28	4.04	5254	1.83
25	28	3.55	4192	0.81

6.3 The $Fe^{3+/2+}$ Redox Couple in Tetramer

Two approaches to the determination of k_{sh} for this couple were employed. The first involves polarisation of a $Fe(CF_3SO_3)_2$ solution at $E_{1/2}$ and the use of ac impedance and the second ac impedance studies of a poised system, i.e. both Fe^{3+} and Fe^{2+} in the solution initially.

6.3.1 AC Impedance at $E_{1/2}$

Iron (II) triflate was prepared as described in chapter 2 and dissolved in tetramer along with $LiAsF_6$ as the supporting electrolyte. A three electrode cell was used in which the working and counter electrode were formed from platinum.

In aqueous solutions there are a wide choice of well established reference electrodes e.g. calomel electrodes. However in anhydrous tetramer use of a calomel reference electrode is not desirable because of possible ingress of water into the tetramer. Furthermore a significant distortion of the ac impedance response was noted using such reference electrodes. For measurements carried out in tetramer a Li^+/Li reference electrode was used. This was made up of a solution of 0.1M $LiClO_4$ in tetramer inside a tube with a Vicor glass frit into which was placed a lithium wire. The working electrode was then polarised at $E_{1/2}$ as determined by carrying out a cyclic voltammetric study on the system. In the complex impedance plots obtained, using the Li^+/Li reference electrode and the complex impedance collected while polarised at $E_{1/2}$, an additional semicircle was present and is believed to be caused by the presence

of the Vicor glass frit in the reference electrode compartment. In order to present the effect of the Vicor glass frit along with the charge transfer semicircle and the diffusional impedance a scale was chosen so that only the low frequency data points of the additional semicircle have been shown in figure 6.5. To verify that the additional semicircle was due to the presence of the Vicor glass frit and to make sure that its presence did not interfere with the determination of the rate constant, the same experiment was carried out using a coiled platinum wire as a pseudo reference electrode (i.e. one that is stable with time but whose potential is not thermodynamically well defined). A cv was again used to establish $E_{1/2}$ with respect to the platinum reference In this case the additional semicircle did not appear. From table 6.3 below it can be seen that the Vicor glass frit does not affect the measurement of the rate constant (within reasonable experimental error of less than $\pm 30\%$) and so the Li^+/Li reference electrode is used in all work carried out on Fe (II) triflate in tetramer.

Figure 6.5 Complex impedance plots obtained for the Li^+/Li reference electrode.

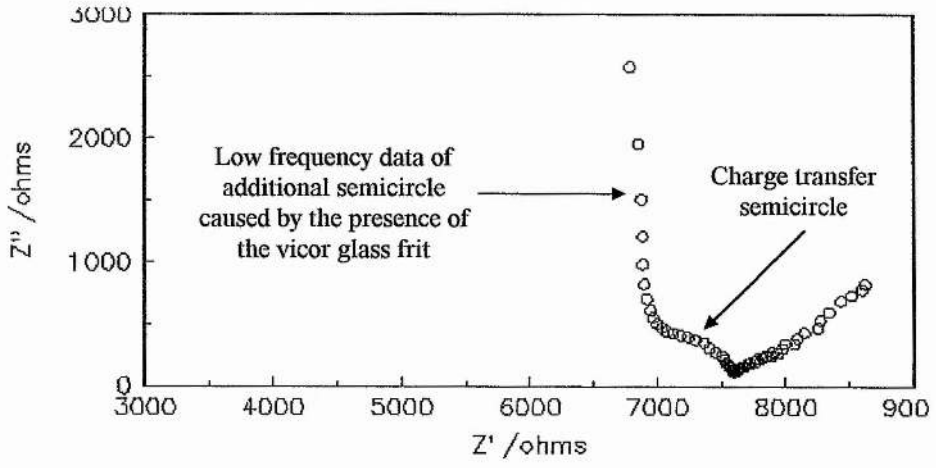

Table 6.3 Comparison of reference electrodes employed in measurements carried out on the Fe^{2+} species in tetramer.

Reference electrode	D_0 (10^{-6} cm^2s^{-1})	k_{sh} (10^{-4} cms^{-1})
Platinum wire	1.3	1.8
Li^+/Li	1.3	1.4

6.3.1.1 Verification of half wave potential

To confirm that the value of the half wave potential determined from cyclic voltammetry is correct ac impedance spectroscopy was carried out at the assumed $E_{1/2}$ and then at a series of dc potentials varying in steps of approximately ±25mV from the assumed half wave potential up to a maximum of ±200mV. From each of the complex impedance plots the charge transfer resistance (R_{ct}) is determined and plotted vs. $E-E_{1/2}$ where E is the dc potential applied and $E_{1/2}$ is the assumed half wave potential. If the assumed half wave potential is correct then it should correspond closely to the minimum of the curve produced in the plot since the theory of ac impedance for a simple electrode reaction shows that R_{ct} reaches a minimum at $E_{1/2}$ [3]. Figure 6.6 is the plot produced for R_{ct} vs. $E-E_{1/2}$ for 32mM Fe (II) triflate in 0.1M $LiAsF_6$ which shows that this is the case As the assumed half wave potential

corresponds to the minimum of the curve we may be confident about extracting rate constants at dc polarised electrodes in the $Fe^{3+/2+}$ system.

Figure 6.6 A plot R_{ct} vs. $E-E_{1/2}$ [3] for 32mM Fe^{2+} in tetramer with 0.1M $LiAsF_6$.

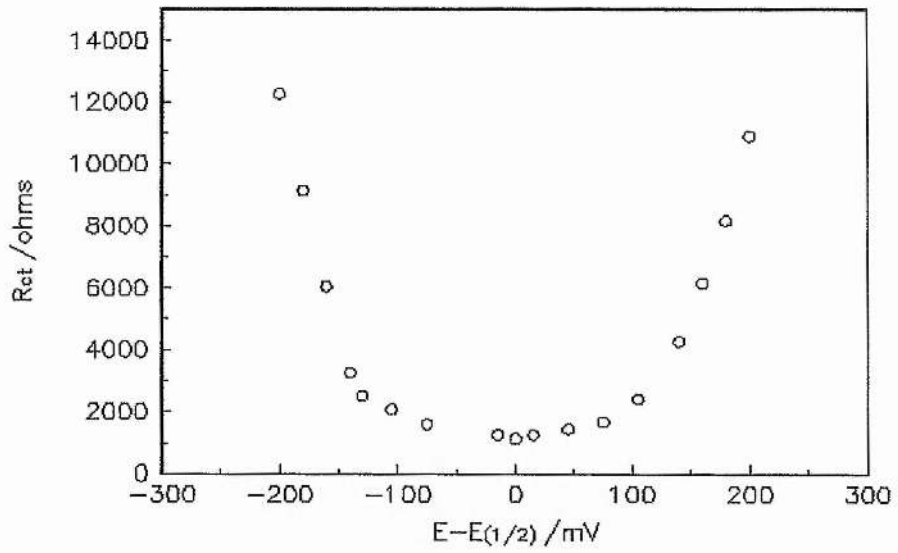

6.3.1.2 Supporting Electrolyte Dependence

Three supporting electrolytes were studied at a concentration of 0.1M with 32mM Fe (II) triflate, they were lithium hexafluoroarsenate ($LiAsF_6$), lithium perchlorate ($LiClO_4$) and lithium triflate ($LiCF_3SO_3$). Ac impedance was carried out at the half wave potential of each solution and the data obtained were analysed using a fitting program (MacDonald [2]). Table 6.4 summarizes the results for the three supporting electrolytes. It can be seen that the supporting electrolyte has a minimal effect on the rate constant for Fe (II) triflate in tetramer. $LiAsF_6$ was chosen as the supporting

electrolyte for the rest of the investigation as it was the quickest and easiest to dissolve.

Table 6.4 Summary of supporting electrolyte dependence for Fe (II) triflate in tetramer

Supporting electrolyte	D_0 (10^{-6} cm^2s^{-1})	k_{sh} (10^{-4} cms^{-1})
$LiAsF_6$	1.4	1.2
$LiClO_4$	1.5	1.9
$LiCF_3SO_3$	1.1	1.2

6.3.1.3 Concentration Dependence

Five different concentrations of Fe (II) triflate (10,20,30,40 and 50mM) were studied in tetramer with 0.1M $LiAsF_6$ and the data obtained were analysed using the MacDonald fitting program [2] after removal of the high frequency data corresponding to the presence of the Vicor frit. An example of the complex impedance plots obtained is shown in Figure 6.7 along with the fitted data. The concentration dependence results are summarised in table 6.5.

Figure 6.7 Complex impedance plot obtained for 32mM Fe^{2+} in tetramer with 0.1M $LiAsF_6$ where O represents the data and — represents the fit.

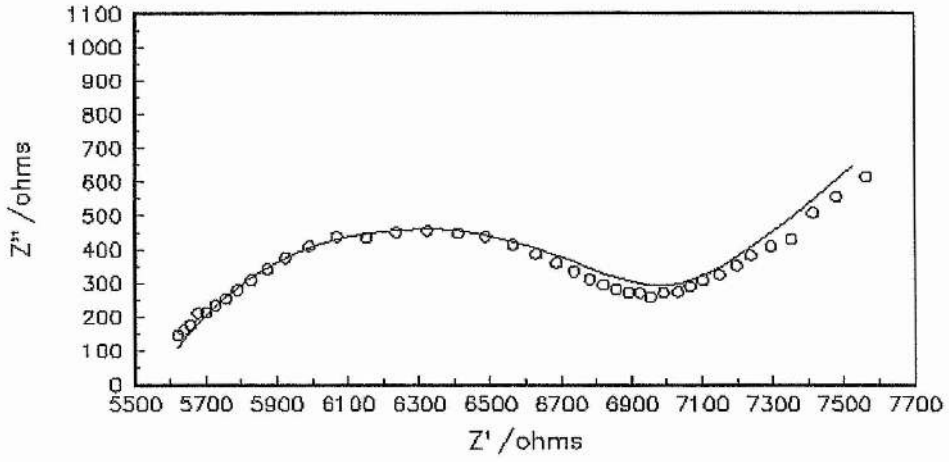

Table 6.5 Summary of concentration dependence for Fe (II) triflate in tetramer with 0.1M $LiAsF_6$.

Bulk concentration of Fe^{2+} (mM)	k_{sh} (10^{-4} cms^{-1})
10	5.3
20	5.6
30	4.5
40	3.0
50	2.8

From table 6.5 it can be seen that there is a slight concentration dependence but this is not as marked as the concentration dependence noted for $CoCp_2^+/CoCp_2$. For a five fold increase in concentration k_{sh} varies only by a factor of 2 and so it can be concluded that concentration dependence has a minimal effect.

6.3.2 AC Impedance at a Poised Potential.

The electrochemistry of the $Fe^{3+/2+}$ couple was in this case, investigated by poising the system with equimolar concentrations of Fe^{2+} and Fe^{3+} in solution (i.e. no dc bias) as in the experiments on the $CoCp_2^+/CoCp_2$ couple described in section 6.2. Again the dependence of supporting electrolyte and concentration of the electroactive species was examined. Close correspondence of the results between the poised and polarised approaches would add confidence to the conclusions of the results and verify that $E_{1/2} = E_0$. In this case the Li^+/Li reference was dispensed with in favour of a platinum wire poised at E_0.

6.3.2.1 Supporting electrolyte dependence

Lithium hexafluoroarsenate and lithium perchlorate were studied at a concentration of 0.1M with 10mM $Fe^{3+/2+}$. The results are summarized in table 6.6 below. From this it can be seen that, again, that there is a slight supporting electrolyte dependence.

Table 6.6 Supporting electrolyte dependence of 10mM $Fe^{3+/2+}$ in tetramer

Supporting electrolyte	k_{sh} (10^{-4} cms^{-1})
$LiAsF_6$	2.5
$LiClO_4$	1.7

6.3.2.2 Concentration dependence

Three concentrations of the $Fe^{3+/2+}$ redox couple (5, 10 and 20mM) were studied with 0.1M $LiAsF_6$ in tetramer and the results were analysed using the MacDonald fitting program [2]. Figure 6.8 shows a typical complex impedance plot obtained incorporating the original and fitted data and table 6.7 summarizes the concentration dependence results. For a four fold increase in concentration k_{sh} varies only by a factor of about 2 and so concentration dependence is a minimal effect. This was also concluded for the investigation of the $Fe^{3+/2+}$ couple at polarised electrodes.

Figure 6.8 Complex impedance plot for 10mM $Fe^{3+/2+}$ with 0.1M $LiAsF_6$ in tetramer with O representing the data and — representing the fit.

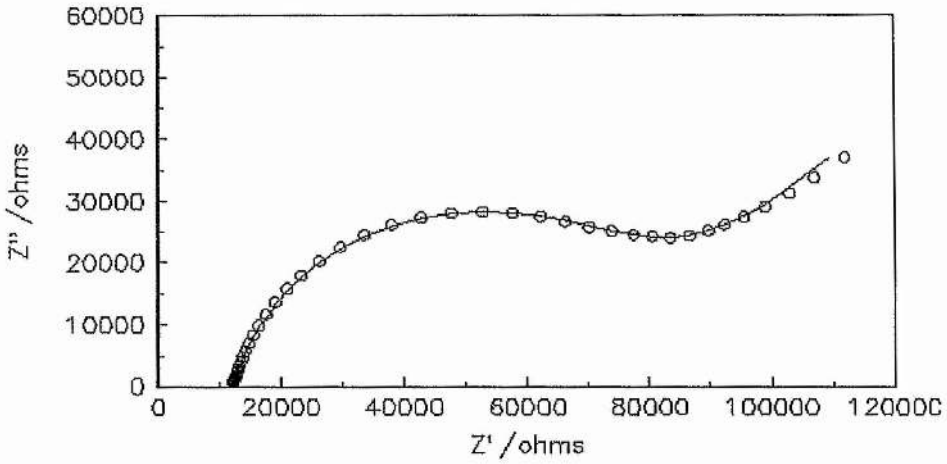

Table 6.7 Concentration dependence for the $Fe^{3+/2+}$ redox couple in tetramer with 0.1M $LiAsF_6$

Concentration of $Fe^{3+/2+}$ (mM)	k_{sh} (10^{-4} cm s^{-1})
5	3.9
10	2.53
20	1.8

6.4 The 1,4 Phenylenediamine Couple PPD^+/PPD

Opallo [4] has carried out in-depth investigations into the solvent effects on the kinetics of this redox couple. In view of the successful use of the couple in the past it was selected as a possible candidate to study in both low dielectric constant ethers.

1,4 phenylenediamine was used as received (Aldrich 99%). It was dissolved in tetramer along with 1M $LiClO_4$. A two electrode cell consisting of a 12.5 μm Pt ultramicroelectrode and a Li^+/Li reference/counter electrode was employed to establish the half-wave potential. Ac impedance spectroscopy was then carried out at this potential using a cell in which the ultramicroelectrode was replaced by a 2mm diameter Pt disk. Five concentrations of PPD were examined, 0.1, 0.2, 0.3, 0.4 and 0.5M with 1M $LiClO_4$ present as the supporting electrolyte. Lower concentrations proved difficult to measure as the kinetics of the electrode reaction were too slow to be seen on the complex impedance plot. After removal of high frequency data caused by the presence of the Vicor glass frit, the data were analysed using the Boukamp method [1] to obtain R_{ct} and then the equations of Sluyters & Sluyters-Rehbach [3] to obtain k_{sh} at $E_{1/2}$ The concentration dependence results are summarized in table 6.8 and an example of the data obtained is shown in Figure 6.9.

Figure 6.9 Complex impedance plot obtained for a bulk concentration for PPD of 0.1M with 1M $LiClO_4$ in tetramer.

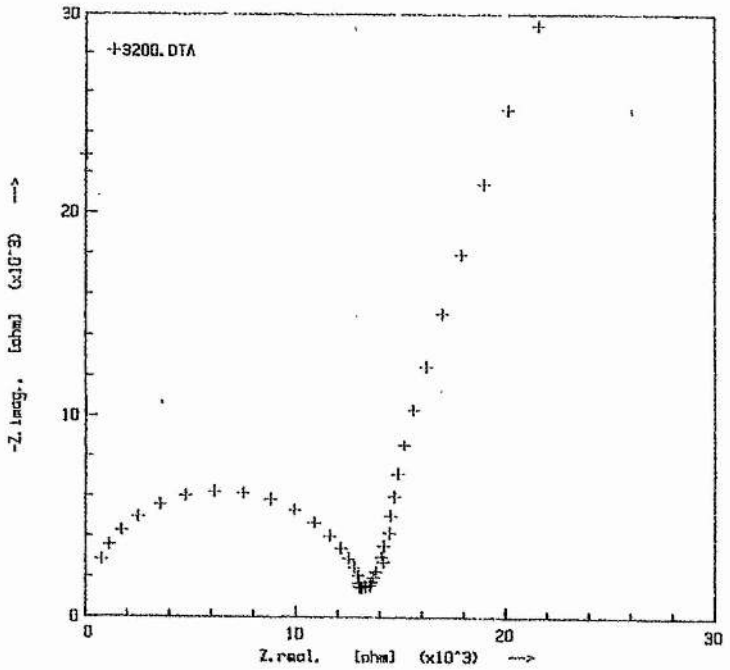

Table 6.8 Summary of concentration dependence for PPD in tetramer with 1M $LiClO_4$.

Bulk concentration of PPD (M)	D_0 (10^{-7} cm^2 s^{-1})	k_{sh} (10^{-4} cm s^{-1})
0.1	2.84	5.69
0.2	1.19	2.39
0.3	1.15	2.31
0.4	8.65	1.73
0.5	6.92	1.39

6.5 Discussion

Three redox couples, which are chemically very different, have been investigated here with the view to finding which, if any, exhibit a simple electrochemical reaction suitable for probing electron transfer.

The $CoCp_2^+/CoCp_2$ couple is attractive because it is known to exhibit minimal inner sphere vibration activation hence it should be an excellent probe of solvent dynamics. However it demonstrated severe variation of k_{sh} with concentration of the redox couple. The reasons for this are not clear at present but may arise from significant ion pairing effects implying that the measured rate constant for this system is not that of electron transfer but of ion association. This negates its use as an electron transfer probe. In addition the attempts to dissolve $CoCp_2$ in poly(ethylene oxide) proved unsuccessful for concentrations greater than 20mM. Since the objective is to follow the rate of the same couple as a function of molecular weight from liquid to solid ethers this also renders cobaltocene inappropriate.

The second couple to be investigated was PPD^+/PPD with only PPD being initially present in solution. Investigation of the couple in tetramer using cyclic voltammetry exhibited evidence of other electrochemical or chemical processes occurring besides that of electron transfer and, although the couple dissolved to high concentrations in the liquid polyether, it was found that the solubility in the solid polyether was less than 15mM. For these reasons the PPD^+/PPD couple was not used in further investigations.

The final couple studied, that of $Fe^{3+/2+}$ seemed to be the most successful. The initial studies found very little supporting electrolyte or concentration dependence suggesting that a simple one electron transfer dominates the electrochemistry of this couple in tetramer. Furthermore the solubility of the $Fe(CF_3SO_3)_2$ and $Fe(CF_3SO_3)_3$ in tetramer and poly(ethylene oxide) seems excellent for providing a wide range of concentrations with which to investigate electron transfer rates. The disadvantage of this couple from the viewpoint of probing solvent effects is that it is expected to demonstrate considerable vibrational activation in tetramer and poly(ethylene oxide) as was found in chapter 5 for the same couple in other non-aqueous solvents. It is hoped, however, that the solvent dynamics will be slow enough in the solid polyethers to demonstrate a dependence on the nature of the outer sphere.

REFERENCES

1 B. Boukamp, *Equivalent Circuit Program,* University of Twente, 1988

2 J.R. MacDonald, J. Scoonman & A.P. Lehner, *J. Electroanal. Chem.*, 131, 77, 1982,

3 Sluyters & Sluyters-Rehbach, *J. Electroanal. Chem.*, 171, 157, 1984

4 M. Opallo, *J. Chem. Soc., Faraday Trans.*, 82, 339, 1986

CHAPTER 7

The $Fe^{3+/2+}$ Redox Couple in the Solid Solvent Poly(ethylene oxide) (PEO)

7.1 Introduction

In chapter 5 the electrochemistry of the $Fe^{3+/2+}$ redox couple was studied and the conclusion derived from the investigation was that there was no influence on the electrode kinetics of the redox couple from outer sphere solvent dynamics. However, liquids can only offer a limited variation on solvent dynamics, hence for example τ_L (the longitudianl relaxation time) can only be varied to a small extent. A much wider variation in the solvent dynamics is possible by investigation with liquid and solid solvents of the same type. In this chapter the work is taken one step further by investigating the kinetics of the $Fe^{3+/2+}$ couple in a solid solvent namely poly(ethylene oxide) (PEO).

In this study comparisons are made between two polyether solvents which differ only in their molecular weight both are based on the repeat unit CH_2-CH_2O; the solid is polyethylene oxide $(CH_2CH_2O)_n$ whereas the liquid is tetraethyleneglycol dimethyl ether, CH_3-$O(CH_2CH_2O)_3CH_3$. In the solid solvent motion (particularly rotation) of the dipoles is greatly restricted whereas the vibration of the metal-ligand bonds is expected to be altered much less in going from the liquid to the solid. If electron transfer is dominated by inner sphere vibration in all cases then values of k_{sh} in the

tetramer and polymer are expected to be similar. On the other hand variation of k_{sh} would signal some influence of solvent dynamics on the rate of electron transfer.

7.2 Results

7.2.1 Dissolution of Salts in the Solid Solvent

Before any kinetic measurements were made on the polymer electrolytes it was necessary to ensure that the iron triflate salts had dissolved in the solid polymer. This was achieved via x-ray crystallography. First x-ray diffraction was carried out on powders of the pure iron (II) and (III) triflates to establish the powder patterns for the crystalline salts. Three polymer electrolytes were then prepared, all containing $LiClO_4$. One containing in addition Fe^{3+} triflate in sufficient quantity to yield an etheroxygen to Fe^{3+} ratio of 10:1, and two containing Fe^{2+} yielding compositions of 10:1 and 20:1. The polymer electrolytes were prepared by heating a cryoground mixture of the salts and polymer at 80°C for 5 hours to promote dissolution of the salts in the polymer matrix. This temperature was chosen after investigation by DSC was carried out on polymer electrolytes containing the supporting electrolyte and a high concentration of iron (II) and iron (III) triflate. The DSC plots obtained for a polymer electrolyte containing $LiClO_4$ at a ratio of 20:1 and an equimolar ratio of Fe^{2+} and Fe^{3+} of 100:1 are shown in figure 7.1. X-ray powder patterns were taken of the three individual polymer electrolytes at room temperature. If the salts are completely dissolved at these concentrations then there should be no peaks present from the pure

salt and peaks present from a crystalline complex formed between the salt and the polymer.

Figure 7.2 shows three powder patterns; one for pure PEO, one for pure Fe (II) triflate and one for $PEO_{20}Fe$ (II) triflate. The pattern for the $PEO_{20}Fe$ (II) triflate systems shows no peaks pertaining to pure Fe (II) triflate but does show peaks that correspond to a crystalline complex formed between PEO and the salt showing that the Fe (II) triflate has dissolved. Figure 7.3 is similar except that it is the powder pattern for $PEO_{10}Fe$ (II) triflate. In this instance there are peaks corresponding to both the crystalline PEO-salt complex and the pure crystalline salt. From this it can be concluded that Fe (II) triflate does not fully dissolve at this concentration, and the solubility limit occurs between the ratios of 20:1 and 10:1. The powder pattern for $PEO_{10}Fe$ (III) triflate and pure Fe (III) triflate is shown in figure 7.4. Once again peaks arise due to a crystalline PEO-salt complex formed between the PEO and the Fe (III) salt indicating the dissolution of Fe (III) triflate All these powder patterns were obtained at room temperature, however, all electrochemical measurements are taken at temperatures above 60°C and the presence of a crystalline PEO-salt complex is not desired for these measurements. Therefore, further powder patterns were obtained at 60°C and 70°C to see if the crystalline salt complex disappears. The powder patterns are shown in figure 7.5 and, as can be clearly seen, the complex does in fact disappear at temperatures at which the electrochemical measurements are made. From this it can be concluded that during electrochemical measurements all iron salts and crystalline complexes are completely dissolved and do not complicate any measurements taken.

Figure 7.1 DSC plots of the $PEO_{20}LiClO_4$ system with a ratio of $PEO_{100}Fe^{3+/2+}$.

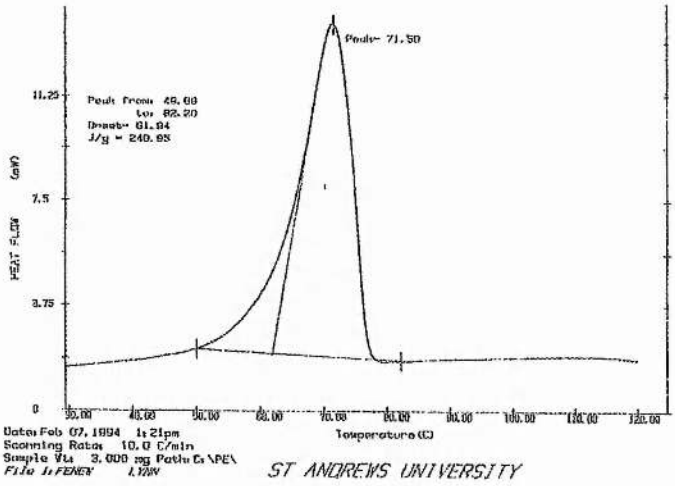

The polymer melts at a temperature of 71.5°C with no evidence of other thermal events up to 120°C

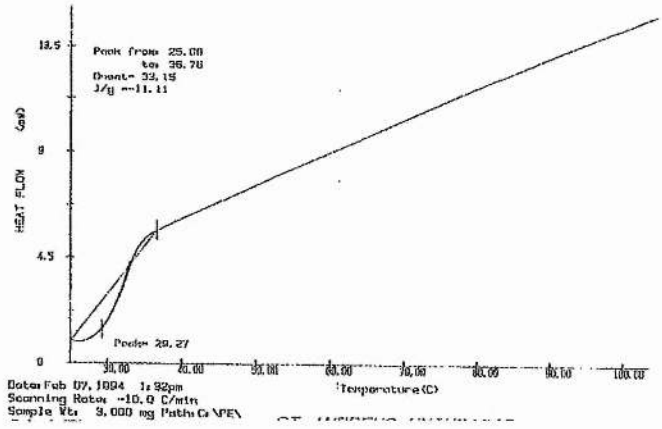

Cooling curve for the same polymer: the polymer solidifies at a temperature of about 33°C. This is the temperature at which the polymer electrolyte is pressed to produce films for use in the cells for electrochemical investigations.

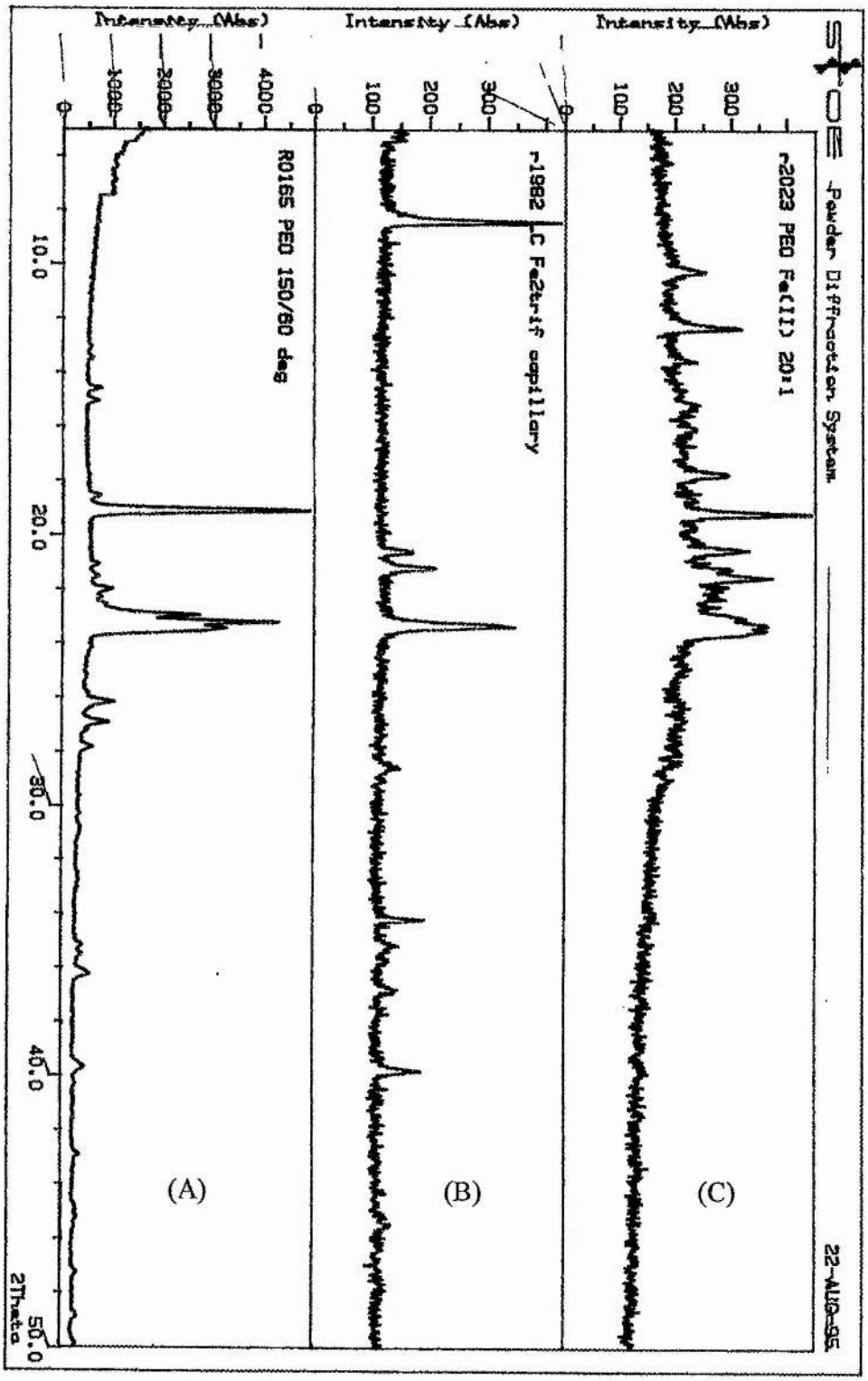

Figure 7.2 X-ray powder pattern for (A) pure PEO, (B) pure Fe (II) triflate and (C) $PEO_{20}Fe$ (II) triflate

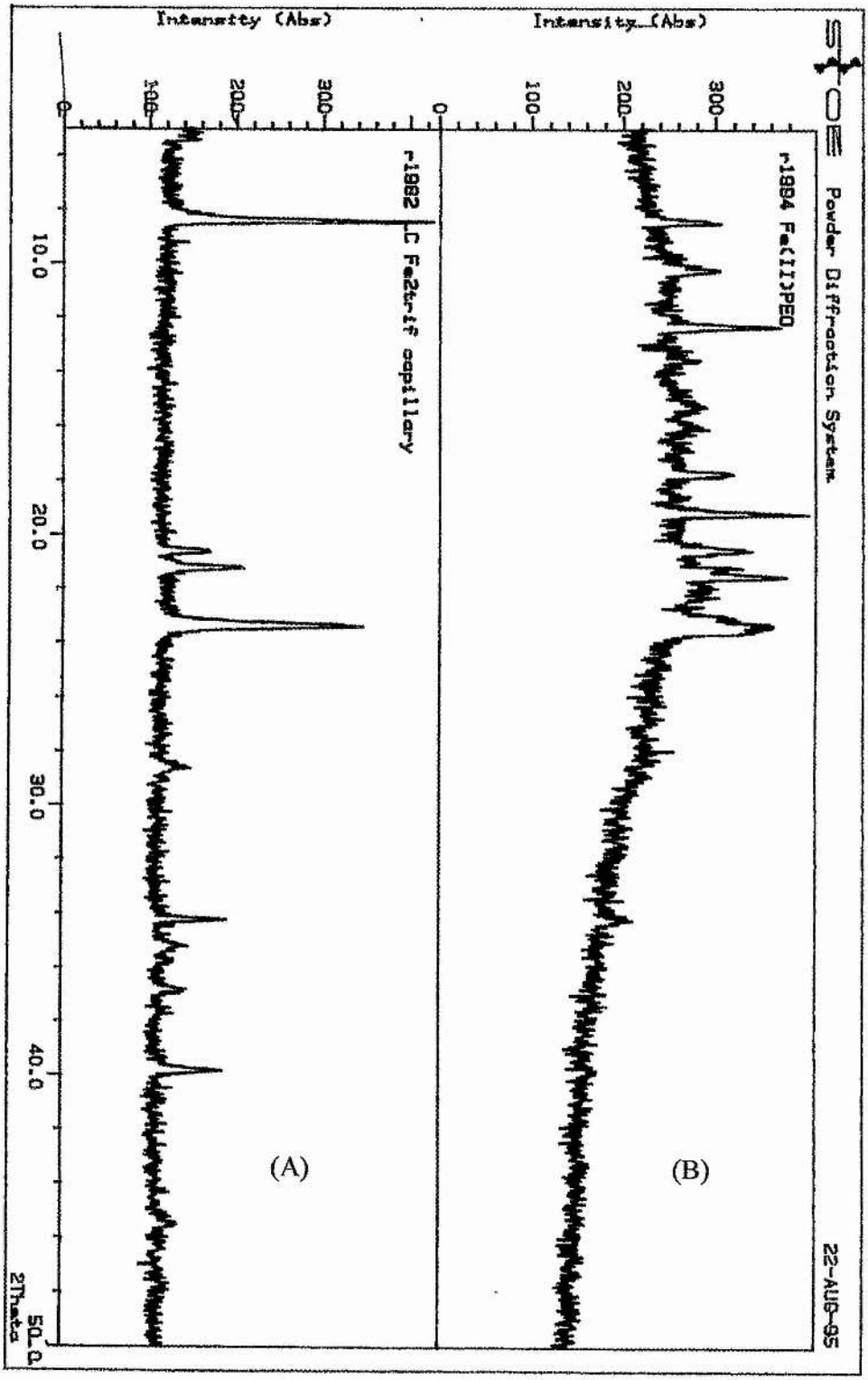

Figure 7.3 X-ray powder pattern for (A) pure Fe (II) triflate and (B) $PEO_{10}Fe$ (II) triflate.

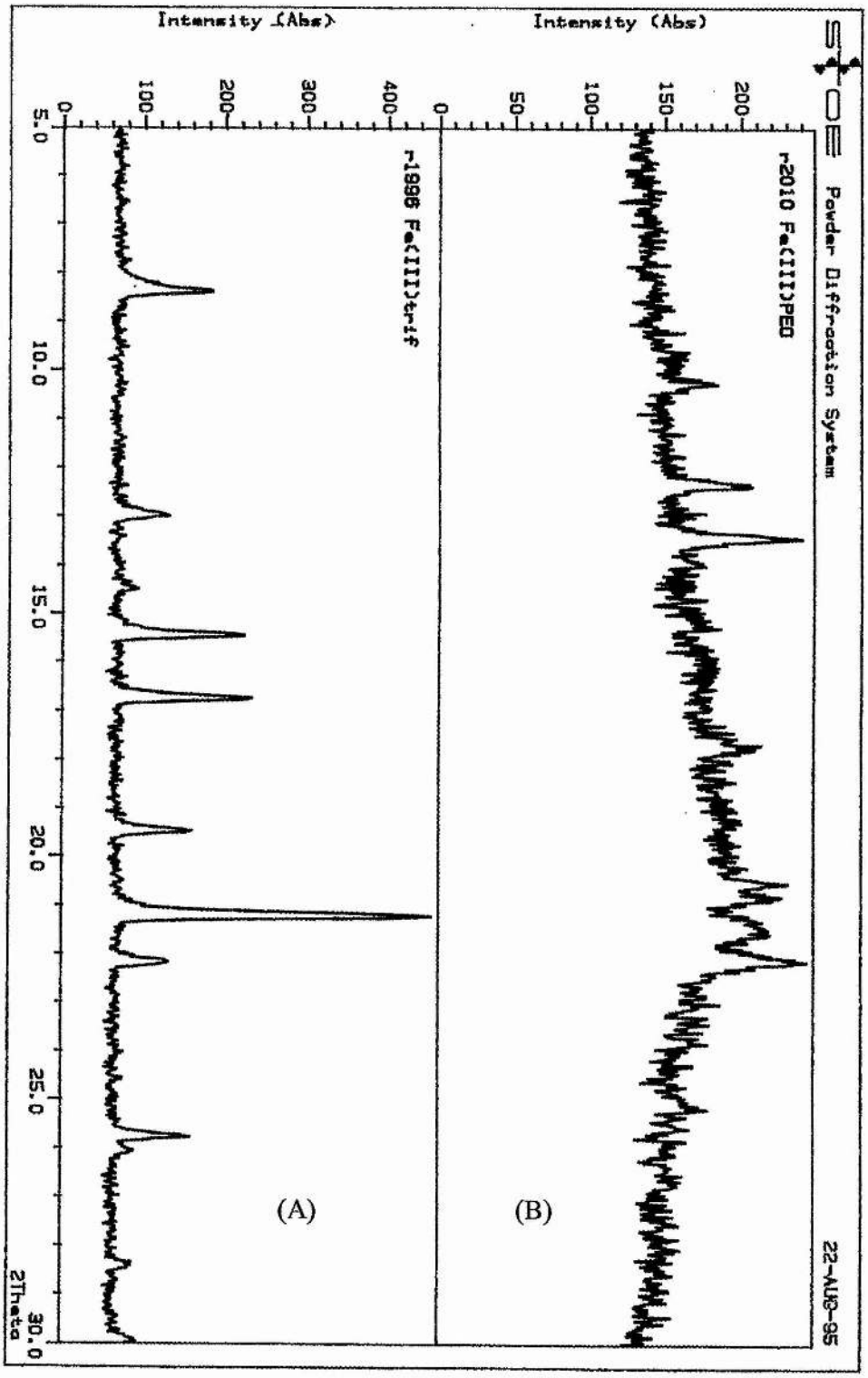

Figure 7.4 X-ray powder pattern for (A) pure Fe (III) triflate and (B) $PEO_{10}Fe$ (III) triflate.

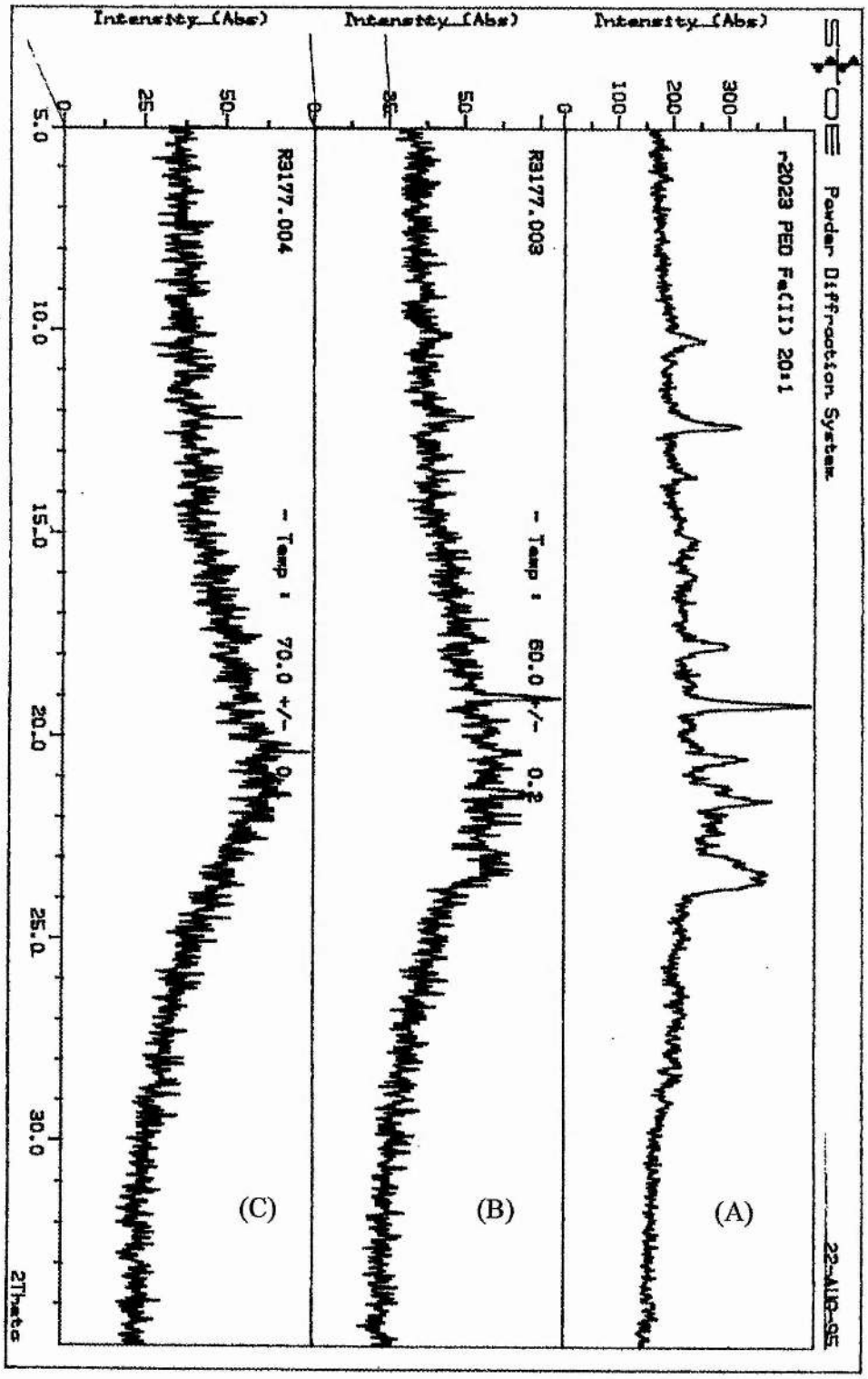

Figure 7.5 X-ray powder pattern for $PEO_{20}Fe$ (II) triflate at (A) 25°C, (B) 60°C and (C) 70°C.

7.2.2 Kinetic Measurements on the Polymer Electrolytes

When comparing liquid and solid solvent systems there are two main differences which are important in the context of measuring interfacial kinetics. The first concerns the large electrolyte resistance associated with the solid solvent; typically this can be three orders of magnitude higher than in comparable liquids. One way to reduce this is to employ an ultramicroelectrode the radius of which should not exceed a few micrometers. Current densities comparable to those used on electrodes of normal dimensions are associated with currents in the pA to nA range with ultramicroelectrodes. The advantage of employing ultramicroelectrodes is that the iR drop associated with the bulk resistance is much reduced. The second difficulty arises from the slower diffusion of electroactive species to and from the electrode in a solid solvent compared with a liquid. Typically diffusion coefficients are at least three orders of magnitude lower in the solid state. In principle microdisk electrodes can also help here in that upon electrolysis the planar semi-infinite diffusion obtained at short times (high frequencies) gives way to near spherical diffusion, and as a consequence enhanced flux is anticipated compared with an electrode of normal dimensions at which linear diffusion continues to grow and the current decays continuously with $t^{1/2}(\omega^{1/2})$ dependence.

Ultramicroelectrodes are therefore of considerable value in studying electrochemistry of polymer electrolytes. However by combining ac impedance measurements and ultramicroelectrodes a powerful technique becomes available which is suited to the study of polymer electrolytes since it permits full characterisation of the

electrochemical reaction at a polymer electrolyte/electrode interface and extraction of the kinetic parameters at high frequencies. An estimate of the frequency above which semi-infinite diffusion to a microdisk dominates can be obtained from the following equation [1-3]: $\omega \approx 100D/a^2$ where D is the diffusion coefficient of the electroactive species, a is the radius of the microdisk and ω is the angular frequency. Similarly, the frequency below which hemispherical diffusion dominates is given by [1-3]: $\omega \approx 0.1D/a^2$. The intermediate region of frequencies is characterised by a mixture of linear and hemispherical diffusion. For disks with a radius of several microns in solid polymers the semi-infinite region dominates down to 0.15Hz in which case flux enhancement due to the use of an ultramicroelectrode may not be obtained within the frequency range of the interfacial processes. Nevertheless a combination of an ultramicroelectrode with its small iR_u drop (and low R_uC_{dl} time constant) and ac impedance spectroscopy, offers the best tool with which to probe the nature of the redox reactions in polymer electrolytes at metal electrodes.

Fleischmann and Pons [1] considered the diffusional impedance at a microdisk and proposed expressions describing the real and imaginary parts of the microdisk impedance using relatively complicated functions of a dimensionless parameter $(\omega a^2/D)$. They found that at high frequencies the diffusional impedance resembles a Warburg impedance and at low frequencies a steady state mass transport limit is obtained due to the spherical diffusional field around the disk. On the basis of this finding the diffusional impedance at a microdisk can be approximated by a parallel combination of a Warburg impedance and non-linear resistance [3,4]. Consequently it is possible to use, for the microdisk, an equivalent circuit identical to that for a

hemispherical electrode, modified only by a geometrical factor. Although this approach to the impedance of a microdisk is only an approximation, the "hemispherical approximation" enables the kinetic parameters (including the diffusion coefficient) to be easily obtained from analysis of the ac impedance response of a microdisk. The complete equivalent circuit which approximates a microdisk at which a simple one-step reaction is occurring is shown in figure 7.6. The real and imaginary components Z' and Z'' obtained for all frequencies are analysed using the CNLS [5] program modified in order to extract the experimental values of the uncompensated solution resistance R_u, the double layer capacitance C_{dl}, the diffusion coefficient D and the standard apparent rate constant k_{sh}

Figure 7.6 The equivalent circuit for a simple one-step reaction at a microdisk.

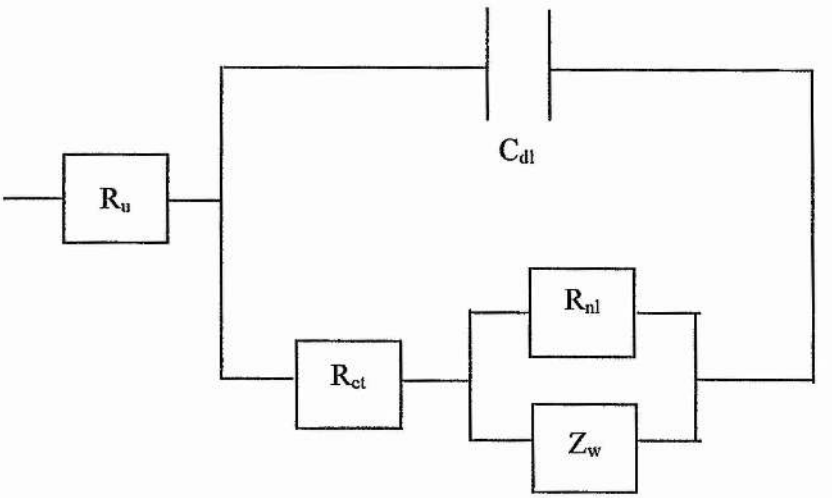

Five different polymer electrolyte systems were studied containing 2,7,13,20,50 and 200mM of Fe^{2+} and Fe^{3+} in equal concentrations. For each of these concentrations the interfacial kinetics of the system were measured at a minimum of four different

temperatures between 65°C and 90°C. The temperature limits were set on the one hand by crystallisation of the PEO, at which point the impedances were to great to measure, and on the other by the fluidity of the polymer becoming too great for the solid state cell with the resulting loss of contact.

To ensure contact between the ultramicroelectrode surface and the polymer electrolyte film a measurement was taken before heating the cell. The cell was then heated over night at 55-60°C and the cell tighten up until a stable impedance was obtained. Figure 7.7 below shows complex impedance plots taken before the cell was heated and after 12 hours of heating. As can be seen from the diagram electrode contact is ensured after this treatment.

Figure 7.7 Complex impedance plots indicating electrical contact after heat treatment.

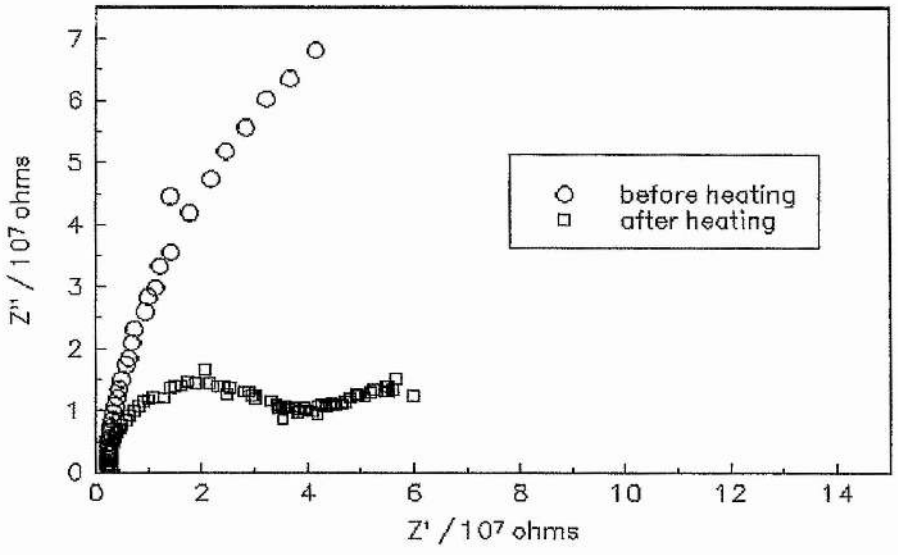

7.2.2.1 200mM and 50mM Fe (II)/(III) Triflate

Initial studies of the $Fe^{3+/2+}$ redox couple in a solid polymer solvent were carried out on the polymer electrolyte $PEO_{20}LiClO_4$ containing 273mM Fe (II) and Fe (III) triflate. Ac impedance spectroscopy was conducted at the open circuit potential ($0V \pm 5mV$), in the frequency range 150kHz to 0.1Hz. For low frequency sweeps a high current amplification was used (10^9) whereas for the higher frequency sweeps a lower amplification was required (10^4-10^6). Complex impedance plots for the system were produced for temperatures of 65, 71, 75, 80 and 85°C and figure 7.8 shows these plots. The plots indicate a decrease in the size of the semicircle with increasing temperature. However, on closer inspection a second semicircle can be seen. An agreement between the data and the equivalent circuit (shown in figure 7.6) could not be obtained, confirming the fact that the process was not a simple one-step reaction. For this polymer electrolyte system the equivalent circuit proposed by Gerischer [6] and Armstrong et. al. [7] was fitted to the data. This equivalent circuit assumes the presence of an adsorbed intermediate. Figure 7.9 shows the results of this fit in conjunction with the data, and, as can be seen, the fit is in excellent agreement with the original data. Other processes such as a coupled chemical reaction or the precipitation of the salt at the interface could also give rise to other semcircles. It is not possible with the data collected to date to identify which of several possible explanations for the semicircle is appropriate in this case. The complex nature of the electrochemistry is supported by cyclic voltammetry at an ultramicroelectrode. For a simple one-step reversible process plateaux should be evident at a sweep rate of $10mVs^{-1}$, in figure 7.10 peaks can be identified that have been distorted by the presence of an adsorbed intermediate [8].

Further investigations of this more complex system were not carried out as the main aim of this work was to investigate the factors influencing the rate of electron transfer for which a simple one-step process is required.

For the solid solvent system containing 50mM Fe (II) and Fe (III) triflate, a similar, although not quite so marked, response to that for 273mM $Fe^{3+/2+}$ was seen. Figure 7.11 shows a typical example of the complex impedance plot obtained for this concentration. Again the equivalent circuit for an adsorbed intermediate fitted the data.

Figure 7.8 Temperature dependence of the polymer electrolyte $PEO_{20}LiClO_4$ containing 273mM $Fe^{2+/3}$

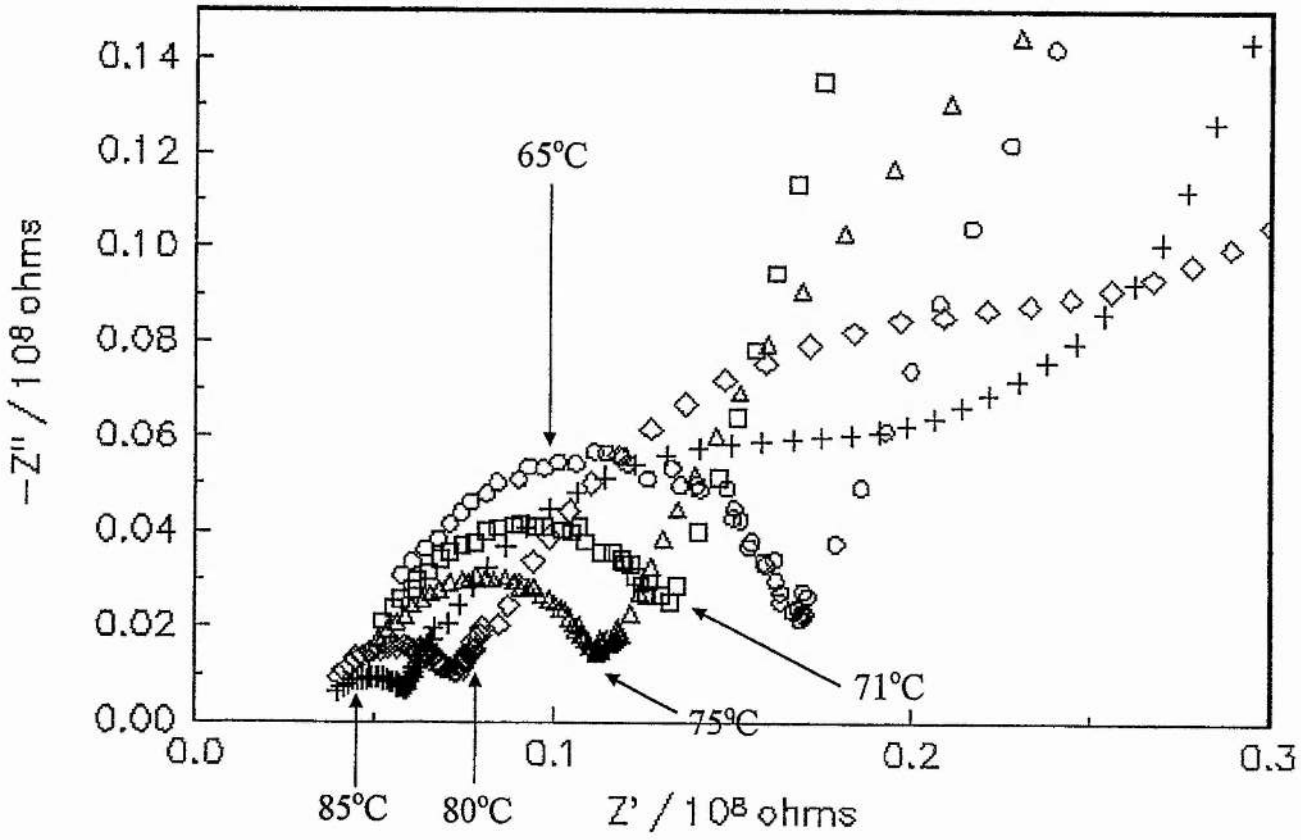

Figure 7.9 Complex impedance plot for $PEO_{20}LiClO_4$ with 273mM $Fe^{3+/2+}$ attributed to a complex electrode reaction. O representing data and — representing fit.

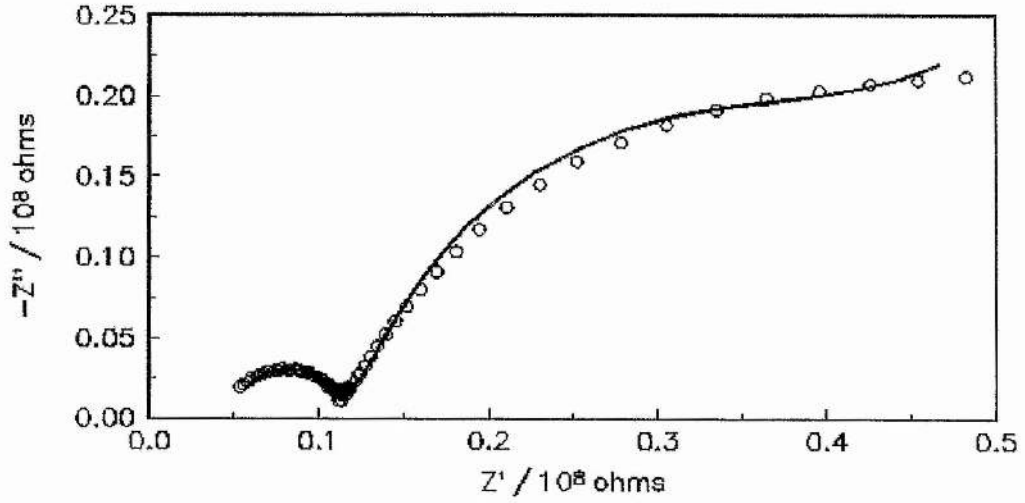

Figure 7.10 Cyclic voltammogram for $PEO_{20}LiClO_4$ with 273mM $Fe^{3+/2+}$ at a sweep rate of $10mVs^{-1}$ and a temperature of 70°C.

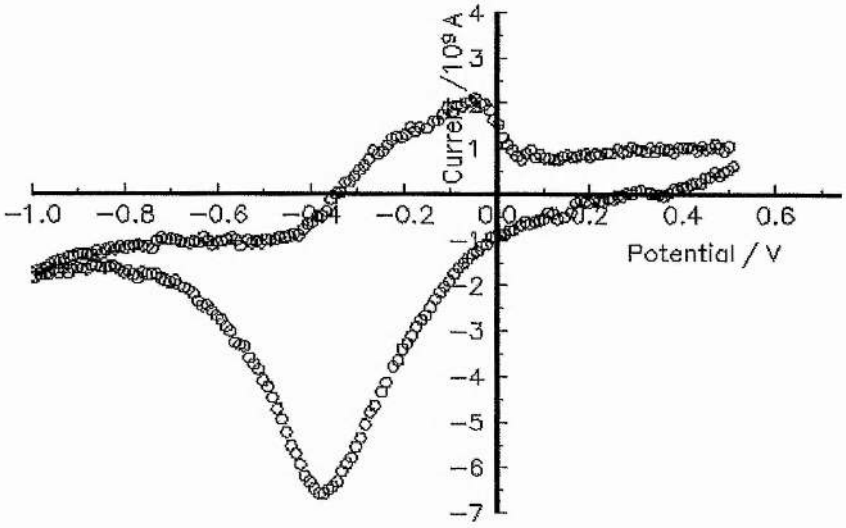

Figure 7.11 Complex impedance plot for 50mM $Fe^{3+/2+}$ in $PEO_{20}LiClO_4$.

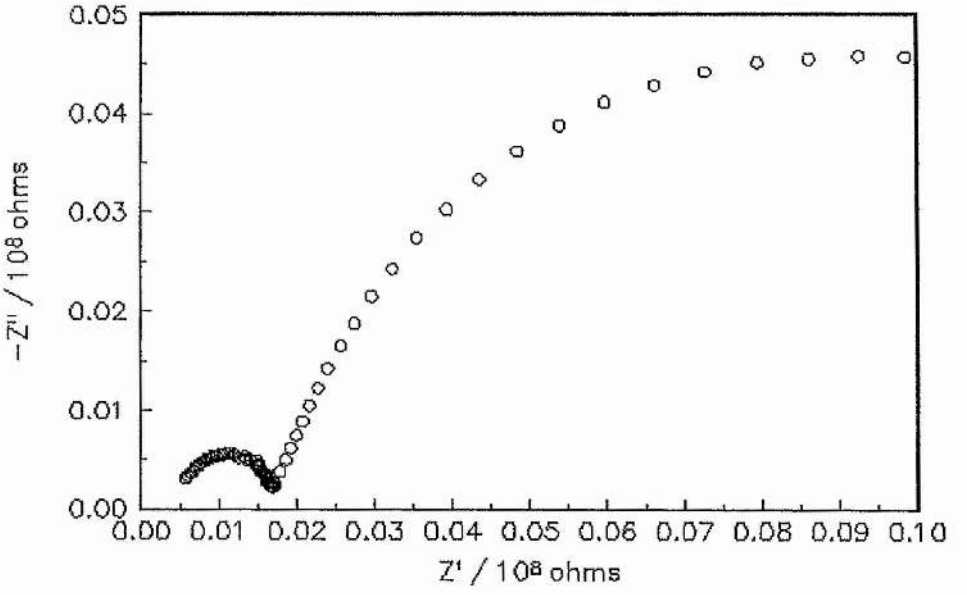

7.2.2.2 2mM, 7mM, 13mM and 20mM Fe (II)/(III) Triflate

Ac impedance spectroscopy was carried out on the systems of lower concentrations and at temperatures between 60 and 95°C. The complex impedance plots are consistent with a simple one-step processes with no adsorbed intermediate or other complex interfacial process. From this initial study of the six concentrations (2,7,13,20,50 and 273mM $Fe^{3+/2+}$) it can be concluded that the ac response of the system is a function of the concentration of the electroactive species, with simple behaviour only being apparent below 20mM. Figures 7.12-7.15 show the complex impedance plots obtained at each temperature for each concentration. All the impedance plots were fitted using the modified CNLS fitting program [5] using the

equivalent circuit for a simple one step process shown in figure 7.6. Figure 7.16 gives an example of a fit obtained along with the data collected for 2mM $Fe^{3+/2+}$ (which is typical for all concentrations). As can be seen the fit is in excellent agreement with the raw data. Tables 7.1-7.4 summarize all the results obtained from the fitting program for each concentration.

From these results, obtained via ac impedance spectroscopy, the specific conductivity κ of the solid electrolyte, $PEO_{20}LiClO_4$, can be checked. From the values of the uncompensated solution resistances κ can be easily calculated from the following equation: $R_u = 1/4\kappa a$ [9]. Choosing one temperature, $\approx 76°C$, the solution resistances and specific conductivities of three concentrations are listed in table 7.5. These values are in good agreement with the literature data the for $PEO_{20}LiClO_4$ system [10]. The values of the diffusion coefficients are also in excellent agreement with those obtained via cyclic voltammetry. The diffusion coefficients are calculated to be 9.64×10^{-9} cm^2s^{-1} at 71°C and 1.32×10^{-8} cm^2s^{-1} at 93°C from cyclic voltammetry and 5.43×10^{-9} cms^{-1} at 71°C and 1.019×10^{-8} cm^2s^{-1} at 93°C from ac impedance spectroscopy.

Figure 7.12 Temperature dependence of the polymer electrolyte $PEO_{20}LiClO_4$ containing 2mM $Fe^{3+/2+}$

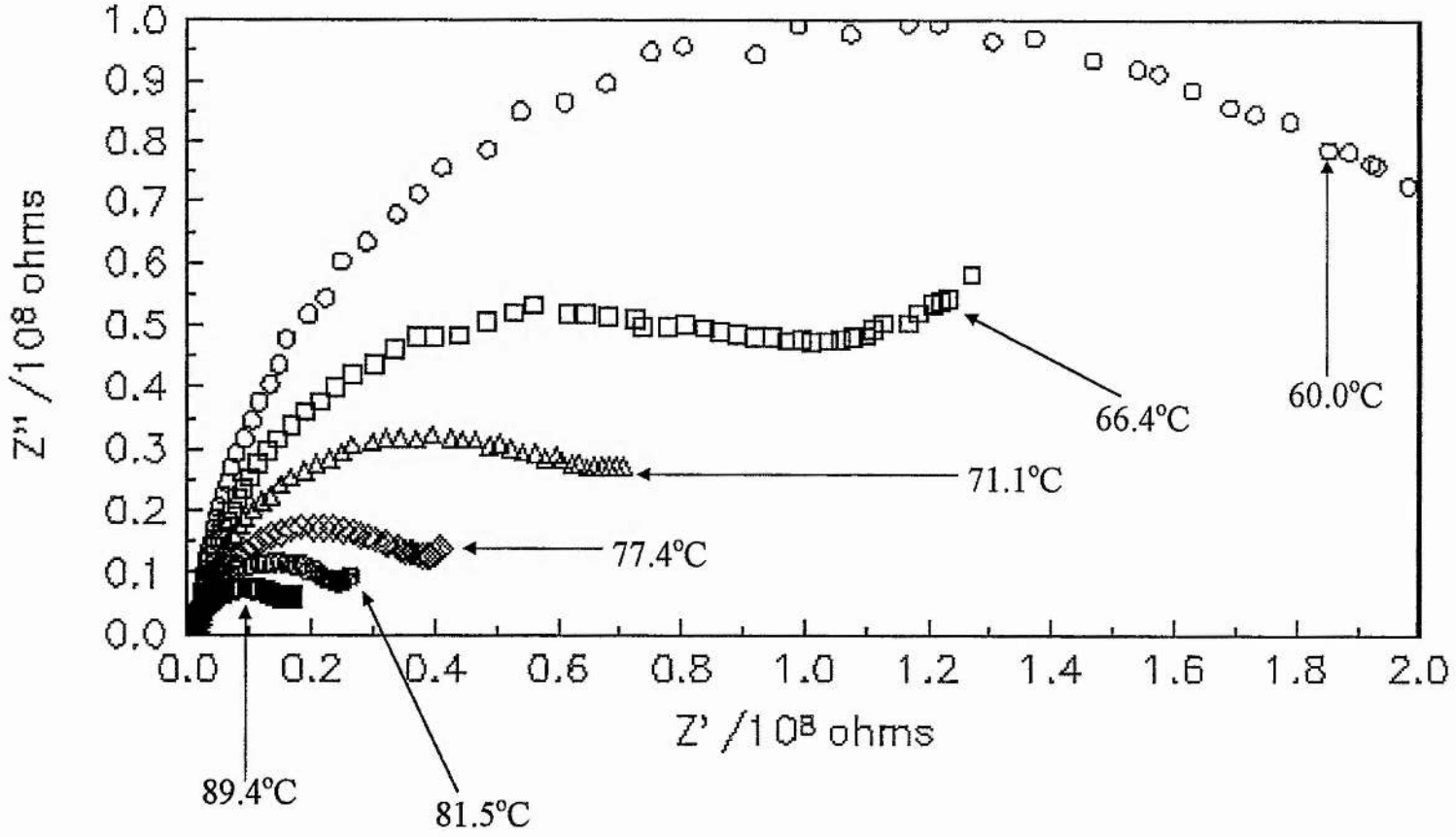

Figure 7.13 Temperature dependence of the polymer electrolyte $PEO_{20}LiClO_4$ containing 7mM $Fe^{3+/2+}$

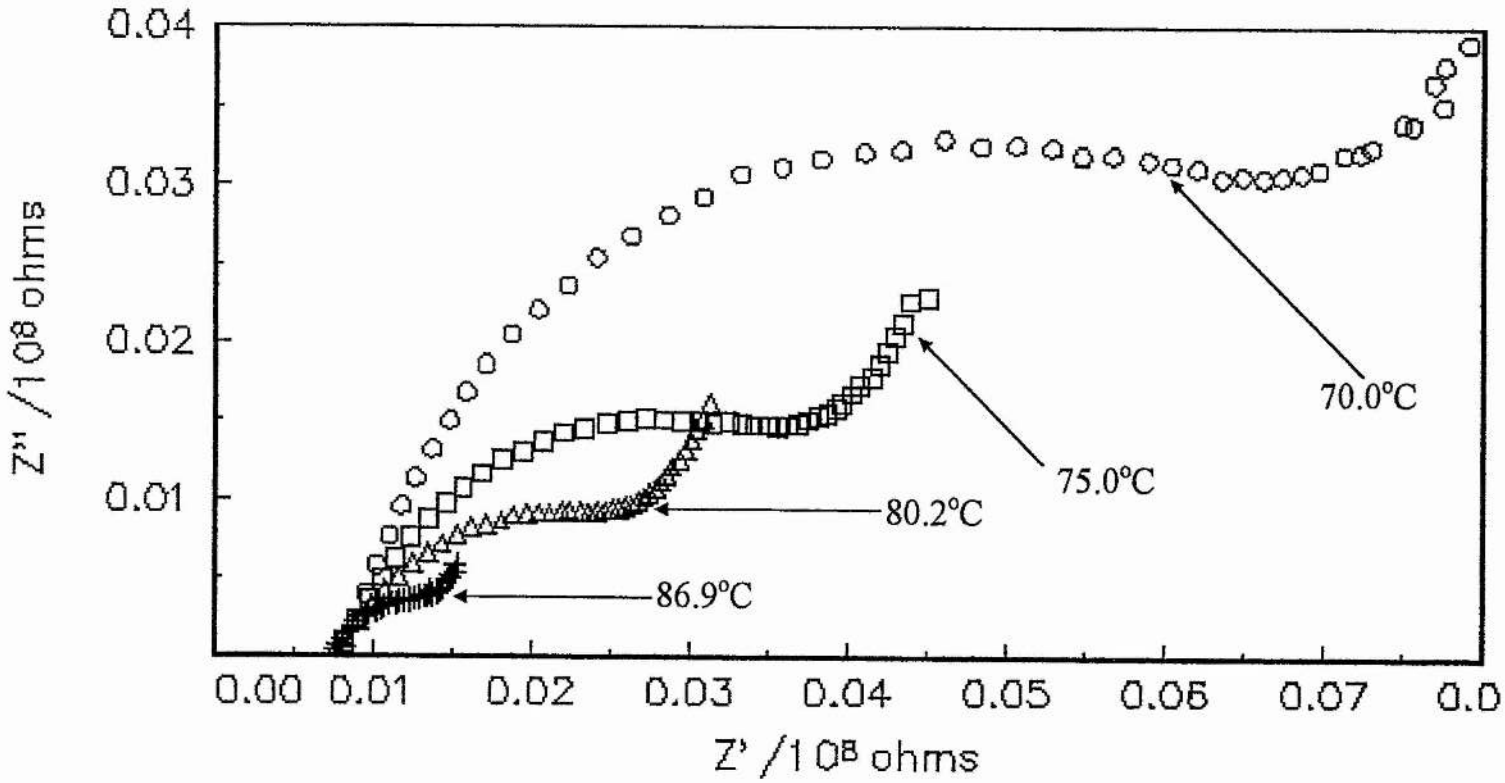

Figure 7.14 Temperature dependence of the polymer electrolyte $PEO_{20}LiClO_4$ containing 13mM $Fe^{3+/2+}$.

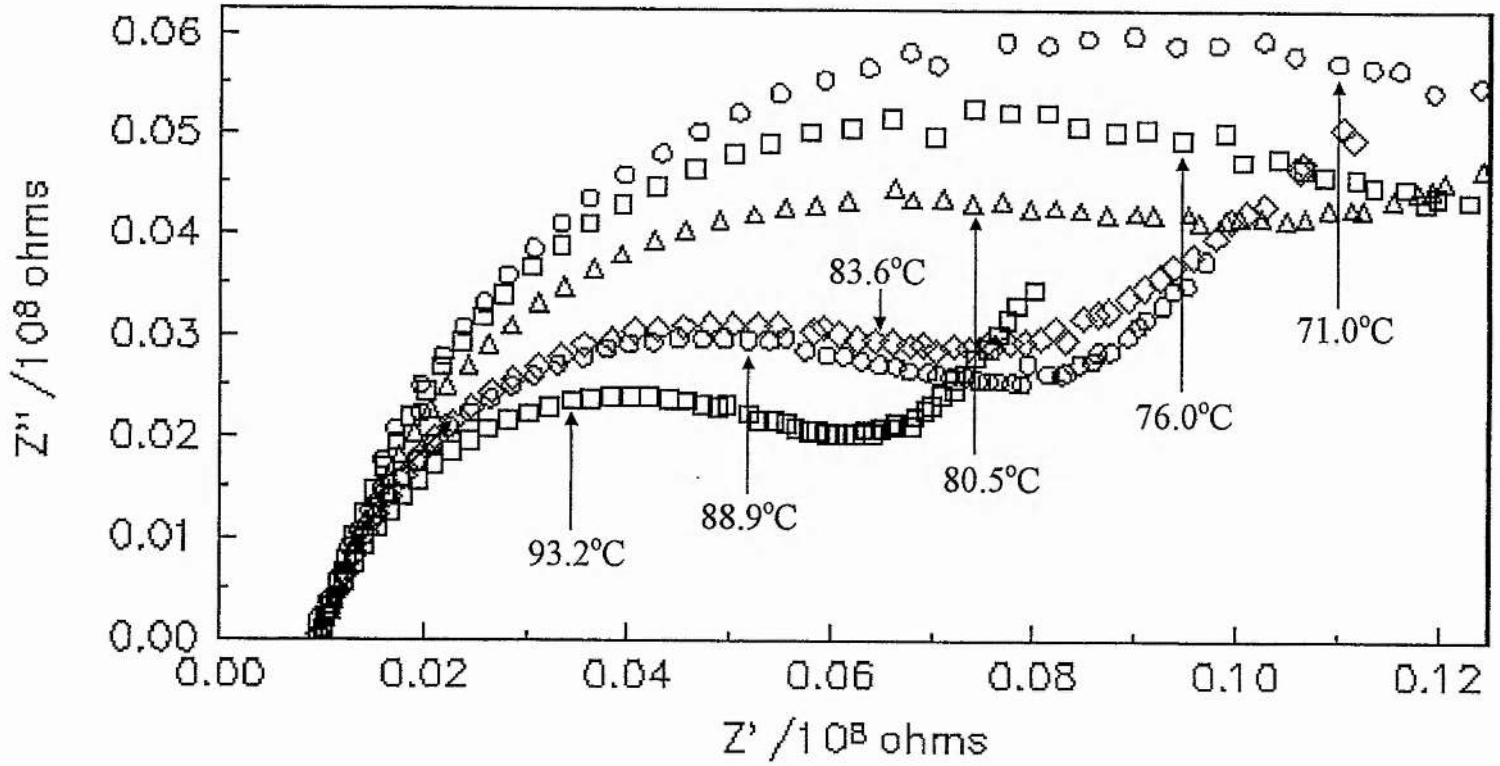

Figure 7.15 Temperature dependence of the polymer electrolyte $PEO_{20}LiClO_4$ containing 20mM $Fe^{3+/2+}$.

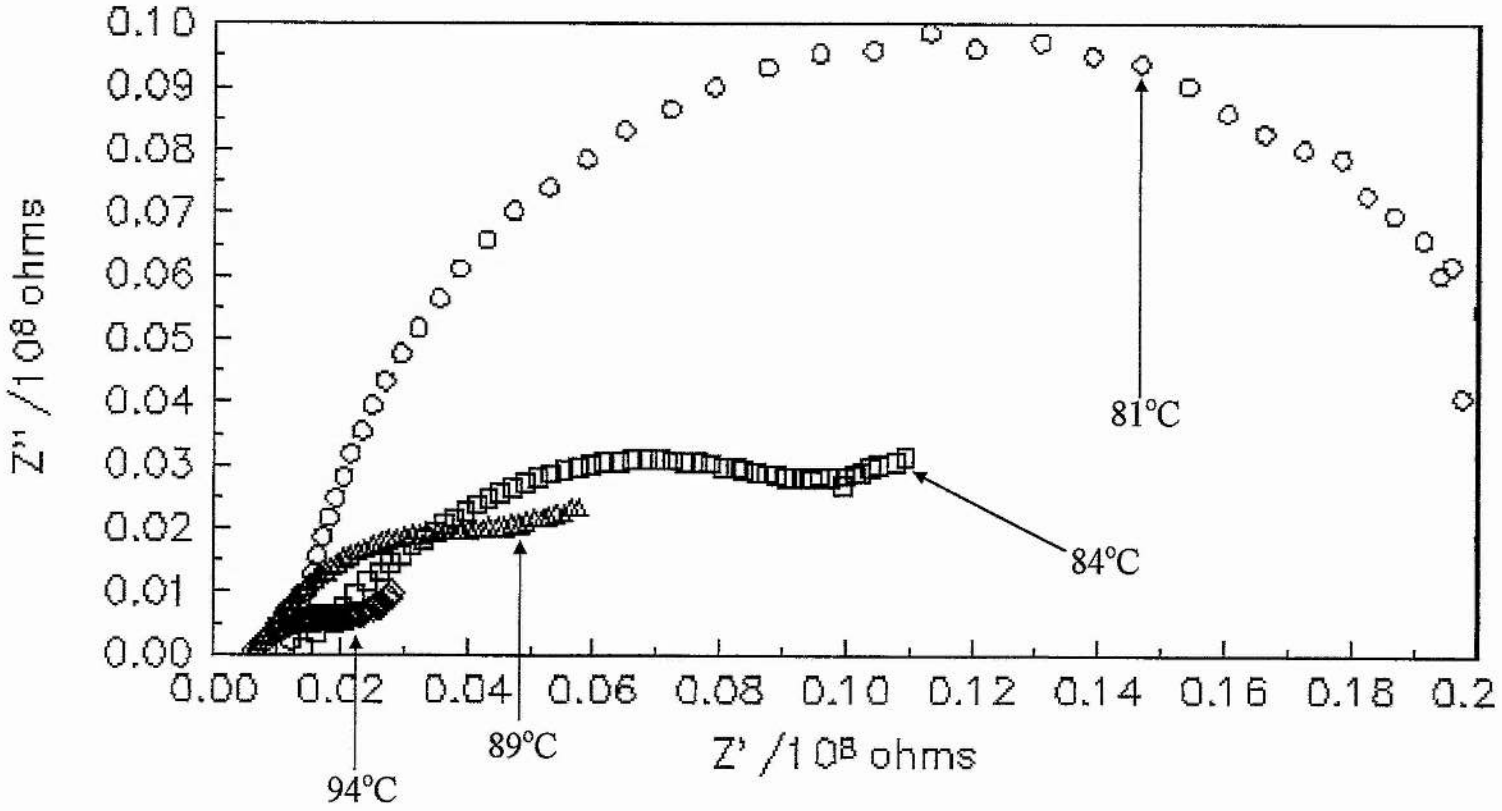

Figure 7.16 Complex impedance plot for $PEO_{20}LiClO_4$ containing 2mM $Fe^{3+/2+}$ at 66.4°C where O is the data and — is the fit.

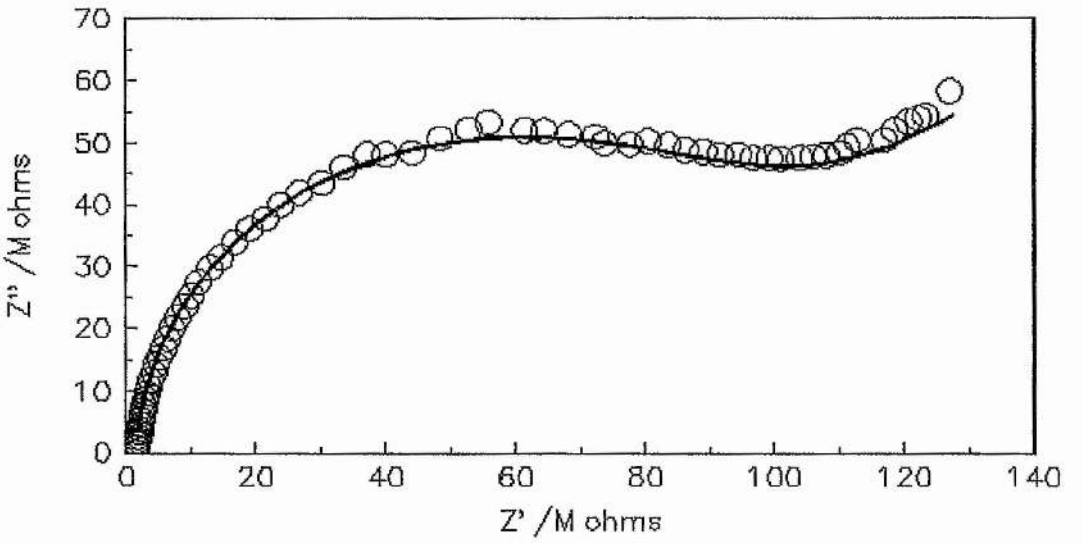

Table 7.1 Summary of results obtained for $PEO_{20}LiClO_4$ containing 2mM $Fe^{3+/2+}$.

Temperature (°C)	**R_u (M ohms)**	**C_{dl} (μFcm^2)**	**k_{sh} (10^{-4} cms^{-1})**	**D_0 (10^{-8} cm^2s^{-1})**
60.0	1.4	2	1.37	0.18
66.4	1.2	2	2.63	0.21
71.1	1.1	2	4.07	0.38
77.4	1	2	7.21	0.68
81.5	0.7	3	9.18	1.38
89.4	0.6	2	18.1	2.05

Table 7.2 Summary of results obtained for $PEO_{20}LiClO_4$ containing 7mM $Fe^{3+/2+}$.

Temperature (°C)	R_u (M ohms)	C_{dl} (μFcm^2)	k_{sh} (10^{-3} cms^{-1})	D_0 (10^{-8} cm^2s^{-1})
66.8	1.32	2	0.709	0.58
70.0	1.30	2	1.17	0.99
75.0	1.24	1	2.65	1.03
80.2	1.01	2	4.21	1.35
86.9	0.93	2	7.9	2.01

Table 7.3 Summary of results obtained for $PEO_{20}LiClO_4$ containing 13mM $Fe^{3+/2+}$.

Temperature (°C)	R_u (M ohms)	C_{dl} (μFcm^2)	k_{sh} (10^{-4} cms^{-1})	D_0 (10^{-8} cm^2s^{-1})
71	2	2	3.54	0.54
76	1	2	4.34	0.69
83.6	0.98	2	6.90	0.83
88.9	0.96	2	7.36	0.99
93.2	0.95	2	8.58	1.09

Table 7.4 Summary of results obtained for $PEO_{20}LiClO_4$ containing 20mM $Fe^{3+/2+}$.

Temperature (^oC)	**R_u (M ohms)**	**C_{dl} (μFcm^2)**	**k_{sh} (10^{-3} cms^{-1})**	**D_θ (10^{-8} cm^2s^{-1})**
81.0	1.22	1	2.1	0.63
84.0	1.41	1	3.4	0.74
89.0	0.63	1	5.9	0.84
94.0	0.66	1	7.6	1.02

Table 7.5 Specific conductivity of the $PEO_{20}LiClO_4$ system calculated for three concentrations of $Fe^{3+/2+}$.

Concentration (mM)	**R_u (M ohms)**	**κ (10^{-4} Scm^{-1})**
2	0.91	2.1
7	1.24	1.7
13	1.01	2

7.2.3 Temperature Dependence of the Standard Apparent Rate Constant and the Diffusion Coefficient

The Standard Apparent Rate Constant k_{sh}

To further understand the electron transfer process it is important to try and calculate the activation energy for the interfacial kinetics. This is normally achieved by modelling the data by the Arrhenius equation defined as:

$$k_{sh} = A \exp(-E_a / RT)$$

where k_{sh} is the rate constant, A is the pre-exponential factor, E_a is the activation energy, R is the gas constant and T is the temperature. Figure 7.17 shows a plot of ln k_{sh} vs. 1000/T.

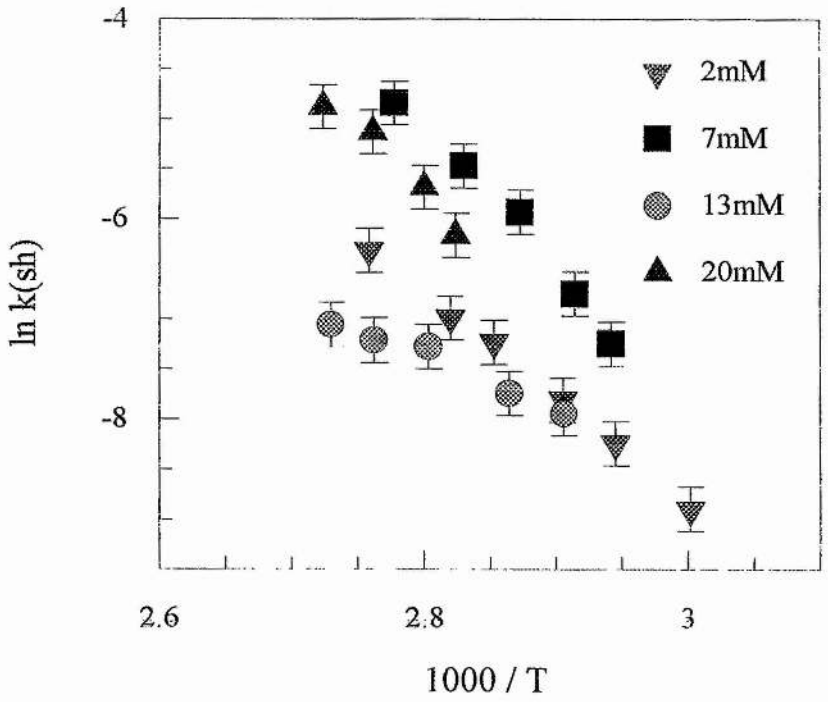

Figure 7.17 Plot of standard apparent rate (k_{sh}) constant vs. temperature (T)

However, as can be seen from figure 7.17, the dependence of k_{sh} on temperature does not appear to follow Arrhenius behaviour, there is some evidence of curvature. For this reason the data were fitted to both the Arrhenius and the Vogel-Tammann-Fulcher (VTF) equations, where the VTF equation is defined as [11]:

$$k_{sh} = AT^{-1/2} exp\{-B\ (T-T_0)\}$$

where k_{sh} is the rate constant, A is a prefactor, T is the temperature, B is an energy divided by the Boltzmann constant, T_0 is the glass transition temperature and T is the temperature.

Table 7.6 show the fitted parameters obtained from using the VTF equation. The table also includes extrapolated values of the rate constants at room temperature. It is necessary to extrapolate values of k_{sh} at room temperature rather than measure them as the polymer crystallises at temperatures below 60°C. The rate given is the rate that would be obtained for PEO at room temperature if it remained amorphous. Table 7.7 shows the fitted parameters and extrapolated room temperature values obtained from the Arrhenius equation. From the values of the room temperature rate constants obtained from each model it can be seen that both models give very similar fits to the data. This is shown graphically in figure 7.17.

Table 7.6 Fitting parameters for VTF behaviour of rate constants

Conc. (mM)	A (10^{-4})	B	T_0 (K)	Extrapolated value for k_{sh} at 25°C (10^{-7} cm s^{-1})
2	5.16 ± 0.36	503.8 ± 40	243 ± 17	9.38
7	0.897 ± 0.06	279.4 ± 22	264 ± 18	4.32
13	93.4 ± 6.5	645.21 ± 51	231 ± 16	106.0
20	22.9 ± 1.6	352.19 ± 28	257 ± 17	7.38

Table 7.7 Fitting parameters for Arrhenius behaviour of rate constants

Concentration (mM)	A (cm s^{-1})	E_A/R (kK)	Extrapolated value for k_{sh} at 25°C (10^{-6} cm s^{-1})
2	22.64 ± 0.68	10.49 ± 0.24	3.54
7	35.89 ± 3.14	14.63 ± 1.09	1.89
13	6.99 ± 1.51	5.14 ± 0.54	35.8
20	30.08 ± 5.34	12.80 ± 1.92	2.63

The results obtained for 13mM $Fe^{3+/2+}$ from both the Arrhenius and the VTF fits are very high when compared to the other concentrations. The reasons for this are unknown and further investigations are necessary to understand this.

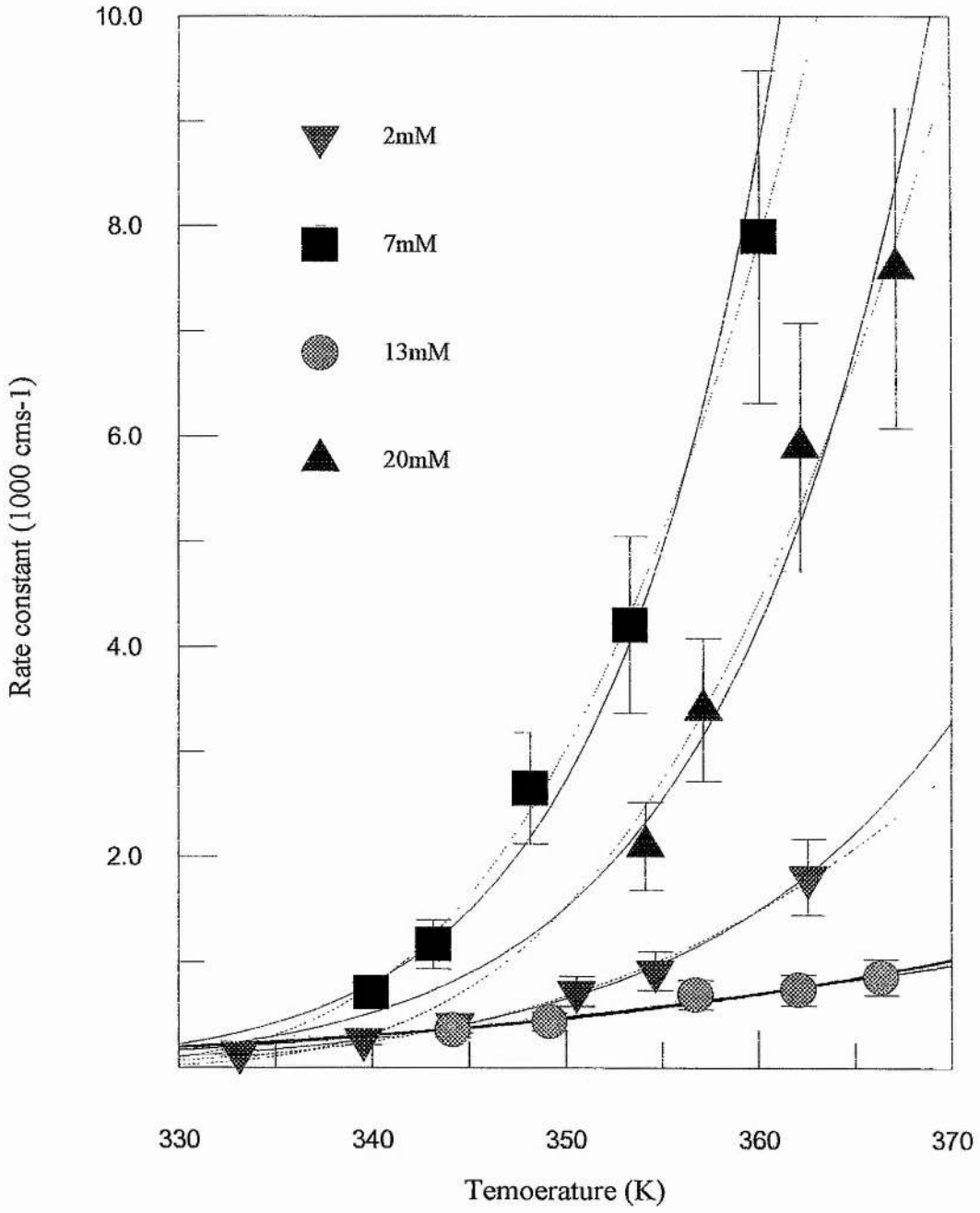

Figure 7.17 VTF (·····) and Arrhenius (——) behaviour of rate constants calculated for 2, 7, 13 and 20mM $Fe^{3+/2+}$.

It appears that the data fits the VTF equation best but taking into account the experimental error when determining k_{sh}, it is not possible to distinguish between VTF and Arrhenius behaviour. This is highlighted in the similarity of the results obtained from both models as given in tables 7.6 and 7.7 It would be intriguing if the temperature dependence of k_{sh} followed VTF behaviour as polymer chain dynamics also follow VTF behaviour [13-18]. One possible explanation for this is that the reorganisation of the solvent molecules should follow VTF behaviour and if the activation of electron transfer is controlled by solvent dynamics then k_{sh} varying with T should be VTF like. However, to say that the dependence of k_{sh} on T follows VTF behaviour would require further work to be carried out, varying T to a much greater extent, as the amount of data presented here is limited.

The Diffusion Coefficient D_0

As was discussed in Chapter 1 the motion of the ions through a polymer electrolyte follows VTF behaviour [13-18]. The temperature dependence of D_0 on T was therefore modelled using the VTF equation [11]. The results of the fit are tabulated in table 7.8. Values of D_0 at room temperature were once again extrapolated from the fitting parameters. The results obtained for 13mM $Fe^{3+/2+}$ are much higher than for each of the other concentrations (c.f. results for k_{sh}) and this is as yet unexplained. The temperature dependence of D_0 with T is shown graphically in figure 7.18.

Table 7.8 Fitting parameters for VTF behaviour of diffusion coefficients

Conc. (mM)	A (10^{-8})	B	T_0 (K)	Extrapolated value for D_0 at 25°C (10^{-11} cm^2s^{-1})
2	0.193 ± 0.013	287.64 ± 23	262 ± 19	1.13
7	2.29 ± 0.16	332.8 ± 26	258 ± 18	9.63
13	54.9 ± 3.84	665.7 ± 53	228 ± 15	70.3
20	5.22 ± 0.37	504.56 ± 40	242 ± 16	11.0

7.4 Discussion

As was discussed in the introduction to this chapter, the solid (PEO) and the liquid solvent (tetramer) only differ in their molecular weight, allowing a direct comparison of the measured kinetics of both systems.

To compare the kinetics of the liquid and solid ethers rate constants have been measured for 20mM Fe (II) and Fe (III) triflate at 81°C for both systems. The value of k_{sh} for the solid was calculated to be 2.1×10^{-3} cm s^{-1} whereas the value of k_{sh} for the liquid system was 3.5×10^{-2} cm s^{-1}. There is not as great a difference between the rate constants at this temperature but they are certainly not equal within experimental error.

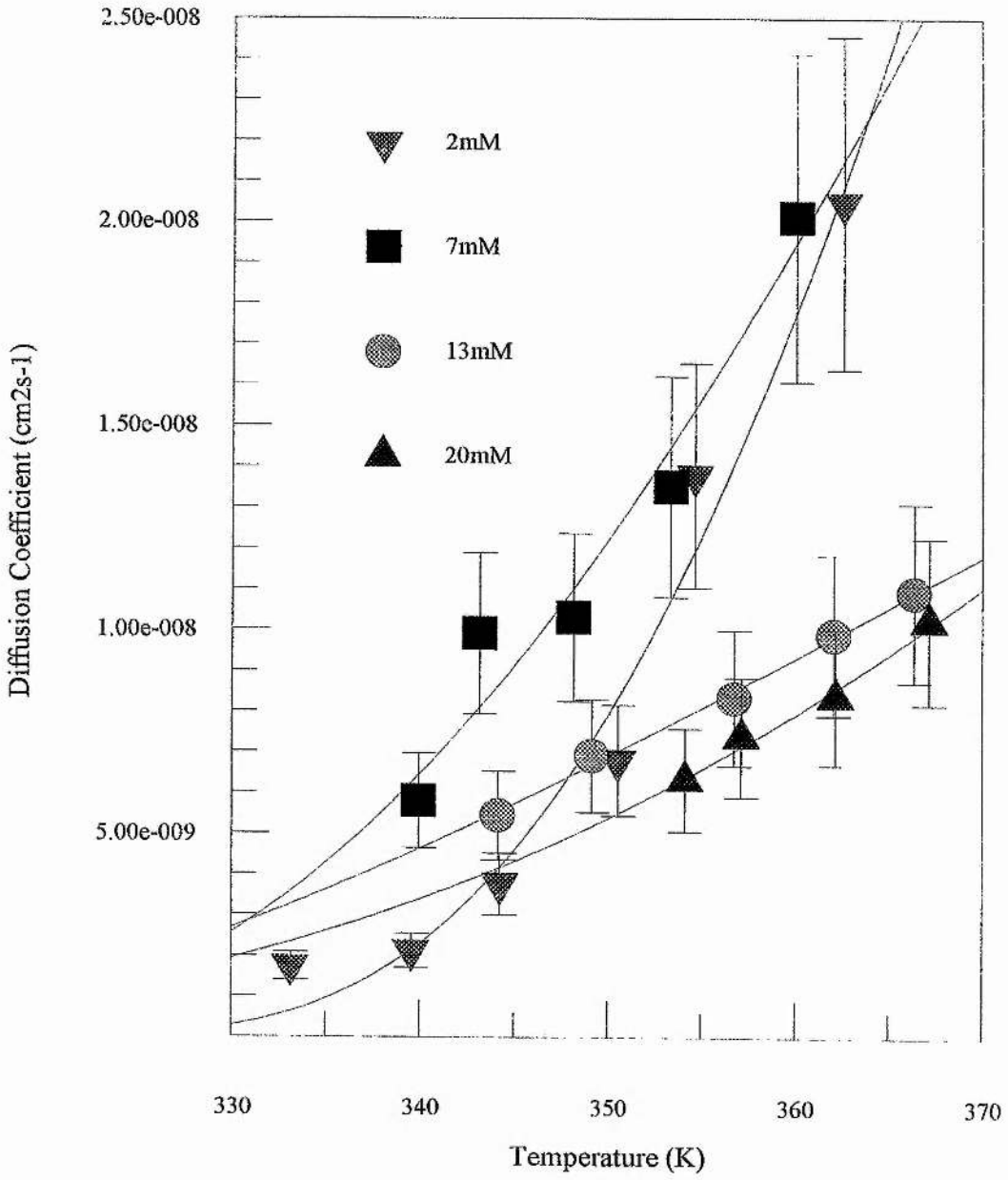

Figure 7.18 VTF behaviour of diffusion coefficients calculated for 2,7,13 and 20mM $Fe^{3+/2+}$.

Therefore, it must be concluded that for polyether solvents outer sphere solvent dynamics must play an important role in the activation of electron transfer and that in the solid the reorganisation of the solvent is much slower than in the liquid polyether: it is not just the influence of the metal-solvent bond vibrations as was concluded in chapter 5. Dipolar coupling between an electron-transfer reactant and the solvent dipole serves to couple the solvent dipole fluctuation or relaxation rate to the barrier crossing rate for electron transfer. In the solid polyether the solvent dipoles are restricted by the segmental motion of the polymer chains to which they are attached. Therefore, the relaxation (or fluctuation times) for these dipoles will be longer than those of the liquid polyether.

Other possibilities arise in the explanation of the differences in the rate constants. The first is that collisional friction may be a factor because the size of the dynamic polymer segments is large, impeding necessary reaction motion. Secondly the nature of the interface between the solid polyether and the platinum working electrode is not fully understood. There may be steric effects arising from the characteristics of macromolecular phase boundaries, and the dynamics of segmental chain motion at the interface may not be the same as in the polymer bulk.

The ion mobility (diffusion coefficient) in the liquid polyethers is higher than in solid polyethers, it is of the order of 10^{-6} cm^2s^{-1} whereas in the solid it is of the order of 10^{-8} cm^2s^{-1} In high molecular weight PEO diffusion occurs via segmental motion, the whole segment moves before passing on the ion and so the movement of the cation

(diffusion) is limited. In liquid polyethers the solvent moves with the ion and so diffusion is not hindered.

REFERENCES

1 M. Fleischmann & S. Pons, *J. Electroanal. Chem.*, 250, 277, 1988

2 S. Sarangapani & R. deLevie, *J. Electroanal. Chem.*, 102, 165, 1979

3 A.S. Baranski, *J. Electroanal. Chem.*, 133, 93, 1986

4 P.G. Bruce, A. Lisowska-Oleksiak, P. Los & C.A. Vincent, *J. Electroanal. Chem.*, 367, 279, 1994

5 J.R. MacDonald, J. Schooonman & A.P. Lehner, *J. Electroanal. Chem.*, 131, 77, 1982

6 H. Gerischer, *Z. Phys. Chem.*, 210, 55, 1952

7 R.D. Armstrong, R.E. Firman & H.R. Thirsk, *Faraday Discuss. Chem. Soc.*, 56, 244, 1973

8 R.H. Wopschall & I. Shain, *Anal. Chem..*, 39, 1514, 1527, 1535, 1967

9 M.I. Montenegro, M.A. Queiros, J.L. Daschbach (Eds.), Microelectrodes: Theory and Applications, NATO ASI Series, Series E: Applied Sciences, 97, Kluwer Academic Publisher, Dordecht, 1991

10 C.D. Robitaille & D. Fauteux, *J. Electrochem. Soc.*, 133, 315, 1986

11 H. Vogel, *Phys. Z.*, 22, 645, 1921; G. Tammann & W. Hesse, *Z. Anorg. Allg. Chem.*, 156, 245, 1926; G.S. Fulcher, *J. Am. Ceram. Soc.*, 8, 339, 1959

12 F.M. Gray, Solid Polymer Electrolytes: Fundamentals and Technological Applications, VCH, 1991

13 M.H. Cohen & D. Turnbull, *J. Chem. Phys.*, 31(5), 1164, 1959

14 J.H. Gibbs & E.A. DiMarzio, *J. Chem. Phys.*, 43(1), 373, 1958

15 G. Adam & J.H. Gibbs, *J. Chem. Phys.*, 43(1), 139, 1965

16 S.D. Druger, M.A. Ratner & A. Nitzan, *Solid State Ionics*, 9&10, 1115, 1983

17 B.L. Papke, M.A. Ratner & D.F. Shriver, *J. Electrochem. Soc.*, 129, 1694, 1982

18 D.F. Shriver, R. Dupon & M. Stainer, *J. Power Sources*, 9, 383, 1983

CHAPTER 8

Concluding Remarks

A successful synthesis has been developed for Fe (II) trifluoromethane sulphonate [$Fe(CF_3SO_3)_2$] and Fe (III) trifluoromethane sulphonate [$Fe(CF_3SO_3)_3$]. Whereas $Fe(CF_3SO_3)_2$ could be prepared by the action of trifluoromethane sulphonic acid on the iron metal, $Fe(CF_3SO_3)_3$ required the oxidation of the Fe^{2+} salt by hydrogen peroxide in the presence of trifluoromethane sulphonic acid. This was surprising as conventional wisdom in inorganic chemistry suggests that Fe^{3+} would be more stable in the acid medium.

The electrochemistry of the $Fe^{3+/2+}$ redox couple was studied in several non-aqueous aprotic systems, namely dimethyl sulphoxide, dimethyl formamide, propylene carbonate, tetrahydrofuran and acetonitrile. In all the systems studied the electrode reaction was simple one electron transfer. The standard apparent rate constant (k_{sh}) varies by a factor of 3 upon variation of the supporting electrolyte (TBAP, $LiClO_4$, $LiAsF_6$, $TEAPF_6$ and $TEABF_4$) indicating minimal supporting electrolyte dependence. However, k_{sh} varies by a factor of 8 upon varying the concentration of $Fe^{3+/2+}$ from 1mM to 20mM. This dependence can be explained, to a certain extent, by poor resolution of data collected and the associated difficulty in calculating k_{sh}. By far the greatest variation of k_{sh} came with variation of the solvent, a factor of 10^2 difference being noted between DMSO and ACN, and so the systems could be used to study

solvent effects on the activation of electron transfer. The solvents were chosen to provide a variation of donor number (DN) and longitudinal relaxation time (τ_L). Electron transfer depends on activation either by vibrations of the species undergoing electron transfer (inner coordination sphere contributions to activation) or by reorganisation of the solvent dielectric (outer coordination sphere contributions to activation) believed to be dependent on τ_L. We have shown, for $Fe^{3+/2+}$, no correlation of k_{sh} with τ_L, However, we have shown inner sphere activation of electron transfer for the FeS_x system, and importantly that k_{sh} is linear with donor number.

A new technique had to be developed and tailored for the investigation of electrode reactions in a solid polymer electrolyte, and was particularly useful for study of relatively fast redox couples. The technique involves making ac impedance spectroscopy measurements at a microelectrode. It allowed measurements to be made in media that are highly resistive (10^3 higher than typical liquids of $10^6\Omega$cm) and in which the diffusion of electroactive species is slow, 10^2 slower than in liquids i.e. 10^{-8} cm^2s^{-1}. The technique provided a greater resolution of interfacial processes than conventional sized electrode studies of the polymer/electrode interface, allowing more accurate calculations to be made of the kinetics involved, and it has proved essential for our studies of the redox kinetics in polyether solvents.

Investigation of $Fe^{3+/2+}$ redox couple was also carried out in PEO with $LiClO_4$ present as the supporting electrolyte. For concentrations of $Fe^{3+/2+}$ of 20mM and less, only one semicircle was seen in the complex impedance plot and the electrode reaction was that of simple one electron transfer. However, at concentrations of

$Fe^{3+/2+}$ greater than 50mM, a second semi-circle was also seen indicating an adsorption or chemical reaction . For 20mM $Fe^{3+/2+}$ the standard apparent rate constant was calculated to be 2.1×10^{-3} cm s^{-1} at 81°C. The value of k_{sh}, for the same couple in the liquid polyether tetramer at the same temperature, was calculated to be 3.5×10^{-2} cm s^{-1}. As the inner sphere contribution to the activation of electron transfer is the same for both solvents, the difference in the two k_{sh} values indicates outer sphere contribution to the activation of electron transfer, i.e. solvent dynamics play an important role in the activation of electron transfer in these media.

Liquid studies of the $Fe^{3+/2+}$ redox couple indicate inner sphere activation of the electron transfer process with a dependence of k_{sh} with DN. However, when moving from a liquid to a solid solvent a dependence of k_{sh} with solvent dynamics is seen. As the DN is particularly similar for the liquid polyether and the solid polyether further investigations of the redox couple in these media should anticipate a similar vibration spectrum of the metal-solvent ligand bond.

Future Work

Many more solvent systems should be investigated, including polyethers of the form $CH_3(CH_2O)_nCH_2CH_3$ where $n \geq 2$, providing a wider range of longitudinal relaxation time, τ_L. Also, it is important that several more redox couples, of the form $M^{n+/(n-1)+}$ are studied in such solvents.

For the liquid and solid polyether systems a molecular compound such as ferrocene must be investigated as coordination of such a compound with the polyethers will be different than for the $Fe^{3+/2+}$ couple and this could influence the activation of electron transfer.

As it has been suggested that the vibration of the Fe-S bond (where S is the solvent) is the same in both tetramer and PEO, the FeS coordination must be investigated in both systems as must the vibrational spectrum, via FTIR and Raman spectroscopy.

Above a concentration of 50mM $Fe^{3+/2+}$ in PEO, the electrode reaction is no longer that of simple one electron transfer; there are two semicircles in the complex impedance plot. This more complex electrode reaction must be investigated to determine whether the process is that of adsorption, or whether the reaction follows an EC or CE mechanism etc. This may be achieved via cyclic voltammetric and chronocoulometric investigations.

The range of temperatures at which the standard apparent rate constant (k_{sh}) is measured in PEO must be expanded further to determine whether ksh follows VTF or Arrhenius behaviour, or indeed a mixture of both. In the same vein of investigation, the temperature dependence of k_{sh} must determined in tetramer and the five aprotic solvents employed in this thesis. This would allow the determination of the activation energies and the preexponential factors for these systems, which in turn could be compared to those calculated for the PEO system.

APPENDIX

Analysis of Iron (II) and Iron (III) Trifluoromethane Sulphonate

Introduction

Iron (II) and (III) triflate were prepared as described in chapter 2. The iron (II) salt gave a blue coloured solution and the iron (III) an orange/brown colour in water which are both typical of their respective oxidation states in water. However such visual observations are inconclusive proof that $Fe(CF_3SO_3)_2$ and $Fe(CF_3SO_3)_3$ have been prepared. The following experiments were carried out to identify the oxidation states.

UV Spectroscopy

Iron (II) triflate was dissolved in 2ml of water to a concentration of 1mol cm^{-3} and uv spectroscopy was then carried out on the solution. Fe^{2+} exhibits a typical peak as observed in the spectrum shown in figure A1.

Cyclic Voltammetry

(i) at an ultramicroelectrode

A three electrode cyclic voltammogram was carried out on an equimolar solution of Fe (II) and Fe (III) triflate to identify the peak potential (E_p) at which Fe^{2+} is oxidised to Fe^{3+} and the peak potential at which Fe^{3+} is reduced to Fe^{2+}. The peak potentials

for the two processes were calculated to be 0.25V and -0.3V respectively. To show that there was no Fe^{3+} present, in the sample of $Fe(CF_3SO_3)_2$, an ultramicroelectrode cv was carried out on a fresh solution containing Fe (II) triflate only. The sweep is started at -0.25V a potential where small traces of Fe^{3+} would be observed on the voltammogram. Figure A2 shows the cyclic voltammogram for 14mM Fe (II) triflate in 0.2M H_2SO_4 at an ultramicroelectrode of 10μm diameter. As can be seen there appears to be no traces of any Fe (III) salt being reduced. In a similar experiment carried out on a solution containing Fe (III) triflate only, the sweep was started at +0.25V. If there were traces of the Fe (II) salt present these would be seen as an oxidation process at this potential. Figure A3 shows the cyclic voltammogram for 10mM Fe (III) triflate in 0.5M H_2SO_4 at a 10μm diameter ultramicroelectrode.

In addition this technique can be used to estimate the molecular weight of the two triflate salts by comparison with a known iron (II) and iron (III) salt. The molecular weight of Fe (II) triflate was estimated by comparison with $FeSO_4.7H_2O$ and the molecular weight of the Fe (III) triflate by comparison with $Fe_2(SO_4).5H_2O$. Cyclic voltammetry at an ultramicroelectrode was first carried out on solutions of 21.55mM $FeSO_4.7H_2O$ in 0.2M H_2SO_4 and 19.62mM $Fe_2(SO_4)_3.5H_2O$. From the voltammograms, the diffusion coefficients of the Fe^{2+} and Fe^{3+} species can be calculated from the steady state current plateaux and the following equation: $D_0 = I_0r/nFC^{\infty}$ prepared using 0.1456 g of Fe (II) triflate and 0.2034 g of Fe (III) triflate and ultramicroelectrode cyclic voltammetry was performed. Using values of current density from each plateau and assuming the diffusion coefficients of the Fe^{2+} and Fe^{3+}

species were the same as for the Fe^{2+} and Fe^{3+} species in $FeSO_4.7H_2O$ and $Fe_2(SO_4).5H_2O$, the concentrations of Fe (II) and Fe (III) triflate present in solution were estimated using the above equation. The diffusion coefficients was calculated to be 8.0×10^{-7} cm^2s^{-1} and 1.2×10^{-6} cm^2s^{-1} for $FeSO_4.7H_2O$ and $Fe_2(SO_4)_3.5H_2O$ respectively. Similar solutions were then The concentrations were calculated to be 20mM and 20.34mM (for Fe^{2+} and Fe^{3+} respectively) and the molecular weight of each was then calculated from these figures and the known masses of salt dissolved. The calculated molecular weights were 364 for the Fe (II) salt and 500 for the Fe (III) salt. The actual molecular weight of Fe (II) triflate is 353.9 and that of Fe (III) triflate is 503.04, and so this experiment has confirmed the identities of the Fe (II) triflate and the Fe (III) triflate.

(ii) at a conventional sized electrode

As further visual evidence for the lack of an Fe^{3+} species and the presence of an Fe^{2+} species, cyclic voltammetry was carried at a conventional sized electrode in a three electrode configuration. The cell was initially swept from 0.15V to -0.3V, the potential region where Fe^{3+}, if present, should reduce to Fe^{2+}, then continued 0.85V, the range in which Fe^{2+} is oxidised to Fe^{3+}. As can be seen in figure A4 there is no evidence to support the presence of Fe^{3+}. The large cathodic peak, is actually the reduction of water with the production of H_2 gas.

Microanalysis

Samples of Fe (II) triflate and Fe (III) triflate were subjected to chemical analysis. The formula weight of Fe (II) triflate should be 353.9 and that for Fe (III) triflate should be 503.04. The microanalysis results are presented below (tables A1 and A2) such that the weights of each element present are given as a percentage of the overall formula. The expected percentages are those for the pure salt and the actual percentages are those obtained from microanalysis.

Table A1 Microanalysis results for Fe (II) triflate

ELEMENT	EXPECTED %	ACTUAL %
Sulphur	18.12	17.7
Fluorine	32.2	32.0
Iron	15.7	13.9

Table A2 Microanalysis results for Fe (III) triflate

ELEMENT	EXPECTED %	ACTUAL %
Sulphur	19.12	17.5
Fluorine	33.9	30.8
Iron	11.1	9.68

Figure A1 UV spectrum for Fe (II) Triflate

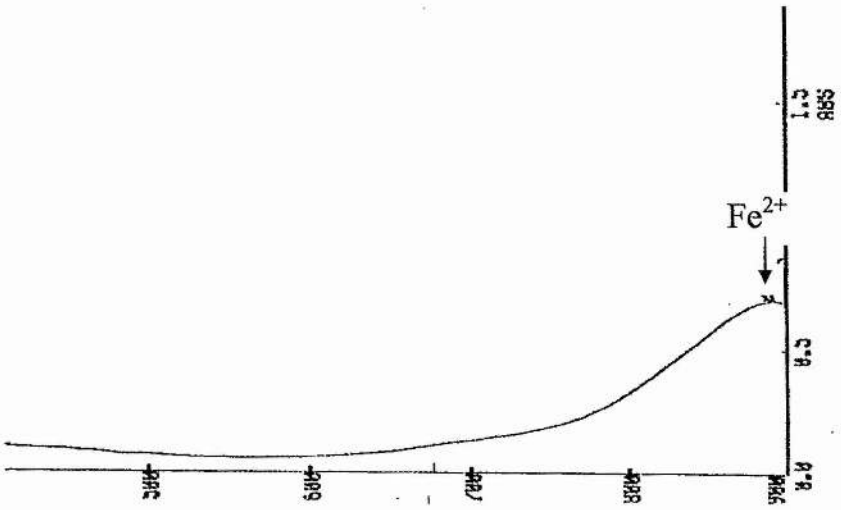

Figure A2 Cyclic voltammogram for 14mM Fe (II) Triflate in 0.2M H_2SO_4 at a 10μm diameter platinum ultramicroelectrode.

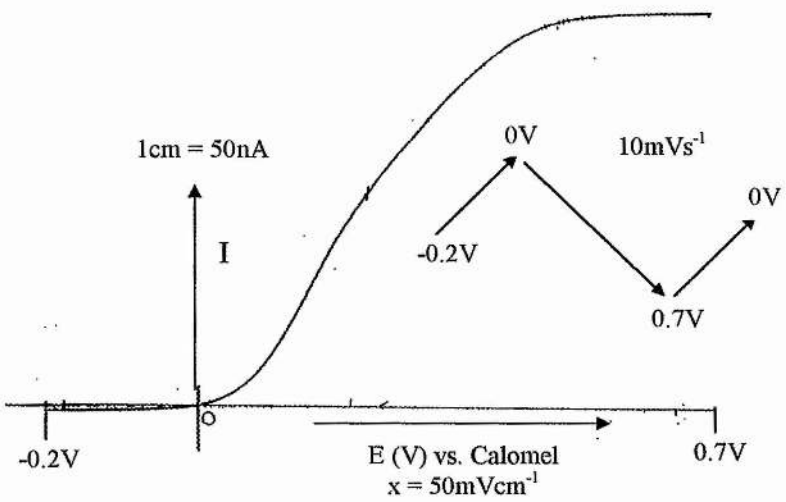

Figure A3 Cyclic voltammogram for 10mM Fe (III) Triflate in 0.5M H_2SO4 at a 10μm diameter platinum ultramicroelectrode.

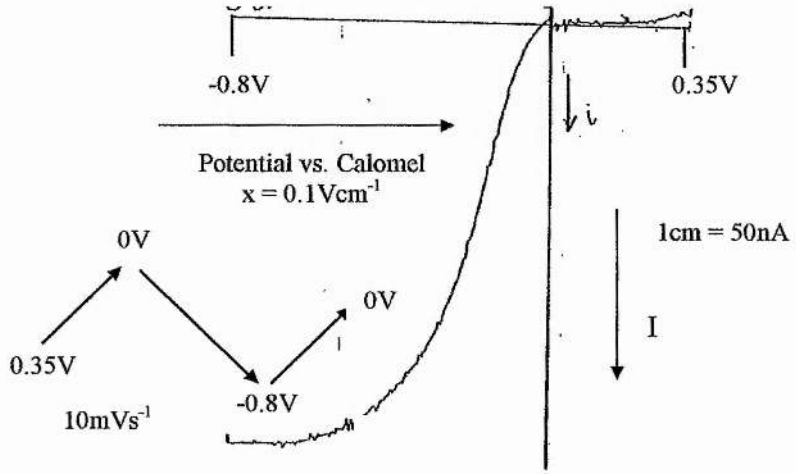

Figure A4 Cyclic voltammogram of 14mM Fe (II) triflate in 0.2M H_2SO_4 at a 2mm diameter platinum electrode.